공학박사 학위논문

Dehydrogenation of n-Butane to n-Butene and 1,3-Butadiene over Magnesium Vanadate and Platinum-Tin Catalysts

마그네슘 바나데이트와 백금-주석 촉매 상에서 노르말-부탄의 탈수소화 반응을 통한 노르말-부텐과 1,3-부타디엔 제조

2016년 2월

서울대학교 대학원

화학생물공학부

이 종 권

Abstract

Dehydrogenation of n-Butane to n-Butene and 1,3-Butadiene over Magnesium Vanadate and Platinum-Tin Catalysts

Jong Kwon Lee

School of Chemical and Biological Engineering

The Graduate School

Seoul National University

Because of extensive use as chemical building blocks, C4 olefins, such as n-butenes and 1,3-butadiene, are important raw materials in the petrochemical industries. C4 olefins are major feedstocks for the production of various chemicals such as synthetic resins (low density polyethylene (LDPE) and high density polyethylene (HDPE)) and synthetic rubbers (acrylonitrile butadiene styrene (ABS), polybutadiene rubber (BR), styrene butadiene rubber (SBR), and styrene butadiene latex (SBL)). The demand of C4 olefins has increased steadily due to the development of synthetic rubber industry in the developing countries. With the growth of shale gas industry, the production of C4 olefins has been reduced because of the switch to lighter

feedstocks (naphtha → ethane). At present, n-butene and 1,3-butadiene in the petrochemical industry are mainly produced from naphtha cracking process. However, naphtha cracking process operated at relatively high temperature (>800 ^{o}C) involves many problems in both marketing and energy management, because this process produces not only butenes and butadiene but also ethylene, propylene, and isobutene. For these reasons, dehydrogenation of n-butane has been considered as the effective method to produce n-butene and 1,3-butadiene. In this work, various magnesium vanadate and platinum-tin catalysts were employed for the dehydrogenation of n-butane.

Magnesium vanadate catalyst has been considered as the most feasible catalyst for oxidative dehydrogenation of n-butane due to its high intrinsic activity. However, it was known that the catalytic performance of $Mg_3(VO_4)_2$/MgO catalyst was unstable due to its low oxygen mobility. The low oxygen mobility of $Mg_3(VO_4)_2$/MgO catalyst impeded oxygen make-up during the catalytic reaction, and thus, led to a severe catalytic deactivation in the oxidative dehydrogenation of n-butane. To overcome this problem, many attempts have been made to improve the stability of $Mg_3(VO_4)_2$/MgO catalyst by adding a metal oxide stabilizer (TiO_2, Cr_2O_3, SiO_2, and ZrO_2) to $Mg_3(VO_4)_2$/MgO catalyst. The addition of ZrO_2 to $Mg_3(VO_4)_2$/MgO catalyst resulted in excellent stability of catalyst by improving oxygen mobility of catalyst. This means that well-developed $Mg_3(VO_4)_2$/MgO-ZrO_2 catalyst not only improved oxygen mobility of the catalyst but also enhanced the intrinsic activity of the catalyst, resulting in a high catalytic performance without catalyst deactivation. Thus, $Mg_3(VO_4)_2$/MgO-ZrO_2 catalysts have received much attention for improving both catalytic activity and stability in the oxidative dehydrogenation of n-butane. In this work, in order to optimize n-

butene and 1,3-butadiene production efficiency in the oxidative dehydrogenation of n-butane, $Mg_3(VO_4)_2/MgO\text{-}ZrO_2$ catalysts were prepared by various chemical compositions such as vanadium content and Mg:Zr ratio in the catalysts.

A series of X-$Mg_3(VO_4)_2/MgO\text{-}ZrO_2$ catalysts were prepared by a citric acid sol-gel method and a wet impregnation method with variation of vanadium content (X = 6.6, 9.9, 12.8, 15.2, and 19.1 wt%). The effect of oxygen capacity (the amount of oxygen in the catalyst involved in the reaction) and oxygen mobility (the intrinsic mobility of oxygen in the catalyst involved in the reaction) of X-$Mg_3(VO_4)_2/MgO\text{-}ZrO_2$ catalysts on the catalytic performance in the oxidative dehydrogenation of n-butane was investigated. Catalytic performance of X-$Mg_3(VO_4)_2/MgO\text{-}ZrO_2$ catalysts was strongly dependent on vanadium content. TPRO (temperature-programmed reoxidation) measurements revealed that the catalytic performance of X-$Mg_3(VO_4)_2/MgO\text{-}ZrO_2$ catalysts was closely related to oxygen capacity and oxygen mobility of the catalysts. Experimental results revealed that oxygen capacity of the catalyst was closely related to the catalytic activity in the oxidative dehydrogenation of n-butane, while oxygen mobility of the catalyst played an important role in the catalyst stability.

$Mg_3(VO_4)_2/MgO\text{-}ZrO_2$ (X) catalysts were prepared by a citric acid sol-gel method and a wet impregnation method with a variation of Mg:Zr ratio (X = 16:1, 8:1, 4:1, 2:1, and 1:1) for the purpose of elucidating the effect of Mg:Zr ratio on the catalytic performance of the catalyst. Catalytic performance of $Mg_3(VO_4)_2/MgO\text{-}ZrO_2$ (X) catalysts was strongly dependent on Mg:Zr ratio. It was observed that all the catalysts showed a stable catalytic performance in the oxidative dehydrogenation of n-butane during the whole

reaction time. Yield for total dehydrogenation products (TDP, n-butene and 1,3-butadiene) showed a volcano-shaped trend with respect to Mg:Zr ratio. Effect of oxygen property of $Mg_3(VO_4)_2$/MgO-ZrO_2 (X) catalysts on the catalytic performance in the oxidative dehydrogenation of n-butane was investigated. Experimental results revealed that the catalytic activity of $Mg_3(VO_4)_2$/MgO-ZrO_2 (X) catalysts increased with increasing oxygen capacity of the catalyst.

Pt-Sn catalyst supported on Al_2O_3 has been widely employed for direct dehydrogenation of n-butane due to its high catalytic activity and high selectivity for n-butene and 1,3-butadiene. It has been reported that platinum is an active metal and tin serves as an efficient activity modifier for platinum in the direct dehydrogenation of n-butane. It is generally accepted that platinum and acid property in the alumina-supported platinum catalyst play key roles in the direct dehydrogenation of n-butane. It has been reported that platinum is an active metal and the high dispersion of platinum is necessary to achieve high selectivity to dehydrogenation relative to undesirable side reactions. The typical alumina supports employed have acidic sites that accelerate skeletal isomerization, cracking, and polymerization of olefinic materials, and enhance “coke” formation. Furthermore, coke formation causing catalyst deactivation is inevitable under high-temperature catalytic reaction conditions in this reaction. Therefore, developing an efficient Pt/Sn/Al_2O_3 catalyst with high catalytic activity and catalyst stability is of great importance. In this work, various platinum-tin catalysts, including Pt/Sn/M/Al_2O_3 (M = Zn, In, Y, Bi, and Ga), a series of Pt/Sn/Zn/Al_2O_3 catalysts with a variation of Zn content (X = 0, 0.25, 0.5, 0.75, and 1.0 wt%), Pt/Sn/Al_2O_3 (various Al_2O_3 support preparation method), and Pt/Sn/Al_2O_3

(different Al_2O_3 support calcination temperature), were prepared by a sequential impregnation method.

A series of $Pt/Sn/M/Al_2O_3$ catalysts with different third metal (M = Zn, In, Y, Bi, and Ga) were prepared by a sequential impregnation method. The effect of third metal addition on the physicochemical properties and catalytic activities of $Pt/Sn/M/Al_2O_3$ catalysts was investigated. It was found that chemical and electronic properties of the catalysts were affected by the addition of third metal. It was revealed that yield for TDP increased with increasing metal-support interaction and Pt surface area of the catalyst. Metal-support interaction and Pt surface area played important roles in determining the catalytic performance. In the direct dehydrogenation of n-butane, $Pt/Sn/Zn/Al_2O_3$ catalyst showed the best catalytic performance.

A series of $Pt/Sn/XZn/Al_2O_3$ catalysts with different Zn content (X, wt%) were prepared by a sequential impregnation method. The effect of zinc content of $Pt/Sn/XZn/Al_2O_3$ catalysts on their physicochemical properties and catalytic activities in the direct dehydrogenation of n-butane was investigated. TPR (temperature-programmed reduction) and chemisorption experiments showed that metal-support interaction and Pt surface area of the catalysts were closely related to the catalytic performance. Catalytic activity increased with increasing metal-support interaction and Pt surface area of the catalysts. In the direct dehydrogenation of n-butane, $Pt/Sn/0.5Zn/Al_2O_3$ catalyst, which retained the strongest metal-support interaction and the highest Pt surface area, showed the best catalytic performance in terms of conversion of n-butane and yield for TDP.

Al_2O_3 (X) supports were prepared by precipitation method (Al_2O_3 (P)), alkoxide-based sol-gel method (Al_2O_3 (AS)), and epoxide-driven sol-gel

method (Al_2O_3 (ES)). For comparison, a commercially available Al_2O_3 (Alfa Aesar) was used as a support (denoted as Al_2O_3 (C)). $Pt/Sn/Al_2O_3$ (X) catalysts were then prepared by a sequential impregnation method. The effect of preparation method of alumina support on the physicochemical properties and catalytic activities of $Pt/Sn/Al_2O_3$ (X) catalysts in the direct dehydrogenation of n-butane was investigated. BET surface area and pore volume of $Pt/Sn/Al_2O_3$ (X) catalysts decreased in the order of $Pt/Sn/Al_2O_3$ (ES) > $Pt/Sn/Al_2O_3$ (AS) > $Pt/Sn/Al_2O_3$ (P) > $Pt/Sn/Al_2O_3$ (C). It was revealed that the platinum dispersion and platinum surface area of $Pt/Sn/Al_2O_3$ (X) catalysts decreased in the order of $Pt/Sn/Al_2O_3$ (ES) > $Pt/Sn/Al_2O_3$ (AS) > $Pt/Sn/Al_2O_3$ (P) > $Pt/Sn/Al_2O_3$ (C). In the direct dehydrogenation of n-butane, $Pt/Sn/Al_2O_3$ (ES) catalyst with the highest platinum surface area showed the best catalytic performance in the direct dehydrogenation of n-butane.

Al_2O_3-X supports prepared by a sol-gel method were calcined at various temperatures, and $Pt/Sn/Al_2O_3$-X catalysts were then prepared by a sequential impregnation method. The effect of calcination temperature of alumina on the catalytic performance of $Pt/Sn/Al_2O_3$-X catalysts in the direct dehydrogenation of n-butane was investigated. Physicochemical properties of $Pt/Sn/Al_2O_3$-X catalysts were strongly influenced by the calcination temperature of alumina. It was found that platinum surface area and acidity of $Pt/Sn/Al_2O_3$-X catalysts decreased with increasing calcination temperature of alumina. In the dehydrogenation of n-butane, platinum surface area and acidity of $Pt/Sn/Al_2O_3$-X catalysts were closely related to conversion of n-butane and selectivity for TDP, respectively. Conversion of n-butane decreased with decreasing platinum surface area of the catalyst and selectivity for TDP decreased with increasing acidity of the catalyst. Among the catalysts

tested, $Pt/Sn/Al_2O_3$-700 (a platinum-tin catalyst supported on alumina that had been calcined at 700 ^oC) showed the best catalytic performance in terms of yield for TDP.

In summary, various magnesium vanadate catalysts and platinum-tin catalysts were prepared and they were applied to the dehydrogenation of n-butane to n-butene and 1,3-butadiene in this study. In order to explain catalytic performance of the prepared catalysts in the dehydrogenation of n-butane, several characterizations such as N_2 adsorption-desorption, XRD, Raman spectroscopy, TPR, TPRO, HR-TEM, chemisorption, and NH_3-TPD analyses were carried out. From experimental findings, it is concluded that oxygen capacity and oxygen mobility of magnesium vanadate catalyst served as crucial factors determining the catalytic performance in the oxidative dehydrogenation of n-butane, Pt surface area and acidity of platinum-tin catalysts played key roles in determining the catalytic performance in the direct dehydrogenation of n-butane.

Keywords: Oxidative dehydrogenation, Direct dehydrogenation, n-Butane, n-Butene, 1,3-Butadiene, Magnesium vanadate catalyst, Platinum-tin catalyst

Student Number: 2011-21067

Contents

List of Tables

List of Figures

Chapter 1. Introduction

1.1. n-Butene and 1,3-butadiene

C4 olefins (n-butene and 1,3-butadiene) are important raw materials for synthetic resins, plastics, rubbers, and other petrochemical products. n-Butene is used as alkylate, monomer for polybutene, and monomer for synthetic resins such as low density polyethylene (LDPE) and high density polyethylene (HDPE). 1,3-Butadiene is an important material for manufacturing synthetic rubbers such as acrylonitrile-butadiene-styrene (ABS), polybutadiene rubber (BR), and styrene-butadiene rubber (SBR) (Fig. 1.1) [1-3].

The shale gas revolution has decreased the production of C4 olefins available for conventional chemical processes because of the switch to lighter feedstocks. Furthermore, the demand for C4 olefins has continuously increased due to the development of rubber industry for motor vehicle tires in the developing countries. At present, n-butene and 1,3-butadiene in the petrochemical industry are mainly produced from naphtha cracking process. However, naphtha cracking process operated at relatively high temperature (>800 ^{o}C) involves many problems in both marketing and energy management, because this process produces not only n-butene and 1,3-butadiene but also ethylene, propylene, and isobutene (Fig. 1.2) [4,5].

Dehydrogenation of light paraffins and catalytic conversion of ethanol have been recognized as alternative processes for producing n-butene and 1,3-

butadiene because of the abovementioned disadvantages of naphtha cracking process. Catalytic conversion of ethanol is an industrially well proven process for the production of 1,3-butadiene [6,7]. This process has an advantage in a sense that it uses a renewable resource (ethanol) as a feedstock. Furthermore, investment cost for this process is low. However, this process has some disadvantages such as high operating cost and formation of many by-products. Although dehydrogenation of light paraffins is more energy intensive than ethanol conversion process, the former process is more efficient for selective production of C4 dehydrogenation products [8-10]. In particular, dehydrogenation of n-butane produces large amount of n-butene rather than 1,3-butadiene, which is also of great importance for n-butene application.

Dehydrogenation of n-butane can be operated at lower temperature than naphtha cracking process and is independent of naphtha cracking process in the production of n-butene and 1,3-butadiene. n-Butane, which is used as a reactant in the dehydrogenation reaction, has various advantages such as wide availability, low price, and environmentally friendly nature in its inert state. Therefore, many recent studies have been conducted on the dehydrogenation of n-butane for producing n-butene and 1.3-butadiene in a single unit [11-16].

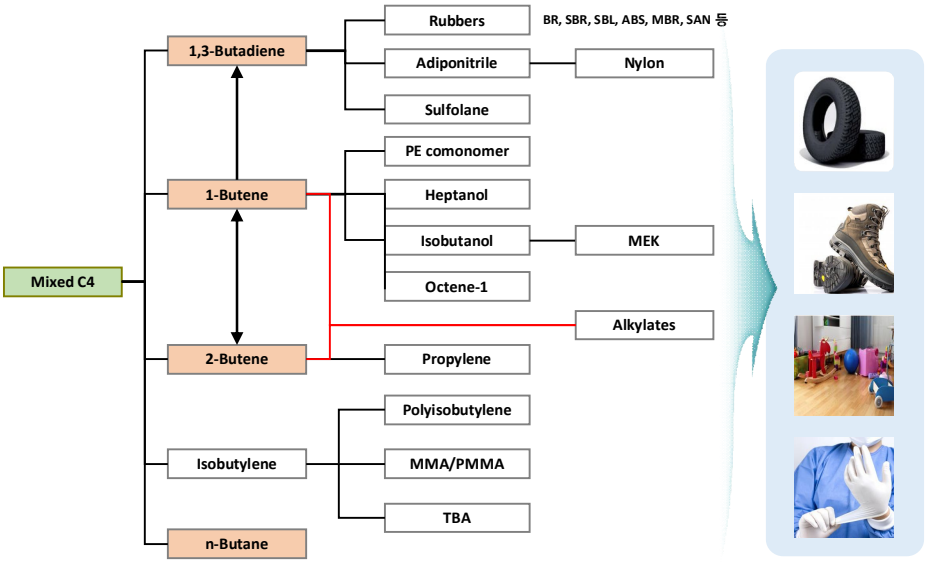

Fig. 1.1. Applications of C4 olefins.

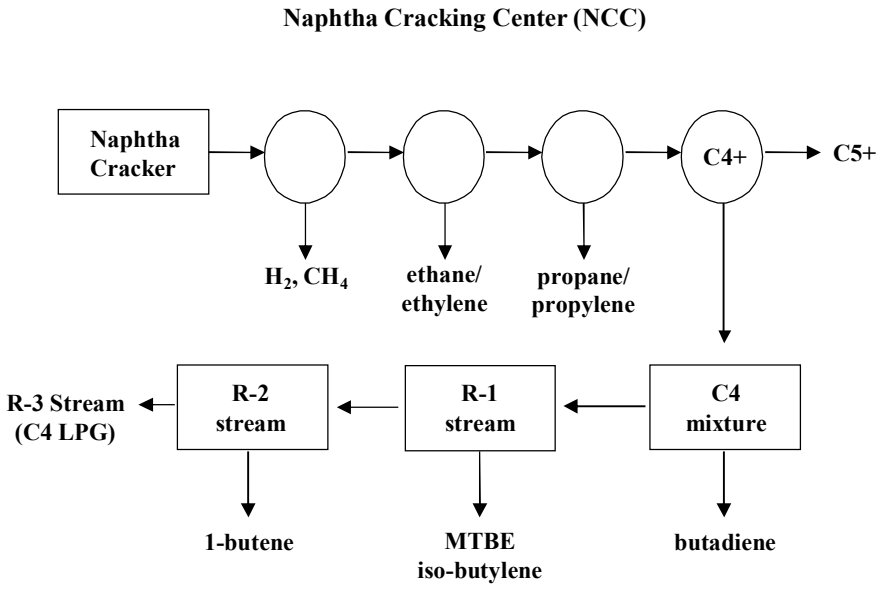

Fig. 1.2. Scheme for naphtha cracking process.

1.2. Dehydrogenation of n-butane

Dehydrogenation of light paraffins has been recognized as an alternative route for the production of light olefins because of wide availability and low price of light paraffin feedstocks. In particular, dehydrogenation of n-butane has attracted much attention as a promising process for producing C4 olefins such as n-butene and 1,3-butadiene. Increasing demand for n-butene and 1,3-butadiene makes this process more economical, because cheap and abundant n-butane is employed as a starting material for producing n-butene and 1,3-butadiene.

There are two methods in the dehydrogenation of n-butane (Fig. 1.3) [17-20]. Direct dehydrogenation of n-butane is an endothermic reaction that requires relatively high temperature to obtain a high yield for n-butene and butadiene. High reaction temperature favors thermal cracking reactions to lower alkanes and coke formation, resulting in a decrease of product yield and catalyst deactivation. The catalyst deactivated by coke formation is required to conduct coke burning in the catalyst regeneration process. Nonetheless, high selectivity and high yield for dehydrogenation products can be obtained in the direct dehydrogenation of n-butane. On the other hand, oxidative dehydrogenation of n-butane using oxygen as a reactant is thermodynamically favorable due to the exothermic nature, the practical application of this process has some problems such as direct combustion of hydrocarbon and formation of CO_x lowing product selectivity. However, this reaction can be attained even at low temperatures and high pressures, bringing enormous

advantages from the economic and process engineering points of view. For these reasons, many studies have been focused on the direct and oxidative dehydrogenation of n-butane for producing n-butene and 1,3-butadiene.

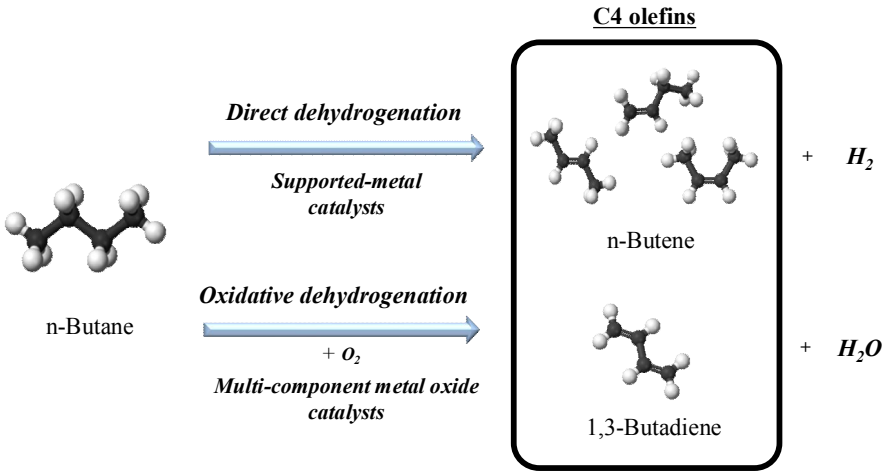

Fig. 1.3. Dehydrogenation of n-butane.

1.3. Catalyst for dehydrogenation of n-butane

1.3.1. Magnesium vanadate catalyst

Various catalysts such as magnesium vanadate [21-25], pyrophosphate [26-28], nickel molybdate [29-31], and ferrite-type [32] catalyst have been investigated for the oxidative dehydrogenation of n-butane. Among these catalysts, magnesium vanadate catalyst is known to be the most efficient catalyst in the oxidative dehydrogenation of n-butane [33-35]. It has been reported that active phase of magnesium vanadate catalyst strongly depends on vanadium content, identity of precursor, or nature of the support [36-38]. It is known that magnesium orthovanadate ($Mg_3(VO_4)_2$) serves as a more efficient and active phase in the oxidative dehydrogenation of n-butane than the other phases such as magnesium pyrovanadate ($Mg_2V_2O_7$) and magnesium metavanadate (MgV_2O_6) [23, 39-41].

Among various $Mg_3(VO_4)_2$ catalysts, $Mg_3(VO_4)_2$/MgO catalyst has been widely studied as an efficient catalyst for the oxidative dehydrogenation of n-butane due to its high catalytic performance in this reaction. However, it was previously reported that the catalytic performance of $Mg_3(VO_4)_2$/MgO catalyst was unstable due to its low oxygen mobility [42,43]. It was expected that low oxygen mobility of $Mg_3(VO_4)_2$/MgO catalyst impeded oxygen make-up during the catalytic reaction, thus, led to a severe catalytic deactivation in the oxidative dehydrogenation of n-butane. To overcome this problem, addition of metal oxides such as TiO_2, Cr_2O_3, SiO_2, and ZrO_2 to $Mg_3(VO_4)_2$

catalyst has been attempted to improve the stability of catalyst. In particular, the addition of ZrO_2 to $Mg_3(VO_4)_2$/MgO catalyst resulted in excellent stability of catalyst by improving oxygen mobility of catalyst. This means that presence of excess MgO in the $Mg_3(VO_4)_2$ catalyst enhances the catalytic performance, while ZrO_2 in the $Mg_3(VO_4)_2$ catalyst acts as a stabilizer [44-46]. This implies that an appropriate amount of each metal oxide is required to improve the catalytic performance in the oxidative dehydrogenation of n-butane.

Many attempts have been made to find major factors determining the catalytic performance in the oxidative dehydrogenation of n-butane. Although fundamental reaction mechanisms have not been clearly elucidated, many researchers agree that the oxidative dehydrogenation of n-butane to n-butene and 1,3-butadiene over magnesium vanadate catalyst follows the reaction mechanism by way of alkyl radical-metal cation intermediate based on the Mars-van Krevelen mechanism [42-44,47,48]. Typical reaction mechanism for the oxidative dehydrogenation of n-butane over magnesium vanadate catalyst is shown in Fig. 1.4. Reaction mechanism for the oxidative dehydrogenation of n-butane by way of alkyl radical-metal cation intermediate consists of five sequential elementary step; (step i) chemisorptions of n-butane and activation of C-H bond, (step ii) abstraction of hydrogen from n-butane to form alkyl radical-metal cation intermediate, (step iii) abstraction of one more hydrogen from alkyl radical-metal cation intermediate to form n-butene, (step iv) desorption of n-butene, and (step v) dissociation of oxygen on the gas phase to make up oxygen vacancy in the catalyst and reoxidation of V^{3+} cation. According to this mechanism, (step i)

chemisorption of n-butane and activation of C-H bond and (step ii) abstraction of hydrogen from n-butane to form alkyl radical-metal cation intermediate are important steps in the oxidative dehydrogenation of n-butane [44,47]. It is known that the rates of these steps are enhanced if cation can readily undergo reduction with two electrons transferred from C-H bonds and if concentration of surface lattice oxygen is high [42,44,47]. This implies that oxygen property (capacity and mobility) of catalyst may play an important role in determining the catalytic performance in the oxidative dehydrogenation of n-butane. Therefore, it is expected that a magnesium vanadate catalyst with high oxygen capacity or mobility will show an excellent catalytic performance in the oxidative dehydrogenation of n-butane.

As mentioned above, it can be inferred that oxygen capacity and mobility of the catalyst play important roles in determining the catalytic performance in the oxidative dehydrogenation of n-butane. Therefore, it can be reasonable to expect that the catalytic performance of magnesium vanadate catalyst would be enhanced, if oxygen capacity and mobility of magnesium vanadate catalyst are promoted by the addition of MgO and ZrO_2.

In this work, a series of X-$Mg_3(VO_4)_2$/MgO-ZrO_2 catalysts with a variation of V content (X = 2.8, 5.6, 8.4, 11.2, 14.0, and 16.8 wt%) and $Mg_3(VO_4)_2$/MgO-ZrO_2 (X) catalysts with different Mg:Zr ratio (X = 16:1, 8:1, 4:1, 2:1, and 1:1) were prepared by a wet impregnation method. Prepared $Mg_3(VO_4)_2$/MgO-ZrO_2 catalysts were then applied to the oxidative dehydrogenation of n-butane to n-butene and 1,3-butadiene. Formation of $Mg_3(VO_4)_2$/MgO-ZrO_2 catalysts was confirmed by XRD, Raman spectroscopy, and ICP-AES analyses. Temperature-programmed reoxidation (TPRO)

experiments were carried out to determine oxygen properties of the catalysts.

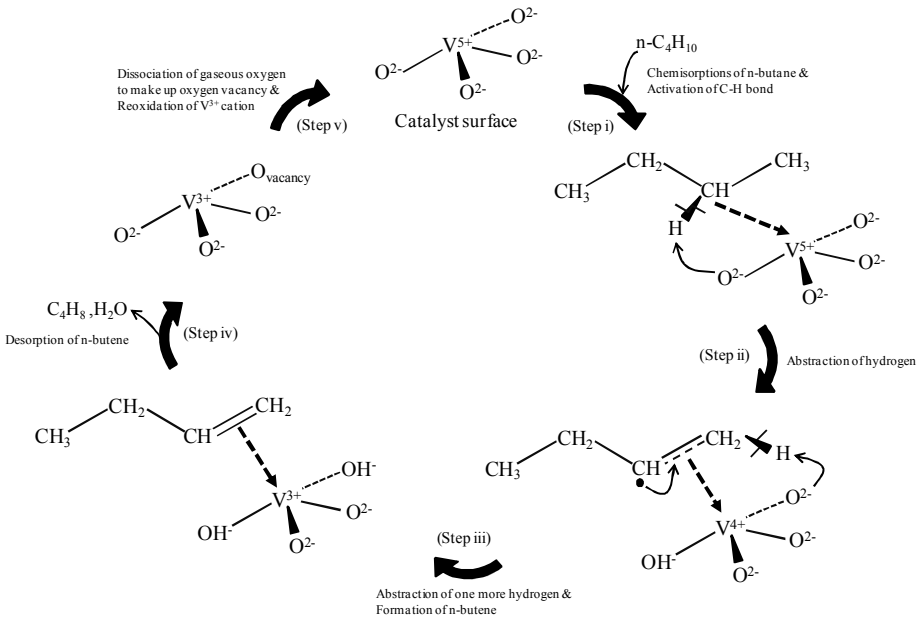

Fig. 1.4. Typical reaction mechanism for the oxidative dehydrogenation of n-butane over magnesium vanadate.

1.3.2. Platinum-tin catalyst

Direct dehydrogenation of n-butane has been investigated over a number of metal catalysts (Cr, Pt, Pd, Ga, and V) supported on various metal oxides (Al_2O_3, SiO_2, $MgAl_2O_4$, and $ZnAl_2O_4$) [49-54]. In 1930s, direct dehydrogenation of n-butane over a chromia-alumina catalyst was practiced for the production of n-butene [49]. The work on direct dehydrogenation of paraffins with noble metal (Pt) catalysts done in the 1960s clearly demonstrated that Pt-based catalysts had high activity and with minimum cracking [49]. In 2000s, vanadium based catalysts have been studied in direct dehydrogenation reaction to substitute for expensive noble metal catalyst [50,51]. Among these catalysts, Pt catalyst supported on Al_2O_3 has been widely employed for dehydrogenation of n-butane. It is known that alumina-supported platinum catalysts are very active but the catalysts are less selective and easily deactivated. The catalytic activity and stability of alumina-supported platinum catalysts can be improved by adding a second metal such as tin [49,55]. The role of second metal is to weaken the platinum-olefin interaction selectively without affecting the platinum-paraffin interaction.

It is generally accepted that platinum and acid property in the alumina-supported platinum catalyst play key roles in the direct dehydrogenation of n-butane [49]. The possible reactions that take place on platinum (Pt) and acid (A) sites in the direct dehydrogenation of n-butane over alumina-supported platinum catalyst, is shown in Fig 1.5. According to this reaction pathway, the main reaction in direct dehydrogenation of n-butane is the formation of n-

butene from n-butane, other reactions include consecutive and side reactions. It has been reported that platinum is an active metal and the high dispersion of platinum is necessary to achieve high selectivity to dehydrogenation relative to undesirable side reactions, such as cracking, isomerization, and polymerization [56]. The typical alumina supports employed have acidic sites that accelerate skeletal isomerization, cracking, and polymerization of olefinic materials, and enhance "coke" formation [57].

Because of the endothermic nature of direct dehydrogenation of n-butane, high reaction temperature is required to obtain high conversion. Under this severe reaction condition, coke formation causing catalyst deactivation is inevitable. To overcome this problem, addition of alkali metal such as Li, Na, and K to Pt-Sn/Al_2O_3 catalyst or modification of preparation method for catalyst has been attempted [52,58]. In particular, the addition of K to Pt-Sn/Al_2O_3 catalyst resulted in high selectivity toward iso-butene in the dehydrogenation of iso-butane by suppressing strong acidity of support [59]. $ZnAl_2O_4$ and $MgAl_2O_4$ have also been used as supports due to their high thermal stabilities and their neutral characteristics to enhance the resistance against catalyst deactivation [60]. However, systematic investigations on the effect of third metal addition or preparation method for catalyst on the catalytic activities of Pt-Sn/Al_2O_3 catalysts in the n-butane dehydrogenation have been rarely reported.

In this work, various platinum-tin catalysts, including Pt/Sn/M/Al_2O_3 (M = Zn, In, Y, Bi, and Ga), a series of Pt/Sn/Zn/Al_2O_3 catalysts with a variation of Zn content (X = 0, 0.25, 0.5, 0.75, 1.0), Pt/Sn/Al_2O_3 (various Al_2O_3 support preparation method), and Pt/Sn/Al_2O_3 (different Al_2O_3 support

calcination temperature), were prepared by a sequential impregnation method for use in the direct dehydrogenation of n-butane to n-butene and 1,3-butadiene. Formation of $Pt/Sn/Al_2O_3$ and $Pt/Sn/M/Al_2O_3$ catalysts was confirmed by XRD and ICP-AES analyses. Nitrogen adsorption-desorption measurements were carried out in order to evaluate textural properties of the catalysts. Chemisorption experiments were conducted to measure the platinum dispersion and platinum surface area of the catalysts. High resolution-transmission electron microscopy analyses were conducted to examine the dispersion of metal species in the catalysts. NH_3-TPD experiments were conducted to determine the acid property of the catalysts.

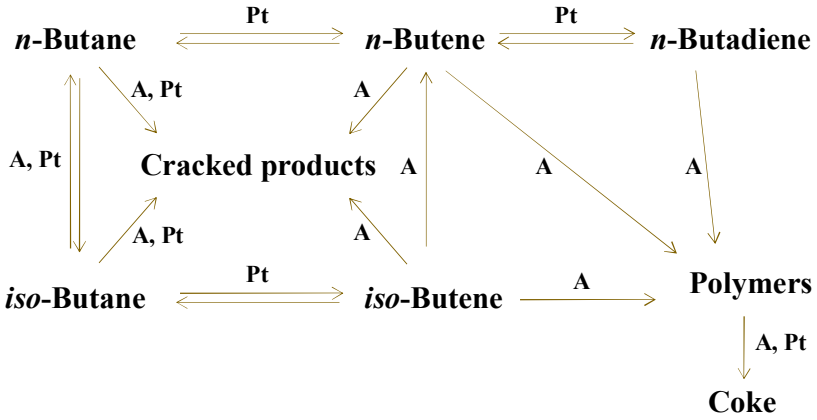

Fig. 1.5. Reaction pathway in the direct dehydrogenation of n-butane over platinum-alumina catalyst.

Chapter 2. Experimental

Part 1 Oxidative dehydrogenation of n-butane to n-butene to 1,3-butadiene

2.1. Preparation of catalysts

2.1.1. X-$Mg_3(VO_4)_2$/MgO-ZrO_2 catalysts

Magnesia-zirconia (MgO-ZrO_2) support was prepared by a sol-gel method, according to the similar method reported in the literatures [61-63]. Known amounts of magnesium nitrate ($Mg(NO_3)_2 \cdot 6H_2O$, Sigma-Aldrich) and zirconium oxynitrate ($ZrO(NO_3)_2 \cdot xH_2O$, Sigma-Aldrich) were dissolved in distilled water. A known amount of citric acid ($C_6H_8O_7$, Sigma-Aldrich) was separately dissolved in distilled water. The citric acid solution was then added into the solution containing magnesium and zirconium precursors. After stirring the mixed solution at 70 ^oC for 3 h, it was evaporated to obtain a gel. The gel was then dried overnight at 170 ^oC. After grinding the dried gel, it was finally calcined at 550 ^oC for 3 h to yield MgO-ZrO_2 support. For the preparation of $Mg_3(VO_4)_2$/MgO-ZrO_2 catalysts with different vanadium content, a known amount of vanadium was impregnated on MgO-ZrO_2 support using an aqueous citric acid solution containing vanadium precursor

(NH_4VO_3, Sigma-Aldrich). The impregnated sample was heated at 70 ^oC, and the resulting solid was dried at 80 ^oC overnight. The dried product was finally calcined at 550 ^oC for 3 h to yield $Mg_3(VO_4)_2/MgO\text{-}ZrO_2$ catalysts. The prepared $Mg_3(VO_4)_2/MgO\text{-}ZrO_2$ catalysts were denoted as X-$Mg_3(VO_4)_2/MgO\text{-}ZrO_2$ (X = 6.6, 9.9, 12.8, 15.2, and 19.1), where X represented vanadium content (wt%) in the catalyst.

2.1.2. $Mg_3(VO_4)_2/MgO\text{-}ZrO_2$ (X) catalysts

A series of $MgO\text{-}ZrO_2$ (X) supports with different Mg:Zr ratios (X = 16:1, 8:1, 4:1, 2:1, and 1:1) were prepared by a sol-gel method, according to the similar method reported in the literatures [61-63]. Known amounts of magnesium nitrate ($Mg(NO_3)_2 \cdot 6H_2O$, Sigma-Aldrich) and zirconium oxynitrate ($ZrO(NO_3)_2 \cdot xH_2O$, Sigma-Aldrich) were dissolved in distilled water. A known amount of citric acid ($C_6H_8O_7$, Sigma-Aldrich) was separately dissolved in distilled water. The citric acid solution was then added into the solution containing magnesium and zirconium precursors. After stirring the mixed solution at 70 ^oC for 3 h, it was evaporated to obtain a gel. The gel was then dried overnight at 170 ^oC. After grinding the dried gel, it was finally calcined at 550 ^oC for 3 h to yield $MgO\text{-}ZrO_2$ support. For the preparation of $Mg_3(VO_4)_2/MgO\text{-}ZrO_2$ (X) catalysts with different Mg:Zr ratios of support (X = 16:1, 8:1, 4:1, 2:1, and 1:1), vanadium was impregnated on the prepared $MgO\text{-}ZrO_2$ support using an aqueous oxalic acid solution containing vanadium precursor (NH_4VO_3, Sigma-Aldrich). The impregnated sample was

heated at 70 ^{o}C, and the resulting solid was dried at 80 ^{o}C overnight. The dried product was finally calcined at 550 ^{o}C for 3 h in the presence of air to yield $Mg_3(VO_4)_2$/MgO-ZrO_2 (X) catalysts. Vanadium contents in all the $Mg_3(VO_4)_2$/MgO-ZrO_2 (X) catalysts were fixed at 12.8 wt%.

2.2. Characterization

2.2.1. Formation of $Mg_3(VO_4)_2$/MgO-ZrO_2 catalysts

Crystalline phases of $Mg_3(VO_4)_2$/MgO-ZrO_2 catalysts were investigated by XRD measurements (Rigaku, D-MAX2500-PC) using Cu-Kα radiation (λ = 1.541 Å) operated at 50 kV and 100 mA. Raman spectra of the prepared catalysts were obtained with a Raman spectrometer (HORIABA Jobin Yvon T64000) using radiation of 514.5 nm from an argon ion. Vanadium contents (wt%) and atomic ratios in the catalysts were determined by ICP-AES (Shimadz, ICP-1000IV) analyses. Surface areas of the catalysts were measured using a BET apparatus (Micromeritics, ASAP 2010).

2.2.2. Oxygen properties of $Mg_3(VO_4)_2$/MgO-ZrO_2 catalysts

In order to determine the oxygen property of the catalysts, TPRO experiments were carried out. For the TPRO experiment, each catalyst was reduced by carrying out the oxidative dehydrogenation of n-butane at 500 ^oC for 1 h in the absence of oxygen feed in order for the catalyst to consume lattice oxygen. After the reduced catalyst was placed in a conventional TPRO apparatus, a mixed stream of oxygen (10%) and helium (90%) was introduced to the catalyst sample. Furnace temperature was raised from room temperature to 900 ^oC at a heating rate of 5 ^oC/min. The amount of oxygen consumed was measured using a TCD (thermal conductivity detector).

2.3. Oxidative dehydrogenation of n-butane

Oxidative dehydrogenation of n-butane to n-butene and 1,3- butadiene was carried out in a continuous flow fixed-bed reactor in the presence of oxygen. Feed composition was fixed at n-butane: oxygen: nitrogen = 4:8:88. Catalytic reaction was carried out at 500 ^{o}C. Gas hourly space velocity (GHSV) was fixed at 2000 h^{-1} on the basis of n-butane. Reaction products were periodically sampled and analyzed with gas chromatographs. Conversion of n-butane, selectivity for total dehydrogenation products (TDP, n-butene and 1,3-butadiene), and selectivity for 1,3-butadiene were calculated on the basis of carbon balance as follows. Yield for TDP was calculated by multiplying conversion of n-butane and selectivity for TDP.

$$\text{Conversion of n-butane} = \frac{\text{moles of n-butane reacted}}{\text{moles of n-butane supplied}}$$

$$\text{Selectivity for TDP} = \frac{\text{moles of n-butenes formed + moles of 1,3-butadiene formed}}{\text{moles of n-butane reacted}}$$

Yield for TDP = (Conversion of n-butane) x (Selectivity for TDP)

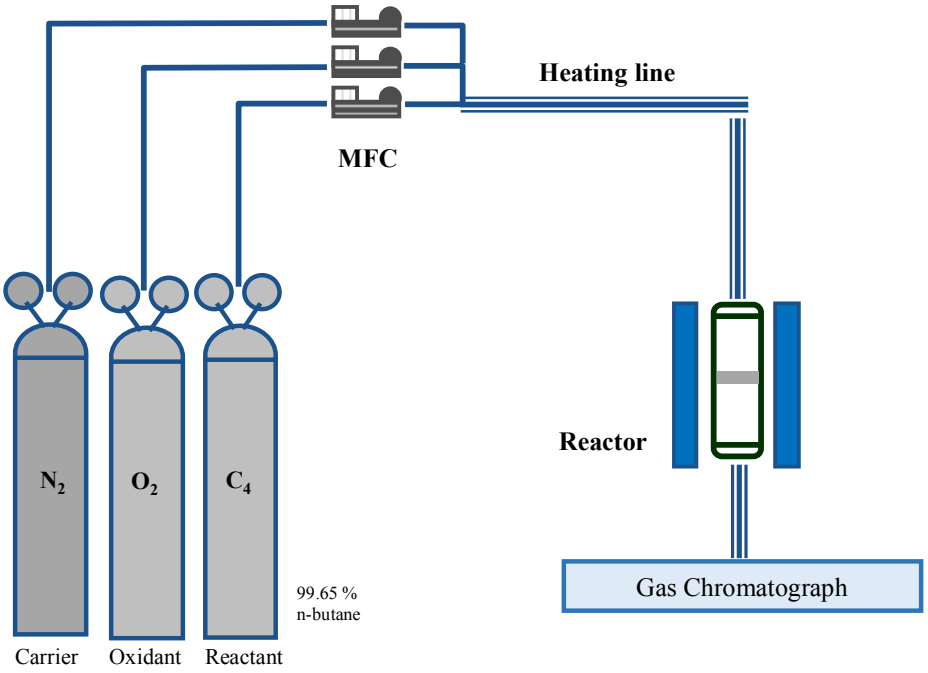

Fig. 2.1. Reaction system for oxidative dehydrogenation of n-butane.

Part 2 Direct dehydrogenation of n-butane to n-butene to 1,3-butadiene

2.4. Preparation of catalysts

2.4.1. Pt/Sn/M/Al_2O_3 catalysts

A series of Pt/Sn/M/Al_2O catalysts with different third metal (M = Zn, In, Y, Bi, and Ga) were prepared by a sequential impregnation method [64,65]. Commercially available Al_2O_3 (Alfa Aesar, S_{BET}: 220 m^2/g) was used as a support. M/Al_2O_3 catalyst was prepared by an impregnation method using an excess aqueous solution of third metal (M) precursor (metal nitrate hydrate, Sigma-Aldrich). After impregnation, it was dried at 80 °C overnight and calcined at 600 °C in air for 4 h. Sn precursor (Tin (II) chloride dihydrate, Sigma-Aldrich) was then impregnated on the prepared M/Al_2O_3 using hydrochloric acid. It was dried at 80 °C overnight and calcined at 600 °C in air for 4 h. For the preparation of Pt/Sn/M/Al_2O_3 catalyst, Pt precursor (Chloroplatinic acid hexahydrate, Sigma-Aldrich) was impregnated on the prepared Sn/M/Al_2O_3 catalyst, followed by drying at 80 °C overnight and calcination at 550 °C in air for 4 h. The contents of Pt, Sn, and third metal in the Pt/Sn/M/Al_2O_3 catalysts were fixed at 1 wt.%, 1 wt.%, and 0.5 wt.%, respectively. For reference, Pt/Sn/Al_2O_3 catalyst was also prepared with the above-mentioned procedures in the absence of third metal.

2.4.2. Pt/Sn/XZn/Al_2O_3 catalysts

A series of Pt/Sn/XZn/Al_2O_3 catalysts with different Zn content (X, wt%) were prepared by a sequential impregnation method [64,65]. A commercially available Al_2O_3 (Alfa Aesar) was used as a support. Zn precursor (Zinc nitrate hexahydrate, Sigma-Aldrich) was impregnated on Al_2O_3 support using an excess aqueous solution. The impregnated sample was dried at 80 ^oC overnight and calcined at 600 ^oC in air for 4 h. For the preparation of Sn/Zn/Al_2O_3 catalyst, Sn precursor (Tin(II) chloride dihydrate, Sigma-Aldrich) was impregnated on Zn/Al_2O_3 catalyst using hydrochloric acid solution. The resultant was dried at 80 ^oC overnight and calcined at 600 ^oC in air for 4 h. Pt precursor (Chloroplatinic acid hexahydrate, Sigma-Aldrich) was finally impregnated on Sn/Zn/Al_2O_3 catalyst, followed by drying at 80 ^oC overnight and calcination at 600 ^oC in air for 4 h. Pt and Sn contents in the Pt/Sn/Zn/Al_2O_3 catalysts were fixed at 1 wt%, respectively. The prepared Pt/Sn/Zn/Al_2O_3 catalysts were denoted as Pt/Sn/XZn/Al_2O_3 (X = 0, 0.25, 0.5, 0.75, and 1.0), where X represented Zn content (wt%) in the catalysts.

2.4.3. Pt/Sn/Al_2O_3 (X) catalysts prepared by various preparation methods

Al_2O_3 supports were prepared by precipitation method, alkoxide-based sol-gel method, and epoxide-driven sol-gel method, according to the similar

methods reported in the literatures [66-68]. Typical preparation procedures for Al_2O_3 support by precipitation method are as follows. A known amount of aluminum precursor (Aluminum nitrate nonahydrate, Sigma-Aldrich) was dissolved in distilled water. The NH_4OH and aluminum precursor solution were then slowly added into distilled water under vigorous stirring. The pH of the mixed solution was adjusted to 9 by controlling the amount of NH_4OH for precipitation. After the resultant was stirred vigorously at room temperature for 3 h, it was aged overnight at room temperature. The precipitate was separated, and subsequently, it was washed and dried overnight at 80 ^oC. The dried product was finally calcined at 600 ^oC for 4 h to yield Al_2O_3 support (denoted as Al_2O_3 (P)). For the preparation of Al_2O_3 support by an alkoxide-based sol-gel method, a known amount of aluminum precursor (Aluminum tri-sec-butoxide, Sigma-Aldrich) was dissolved in ethanol at 80 ^oC with vigorous stirring. Small amounts of distilled water and nitric acid, which had been diluted with ethanol, were slowly added into the solution of aluminum precursor for partial hydrolysis of aluminum precursor. After maintaining the resulting solution at 80 ^oC for a few minutes, a clear sol was obtained. After cooling the alumina composite sol to room temperature, a monolithic gel was obtained by adding an appropriate amount of water diluted with ethanol into the sol. The gel was aged for 2 days, and then it was dried at 80 ^oC for 5 day. The resulting powder was finally calcined at 600 ^oC for 4 h to yield a Al_2O_3 support (denoted as Al_2O_3 (AS)). For the preparation of Al_2O_3 support by an epoxide-driven sol-gel method, a known amount of aluminum precursor (Aluminum nitrate nonahydrate, Sigma-Aldrich) was dissolved in ethanol with vigorous stirring for hydration of Al^{3+} ions. Propylene oxide as a gelation

agent was then added into the aluminum precursor solution to form hydroxyl group on the hydrated ions and to induce polycondensation reaction between Al^{3+} ions. Molar ratio of aluminum precursor:propylene oxide was fixed at 1:10. After maintaining the resulting solution for a few minutes, a white opaque alumina gel was obtained. The gel was aged for 2 days, and then it was dried at 80 ^{o}C. The resulting powder was calcined at 600 ^{o}C for 4 h to yield Al_2O_3 support (denoted as Al_2O_3 (ES)). For comparison, a commercially available Al_2O_3 (Alfa Aesar) was used as a support (denoted as Al_2O_3 (C)).

For the preparation of Sn/Al_2O_3, Sn precursor (Tin (II) chloride dehydrate, Sigma-Aldrich) was impregnated on Al_2O_3 (C, P, AS, and ES) using hydrochloric acid solution. The resultant was dried at 80 ^{o}C overnight and calcined at 600 ^{o}C in air for 4 h. $Pt/Sn/Al_2O_3$ (X) were prepared by impregnating known amounts of a platinum precursor (Chloroplatinic acid hexahydrate, Sigma-Aldrich) on Sn/Al_2O_3 (C, P, AS, and ES), followed by drying at 80 ^{o}C overnight and calcination at 600 ^{o}C in air for 4 h. Pt and Sn contents in the $Pt/Sn/Al_2O_3$ (X) catalysts were fixed at 1 wt% and 1 wt%, respectively.

2.4.4. $Pt/Sn/Al_2O_3$-X prepared by an epoxide-driven sol-gel method and a sequential impregnation method

Al_2O_3 supports were prepared by a sol-gel method, according to the similar methods reported in the literatures [68-70]. A known amount of aluminum precursor (Aluminum nitrate nonahydrate, Sigma-Aldrich) was

dissolved in ethanol with vigorous stirring for hydration of Al^{3+} ions. Propylene oxide as a gelation agent was then added into the aluminum precursor solution to form hydroxyl group on the hydrated ions and to induce polycondensation reaction between Al^{3+} ions. Molar ratio of aluminum precursor:propylene oxide was fixed at 1:10. After maintaining the resulting solution for a few minutes, a white opaque alumina gel was obtained. The gel was aged for 2 days, and then it was dried at 80 ^{o}C. The resulting powder was calcined at various temperatures (600, 700, 800, 900, 1000, and 1100 ^{o}C) for 4 h to yield Al_2O_3 support.

For the preparation of $Pt/Sn/Al_2O_3$ catalyst, Sn precursor (Tin (II) chloride dihydrate, Sigma-Aldrich) was impregnated on the Al_2O_3 support using hydrochloric acid solution. It was dried at 80 ^{o}C overnight and calcined at 600 ^{o}C in air for 4 h. Pt precursor (Chloroplatinic acid hexahydrate, Sigma-Aldrich) was then impregnated on the Sn/Al_2O_3 sample, followed by drying at 80 °C overnight and calcination at 550 °C in air for 4 h. The contents of Pt and Sn in the $Pt/Sn/Al_2O_3$ catalysts were fixed at 1 wt% and 1 wt%, respectively. The prepared $Pt/Sn/Al_2O_3$ catalysts were denoted as $Pt/Sn/Al_2O_3$-X (X = 600, 700, 800, 900, 1000, and 1100), where X represented the calcination temperature of alumina in Celsius degree.

2.5. Characterization

2.5.1. Crystalline structure

X-ray diffraction (XRD) analyses were performed using a D-Max2500-PC (Rigaku) diffractometer operated at 50 kV and 150 mA to examine crystalline characteristics of reduced catalysts. Diffraction data were collected under Cu-Kα radiation (λ = 1.541 Å) with a scan rate of 10 ^{o}/min. For the XRD of reduced catalysts, 0.1 g of each catalysts was reduced with a mixed stream of H_2 (300 ml/h) and N_2 (300 ml/h) at 570 ^{o}C for 3 h.

2.5.2. Physicochemical properties

Chemical compositions of catalysts were determined by ICP-AES (ICP-1000IV, Shimadzu) analyses. Nitrogen adsorption-desorption isotherms of catalysts were obtained with a BELSORP-mini II (BEL Japan) instrument, and pore size distribution of catalysts were determined by the Barret-Joyner-Hallender (BJH) method applied to the desorption branch of nitrogen isotherms. Before the measurements, the catalysts were degassed at 150 ^{o}C for 6 h by rotary vacuum pump for removal of moisture and other adsorbed gases on the surface of samples.

2.5.3. Reduction behavior

In order to examine the reduction behavior of metal species of catalysts, temperature-programmed reduction (TPR) measurements were carried out in a conventional flow system with a moisture trap connected to a thermal conductivity detector (TCD) at temperatures ranging from room temperature to 700 ^{o}C with a ramping rate of 5 ^{o}C/min. For the TPR measurements, a mixed stream of H_2 (2 ml/min) and N_2 (20 ml/min) was used for 0.15 g of catalyst sample.

2.5.4. Morphological feature

High resolution-transmission electron microscopy (HR-TEM) analyses (Jeol, JEM-3000F) were conducted to examine morphological features of metal species in catalysts. For the TEM analyses of reduced catalysts, ex-situ reduction with a mixed stream of H_2 (300 ml/h) and N_2 (300 ml/h) was preliminarily conducted before the analyses.

2.5.5. Chemisorption studies

Hydrogen chemisorption experiments (BELCAT-B, BEL Japan) were conducted to measure Pt dispersion and Pt surface area of the catalysts. 50 mg of each catalyst was preliminarily reduced at 570 ^{o}C for 3 h, and it was then purged with argon (50 ml/min) at 570 ^{o}C for 10 min and cooled to 50 ^{o}C. The

amount of hydrogen uptake was measured by periodically injecting diluted hydrogen gas (5% hydrogen and 95% argon) into the reduced catalyst. Pt dispersion and Pt surface area were calculated by assuming that one hydrogen atom occupies one surface platinum atom.

CO chemisorption experiments (BELCAT-B, BEL Japan) were conducted to measure the platinum dispersion and platinum surface area of the catalysts. Prior to the chemisorption measurements, 50 mg of each catalyst was reduced with a mixed stream of hydrogen (2.5 ml/min) and argon (47.5 ml/min) at 570 °C for 3 h, and subsequently, it was purged with pure helium (50 ml/min) at 570 °C for 10 min and cooled to 50 °C. The amount of carbon monoxide uptake was measured by periodically injecting diluted carbon monoxide gas (5% carbon monoxide and 95% helium) into the reduced catalyst using an on-line sampling valve. Platinum dispersion and platinum surface area were calculated by assuming that one carbon monoxide atom occupies one surface platinum atom.

2.5.6. Acid properties

NH_3-TPD experiments were conducted to determine the acid property of the catalysts (BELCAT-B, BEL Japan). Each catalyst (50 mg) was charged in a quartz cell and it was reduced at 570 ^oC for 3 h with 5% hydrogen/argon flow (50 ml/min). After cooling the cell to 50 ^oC, ammonia (50 ml/min) was introduced into the reactor at 50 ^oC for 30 min to saturate acid sites of the catalyst. Physisorbed ammonia was removed at 100 ^oC for 1 h under a flow of

helium (50 ml/min). After cooling the sample, furnace temperature was increased from 50 to 600 ^{o}C at a heating rate of 5 ^{o}C/min under a flow of helium (30 ml/min). The desorbed ammonia was detected using a TCD.

2.6. Direct dehydrogenation of n-butane

Direct dehydrogenation of n-butane to n-butenes and 1,3-butadiene was carried out in a continuous flow fixed-bed reactor at 550 ^{o}C under atmosphere pressure. Each catalyst was preliminarily reduced with a mixed stream of H_2 and N_2 at 570 ^{o}C for 3 h. For the reaction, n-butane was continuously supplied into the reactor with nitrogen carrier. Feed composition was fixed at n-butane:(hydrogen):nitrogen = 1:(1):1. Reaction products were periodically sampled and analyzed using a gas chromatograph (Varian CP-3380) equipped with a GS-alumina column and a flame ionization detector (FID). Conversion of n-butane and selectivity for total dehydrogenation products (TDP, n-butenes and 1,3-butadiene) were calculated on the basis of carbon balance as follows. Yield for TDP was calculated by multiplying conversion of n-butane and selectivity for TDP.

$$\text{Conversion of n-butane} = \frac{\text{moles of n-butane reacted}}{\text{moles of n-butane supplied}}$$

$$\text{Selectivity for TDP} = \frac{\text{moles of n-butenes formed + moles of 1,3-butadiene formed}}{\text{moles of n-butane reacted}}$$

Yield for TDP = (Conversion of n-butane) x (Selectivity for TDP)

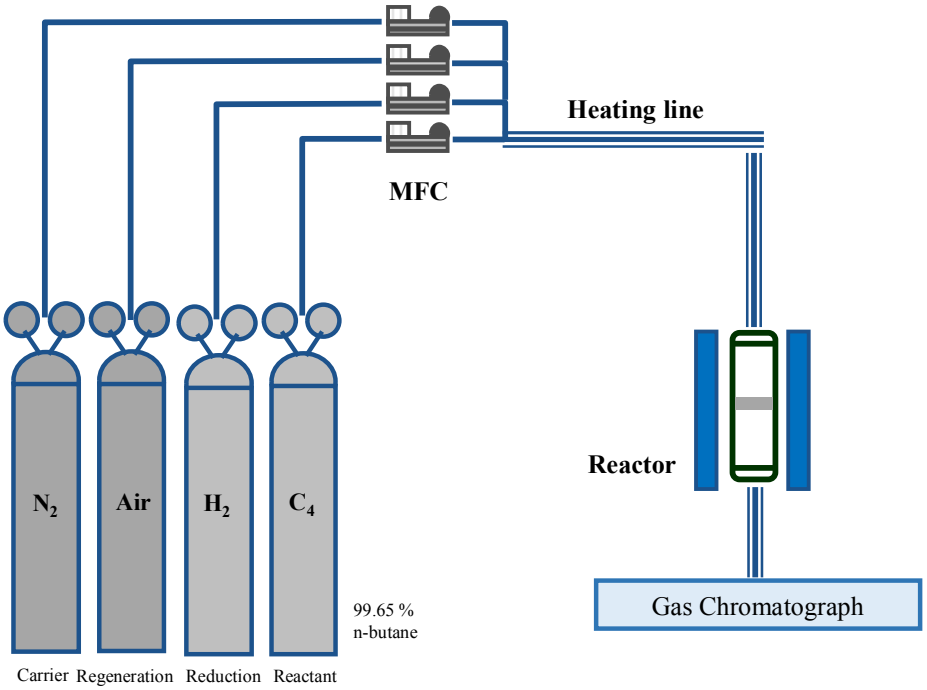

Fig. 2.2. Reaction system for direct dehydrogenation of n-butane.

Table 2.1

Direct dehydrogenation reaction conditions

	Catalyst Weight (g)	Feed ratio (C_4:H_2:N_2)	GHSV on n-butane (cc/h·g-cat.)
Section 3.3	0.25	1:0:1	600
Section 3.4	0.25	1:0:1	600
Section 3.5	0.1	1:1:1	3000
Section 3.6	0.1	1:1:1	3000

Chapter 3. Results and Discussion

Part 1 Oxidative dehydrogenation of n-butane to n-butene and 1,3-butadiene

3.1. Characterization and catalytic performance of X-$Mg_3(VO_4)_2$/MgO-ZrO_2 catalysts

3.1.1. Formation of X-$Mg_3(VO_4)_2$/MgO-ZrO_2 catalysts

The formation of X-$Mg_3(VO_4)_2$/MgO-ZrO_2 catalysts was confirmed by XRD, Raman spectroscopy, and ICP-AES measurements. XRD patterns of X-$Mg_3(VO_4)_2$/MgO-ZrO_2 are shown in Fig. 3.1. Crystalline phases of MgO and ZrO_2 were identified by the characteristic diffraction peaks using JCPDS (Joint Committee on Powder Diffraction Standards). All the catalysts exhibited the mixed peaks of MgO and ZrO_2 phases without any diffraction peaks for $Mg_3(VO_4)_2$. Characteristic XRD peaks for $Mg_3(VO_4)_2$ were not detected due to less crystallized or more finely dispersed $Mg_3(VO_4)_2$ in the catalysts. This result was well consistent with the previous works [42,71] reporting that $Mg_3(VO_4)_2$ diffraction peaks were not detected in the XRD patterns due to its fine dispersion.

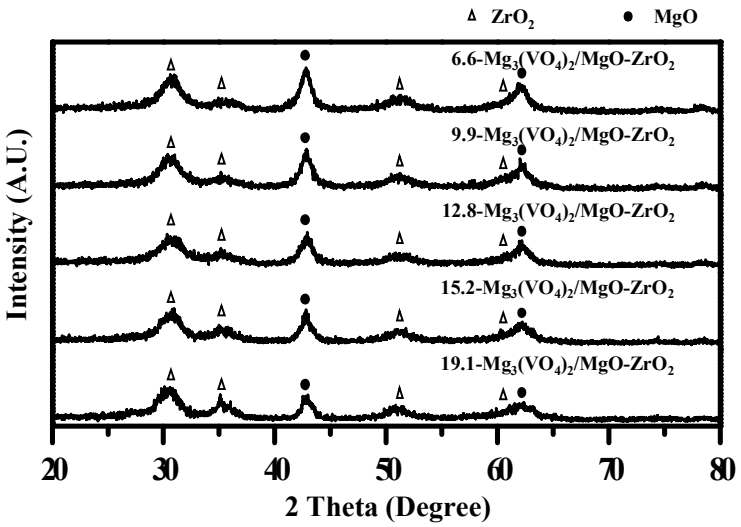

Fig. 3.1. XRD patterns of X-$Mg_3(VO_4)_2$/MgO-ZrO_2 (X = 6.6, 9.9, 12.8, 15.2, and 19.1) catalysts.

Raman spectroscopy measurement was also conducted to confirm the formation of $Mg_3(VO_4)_2$ phase in the X-$Mg_3(VO_4)_2$/MgO-ZrO_2 catalysts. Fig. 3.2 shows the Raman spectra of X-$Mg_3(VO_4)_2$/MgO-ZrO_2 catalysts. For reference, Raman spectra of pure magnesium vanadate ($Mg_3(VO_4)_2$, $Mg_2V_2O_7$, and MgV_2O_6) and vanadium pentoxide (V_2O_5) are also presented in Fig. 3.2. The main characteristic Raman band of X-$Mg_3(VO_4)_2$/MgO-ZrO_2 catalysts appeared at 862 cm^{-1}, which was assigned to isolated VO_4 in $Mg_3(VO_4)_2$ phase [37,38,72,73]. The Raman band position of X-$Mg_3(VO_4)_2$/MgO-ZrO_2 catalysts was identical to that of pure $Mg_3(VO_4)_2$. Furthermore, peak intensity increased with increasing vanadium content in the X-$Mg_3(VO_4)_2$/MgO-ZrO_2 catalysts. These results indicate that $Mg_3(VO_4)_2$ phase was successfully formed in the catalysts. XRD patterns (Fig. 3.1) and Raman spectra (Fig. 3.2) were well consistent with those reported in the previous works [37,38,42,71-73], indicating successful formation of X-$Mg_3(VO_4)_2$/MgO-ZrO_2 catalysts.

Vanadium contents and atomic ratios in the prepared X-$Mg_3(VO_4)_2$/MgO-ZrO_2 catalysts determined by ICP-AES analyses are summarized in Table 3.1. Vanadium contents in the X-$Mg_3(VO_4)_2$/MgO-ZrO_2 catalysts increased with increasing designed values, and atomic ratios were in good agreement with the theoretical values (Mg:Zr = 4:1). This result also supports that all the X-$Mg_3(VO_4)_2$/MgO-ZrO_2 catalysts were successfully prepared in this work. BET surface areas of X-$Mg_3(VO_4)_2$/MgO-ZrO_2 catalysts are also listed in Table 3.1. BET surface areas of X-$Mg_3(VO_4)_2$/MgO-ZrO_2 catalysts showed a volcano-shaped trend with respect to vanadium content in the catalysts.

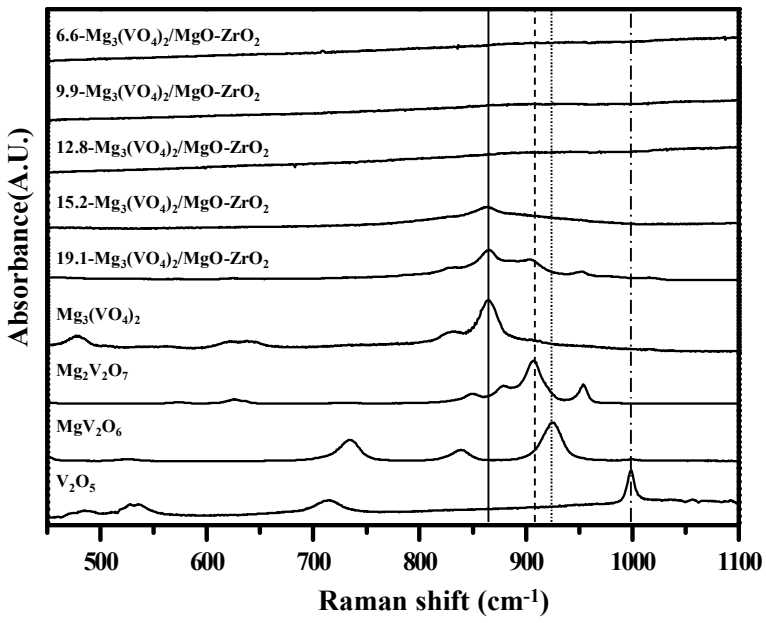

Fig. 3.2. Raman spectra of X-$Mg_3(VO_4)_2$/MgO-ZrO_2 (X = 6.6, 9.9, 12.8, 15.2, and 19.1) catalysts, $Mg_3(VO_4)_2$, $Mg_2V_2O_7$, MgV_2O_6, and V_2O_5.

Table 3.1

V contents, Mg:V atomic ratios, Mg:Zr atomic ratios, and BET surface areas of X-$Mg_3(VO_4)_2$/MgO-ZrO_2 catalysts

Catalyst	V content (wt%)	Mg:V	Mg:Zr	BET surface area (m^2/g)
6.6- $Mg_3(VO_4)_2$/MgO-ZrO_2	6.6	19.0:2	3.9:1 (4:1)[a]	124
9.9- $Mg_3(VO_4)_2$/MgO-ZrO_2	9.9	12.2:2	4.3:1 (4:1)[a]	138
12.8- $Mg_3(VO_4)_2$/MgO-ZrO_2	12.8	8.7:2	4.1:1 (4:1)[a]	136
15.2- $Mg_3(VO_4)_2$/MgO-ZrO_2	15.2	6.9:2	4.1:1 (4:1)[a]	89
19.1- $Mg_3(VO_4)_2$/MgO-ZrO_2	19.1	5.0:2	4.2:1 (4:1)[a]	62

[a] Designed value of Mg:Zr ratio in the X-$Mg_3(VO_4)_2$/MgO-ZrO_2 catalysts.

3.1.2. Catalytic performance of X-$Mg_3(VO_4)_2$/MgO-ZrO_2 catalysts

Fig. 3.3 shows the catalytic performance of X-$Mg_3(VO_4)_2$/MgO-ZrO_2 catalysts in the oxidative dehydrogenation of n-butane at 500 ^oC. Catalytic performance of X-$Mg_3(VO_4)_2$/MgO-ZrO_2 catalysts was strongly dependent on vanadium content. It is noteworthy that 15.2-$Mg_3(VO_4)_2$/MgO-ZrO_2 catalyst showed a slight catalyst deactivation and 19.1-$Mg_3(VO_4)_2$/MgO-ZrO_2 catalyst experienced a severe catalyst deactivation. This indicates that 15.2-$Mg_3(VO_4)_2$/MgO-ZrO_2 and 19.1-$Mg_3(VO_4)_2$/MgO-ZrO_2 catalysts can not serve as an efficient catalyst in the oxidative dehydrogenation of n-butane. On the other hand, 6.6-$Mg_3(VO_4)_2$/MgO-ZrO_2, 9.9-$Mg_3(VO_4)_2$/MgO-ZrO_2, and 12.8-$Mg_3(VO_4)_2$/MgO-ZrO_2 catalysts exhibited a stable catalytic performance during the whole reaction time. Yield for TDP after 1 h-reaction decreased in the order of 12.8-$Mg_3(VO_4)_2$/MgO-ZrO_2 > 9.9-$Mg_3(VO_4)_2$/MgO-ZrO_2 > 6.6-$Mg_3(VO_4)_2$/MgO-ZrO_2 > 15.2-$Mg_3(VO_4)_2$/MgO-ZrO_2 > 19.1-$Mg_3(VO_4)_2$/MgO-ZrO_2. It should be noted that the catalytic performance showed a volcano-shaped trend with respect to vanadium content. Among the catalysts tested, 12.8-$Mg_3(VO_4)_2$/MgO-ZrO_2 catalyst exhibited the best catalytic performance without catalyst deactivation in the oxidative dehydrogenation of n-butane.

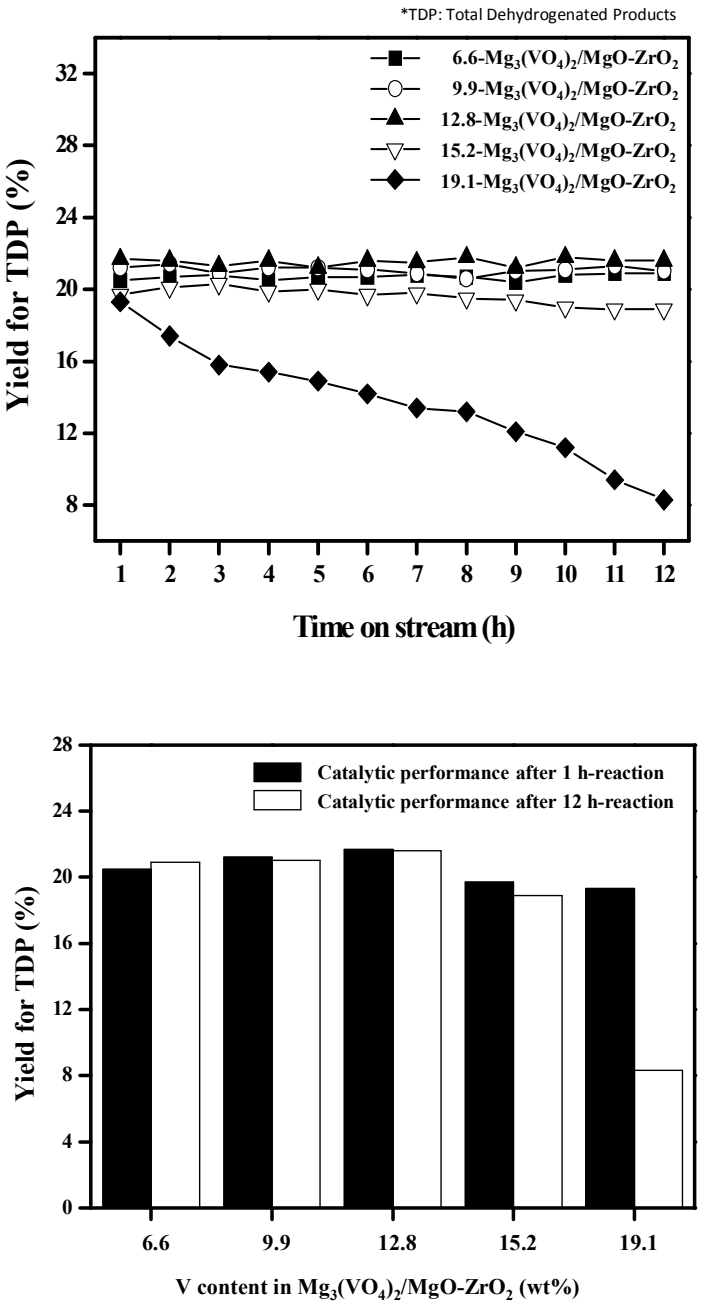

Fig. 3.3. Catalytic performance of X-$Mg_3(VO_4)_2$/MgO-ZrO_2 catalysts.

3.1.3. Effect of V content on the catalytic performance of X-$Mg_3(VO_4)_2$/MgO-ZrO_2 catalysts

In order to elucidate the effect of vanadium content of X-$Mg_3(VO_4)_2$/MgO-ZrO_2 catalysts on the catalytic performance in the oxidative dehydrogenation of n-butane, TPRO measurements were carried out with an aim of determining the oxygen property of the catalysts. According to Mars-van Krevelen mechanism, lattice oxygen in the catalyst directly reacts with n-butane, and in turn, gaseous oxygen makes up oxygen vacancy in the catalyst [42-48]. This means that oxygen mobility of the catalyst may be closely related to the regeneration of the catalyst during the oxidative dehydrogenation of n-butane. Therefore, it is inferred that the catalytic performance of X-$Mg_3(VO_4)_2$/MgO-ZrO_2 would be unstable if oxygen mobility is low.

Fig. 3.4 shows the TPRO profiles of X-$Mg_3(VO_4)_2$/MgO-ZrO_2 catalysts. TPRO peak temperature and TPRO peak area reflect oxygen mobility and oxygen capacity, respectively [74,75]. As shown in Fig. 3.4, oxygen mobility (TPRO peak temperature) of X-$Mg_3(VO_4)_2$/MgO-ZrO_2 catalysts was significantly different. TPRO peak temperature of X-$Mg_3(VO_4)_2$/MgO-ZrO_2 (X = 15.2 and 19.1) catalysts was much higher than that of the other X-$Mg_3(VO_4)_2$/MgO-ZrO_2 (X = 6.6, 9.9, and 12.8) catalysts, indicating that lattice oxygen of X-$Mg_3(VO_{42}$/MgO-ZrO_2 (X = 15.2 and 19.1) catalysts was less mobile than that of the other X-$Mg_3(VO_4)_2$/MgO-ZrO_2 (X = 6.6, 9.9, and 12.8) catalysts. In the oxidative dehydrogenation of n-butane over X-

$Mg_3(VO_4)_2$/MgO-ZrO_2 catalysts (Fig. 3.3), 15.2-$Mg_3(VO_4)_2$/MgO-ZrO_2 catalyst showed a slight catalyst deactivation and 19.1-$Mg_3(VO_4)_2$/MgO-ZrO_2 catalyst experienced a severe catalyst deactivation, while the other X-$Mg_3(VO_4)_2$/MgO-ZrO_2 (X = 6.6, 9.9, and 12.8) catalysts exhibited a stable catalytic performance without catalyst deactivation. Thus, it is believed that the stable catalytic performance of X-$Mg_3(VO_4)_2$/MgO-ZrO_2 (X = 6.6, 9.9, and 12.8) catalysts was attributed to their sufficient oxygen mobility, while X-$Mg_3(VO4_)_2$/MgO-ZrO_2 (X = 15.2 and 19.1) catalysts with low oxygen mobility suffered from a catalyst deactivation. In particular, 19.1-$Mg_3(VO_4)_2$/MgO-ZrO_2 catalyst with the lowest oxygen mobility experienced a severe catalyst deactivation. These results were well consistent with the previous works reporting that oxygen mobility of the catalyst was closely related to the regeneration of the catalyst during the oxidative dehydrogenation of n-butane [74,75].

It was observed that oxygen capacity (TPRO peak area) of the catalyst was much different depending on vanadium content of the catalyst, as shown in Fig. 3.4. As mentioned earlier, oxidative dehydrogenation of n-butane follows the Mars-van Krevelen mechanism. Therefore, it can be inferred that the catalytic performance of X-$Mg_3(VO_4)_2$/MgO-ZrO_2 catalysts may be closely related to the oxygen capacity (the amount of oxygen in the catalyst involved in the reaction). As shown in Fig. 3.4, TPRO peak area of X-$Mg_3(VO_4)_2$/MgO-ZrO_2 catalysts decreased in the order of 12.8-$Mg_3(VO_4)_2$/MgO-ZrO_2 > 9.9-$Mg_3(VO_4)_2$/MgO-ZrO_2 > 6.6-$Mg_3(VO_4)_2$/MgO-ZrO_2 > 15.2-$Mg_3(VO_4)_2$/MgO-ZrO_2 > 19.1-$Mg_3(VO_4)_2$/MgO-ZrO_2.

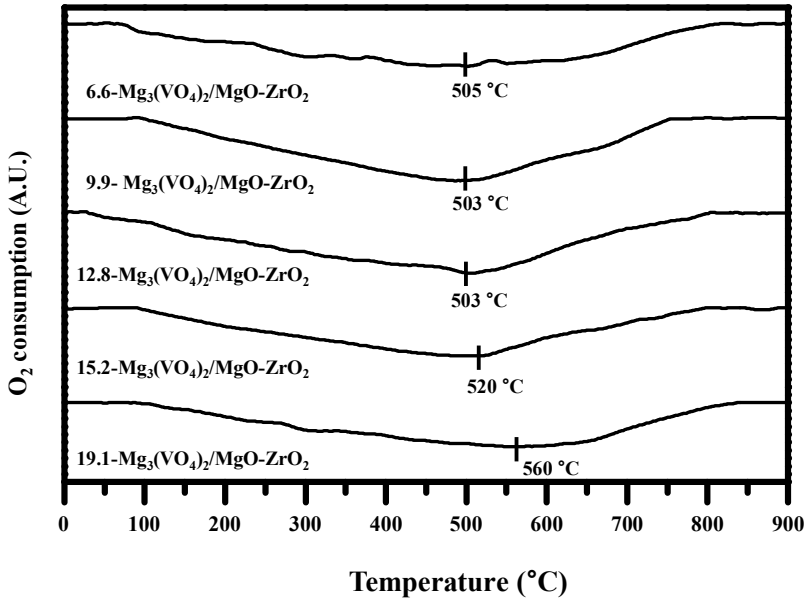

Fig. 3.4. TPRO profiles of X-$Mg_3(VO_4)_2$/MgO-ZrO_2 (X = 6.6, 9.9, 12.8, 15.2, and 19.1) catalysts.

Fig. 3.5 shows the correlation between yield for TDP after 1 h-reaction and oxygen capacity of X-$Mg_3(VO_4)_2$/MgO-ZrO_2 catalysts. Relative oxygen capacity was calculated as the ratio of TPRO peak area of the catalyst with respect to that of 19.1-$Mg_3(VO_4)_2$/MgO-ZrO_2 catalyst. It was observed that yield for TDP after 1 h-reaction increased with increasing oxygen capacity of the catalyst. This result was well consistent with the previous works reporting that there was a reliable correlation between oxygen capacity of the catalyst and catalytic performance in the oxidative dehydrogenation of n-butane [74-77]. Among the catalysts tested, 12.8-$Mg_3(VO_4)_2$/MgO-ZrO_2 catalyst with the largest oxygen capacity showed the best catalytic performance in terms of yield for TDP. In conclusion, oxygen capacity and oxygen mobility of the catalyst were closely related to the catalytic performance and the catalyst stability, respectively, in the oxidative dehydrogenation of n-butane.

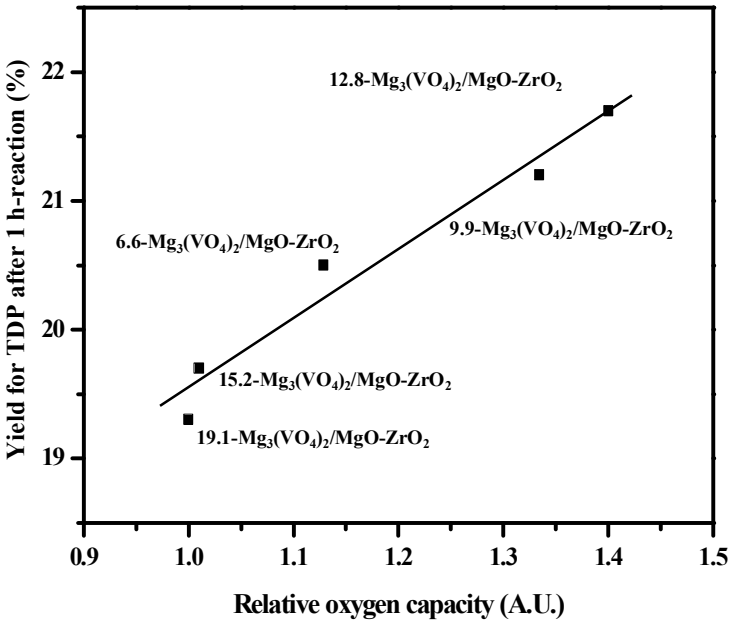

Fig. 3.5. A correlation between yield for TDP after 1 h-reaction and oxygen capacity of X-$Mg_3(VO_4)_2$/MgO-ZrO_2 (X = 6.6, 9.9, 12.8, 15.2, and 19.1) catalysts.

3.2. Characterization and catalytic performance of $Mg_3(VO_4)_2$/MgO-ZrO_2 (X) catalysts

3.2.1. Formation of $Mg_3(VO_4)_2$/MgO-ZrO_2 (X) catalysts

The formation of $Mg_3(VO_4)_2$/MgO-ZrO_2 (X) catalysts was confirmed by XRD, Raman spectroscopy, and ICP-AES measurements. Fig. 3.6 shows the XRD patterns of $Mg_3(VO_4)_2$/MgO-ZrO_2 (X) catalysts (Mg:Zr ratio = 16:1, 8:1, 4:1, 2:1, and 1:1). Crystalline phases of MgO and ZrO_2 were identified by the characteristic diffraction peaks using JCPDS. As shown in Fig. 3.6, a mixed phase of MgO-ZrO_2 supports was observed in all the $Mg_3(VO_4)_2$/MgO-ZrO_2 (X) catalysts. Relative intensities of MgO and ZrO_2 phases in the $Mg_3(VO_4)_2$/MgO-ZrO_2 (X) catalysts were different depending on the Mg:Zr ratio. However, XRD peaks corresponding to $Mg_3(VO_4)_2$ were not detected, indicating the existence of less crystallized or more dispersed form of $Mg_3(VO_4)_2$. This result was well consistent with the previous works [42,71], reporting that MgO and ZrO_2 diffraction peaks were only detected in the XRD patterns obtained from V-Mg-O catalysts with low V content.

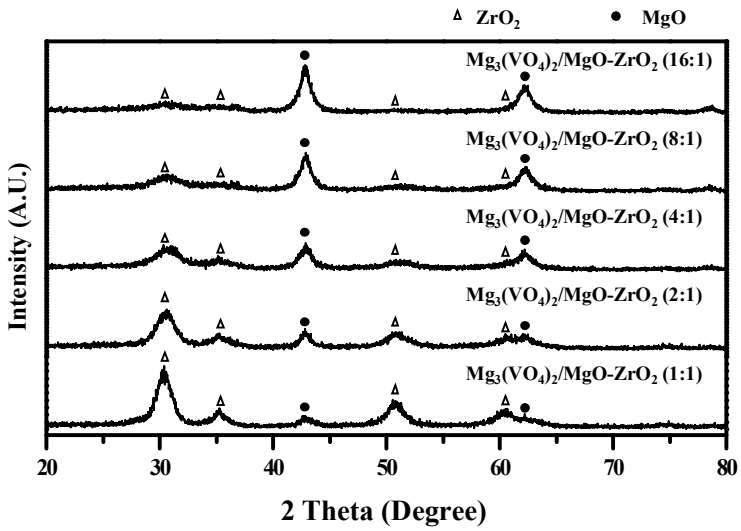

Fig. 3.6. XRD patterns of $Mg_3(VO_4)_2$/MgO-ZrO_2 (X) (Mg:Zr = 16:1, 8:1, 4:1, 2:1, and 1:1) catalysts.

Raman spectroscopy measurement were conducted to confirm the formation of $Mg_3(VO_4)_2$ phase in the $Mg_3(VO_4)_2$/MgO-ZrO_2 (X) catalysts. Fig. 3.7 shows the Raman spectra of $Mg_3(VO_4)_2$/MgO-ZrO_2 (X) catalysts. For reference, Raman spectra of pure magnesium vanadate ($Mg_3(VO_4)_2$, $Mg_2V_2O_7$, and MgV_2O_6) and vanadium pentoxide (V_2O_5) are also shown in Fig. 3.7. The main characteristic Raman band of $Mg_3(VO_4)_2$/MgO-ZrO_2 (X) catalysts appeared at 862 cm^{-1}, which was assigned to isolated VO_4 in $Mg_3(VO_4)_2$ phase [37,38,72,73]. The Raman band position of $Mg_3(VO_4)_2$/MgO-ZrO_2 (X) catalysts was identical to that of pure $Mg_3(VO_4)_2$. Furthermore, peak intensity increased with decreasing magnesium content in the $Mg_3(VO_4)_2$/MgO-ZrO_2 (X) catalysts. These results indicate that $Mg_3(VO_4)_2$ phase was successfully formed in the catalysts. XRD patterns (Fig. 3.6) and Raman spectra (Fig. 3.7) were well consistent with those reported in the previous works [37,38,42,71-73], indicating successful formation of $Mg_3(VO_4)_2$/MgO-ZrO_2 (X) catalysts.

Mg:Zr atomic ratios, Mg:V atomic ratios, and V contents in the $Mg_3(VO_4)_2$/MgO-ZrO_2 catalysts are summarized in Table 3.2. Atomic ratios determined by ICP-AES analyses were in good agreement with the designed values. These results indicate that all the $Mg_3(VO_4)_2$/MgO-ZrO_2 (X) catalysts were successfully prepared in this work. BET surface areas of the catalysts are also summarized in Table 3.2. It was found that BET surface areas of the catalysts showed no consistent trend with respect to Mg:Zr ratio.

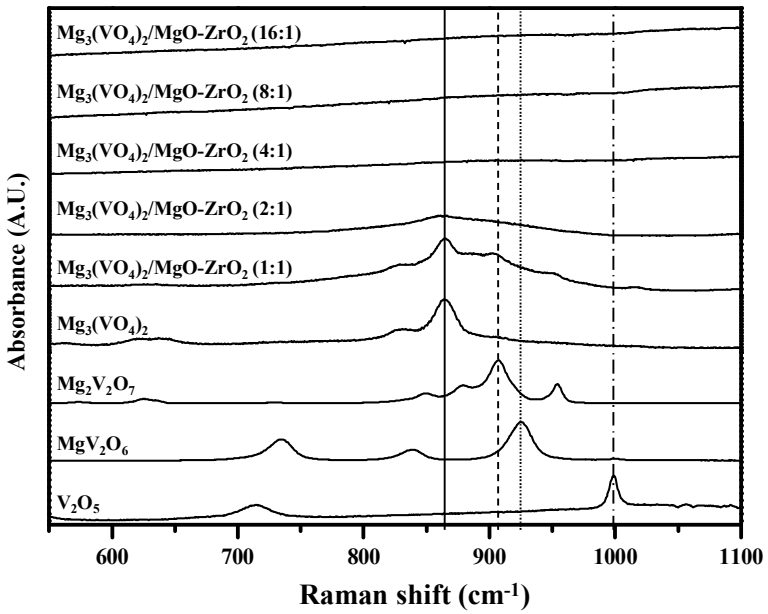

Fig. 3.7. Raman spectra of $Mg_3(VO_4)_2$/MgO-ZrO_2 (X) (Mg:Zr = 16:1, 8:1, 4:1, 2:1, and 1:1) catalysts, $Mg_3(VO_4)_2$, $Mg_2V_2O_7$, MgV_2O_6, and V_2O_5.

Table 3.2

Mg:Zr atomic ratios, Mg:V atomic ratios, V contents, and BET surface areas of $Mg_3(VO_4)_2/MgO\text{-}ZrO_2$ (X) catalysts

Catalyst	Mg:Zr	Mg:V	V content (wt%)	BET surface area (m^2/g)
$Mg_3(VO_4)_2/MgO\text{-}ZrO_2$ (16:1)	16.0:1 (16:1)[a]	12.4:1	13.0 (12.8)[b]	163
$Mg_3(VO_4)_2/MgO\text{-}ZrO_2$ (8:1)	8.0:1 (8:1)[a]	10.9:1	12.9 (12.8)[b]	126
$Mg_3(VO_4)_2/MgO\text{-}ZrO_2$ (4:1)	4.1:1 (4:1)[a]	8.7:1	12.8 (12.8)[b]	136
$Mg_3(VO_4)_2/MgO\text{-}ZrO_2$ (2:1)	1.8:1 (2:1)[a]	5.8:1	12.6 (12.8)[b]	99
$Mg_3(VO_4)_2/MgO\text{-}ZrO_2$ (11:1)	0.8:1 (1:1)[a]	3.4:1	12.2 (12.8)[b]	103

[a] Designed value of Mg:Zr ratio in the $Mg_3(VO_4)_2/MgO\text{-}ZrO_2$ (X) catalysts.

[b] Designed value of V contents in the $Mg_3(VO_4)_2/MgO\text{-}ZrO_2$ (X) catalysts.

3.2.2. Catalytic performance of $Mg_3(VO_4)_2$/MgO-ZrO_2 (X) catalysts

Fig. 3.8 shows the catalytic performance of $Mg_3(VO_4)_2$/MgO-ZrO_2 (X) catalysts in the oxidative dehydrogenation of n-butane at 500 ^oC. Catalytic performance of $Mg_3(VO_4)_2$/MgO-ZrO_2 (X) catalysts was strongly dependent on Mg:Zr ratio. Yield for TDP after 6 h-reaction decreased in the order of $Mg_3(VO_4)_2$/MgO-ZrO_2 (4:1) > $Mg_3(VO_4)_2$/MgO-ZrO_2 (8:1) > $Mg_3(VO_4)_2$/MgO-ZrO_2 (16:1) > $Mg_3(VO_4)_2$/MgO-ZrO_2 (2:1) > $Mg_3(VO_4)_2$/MgO-ZrO_2 (1:1). It was observed that all the catalysts showed a stable catalytic performance in the oxidative dehydrogenation of n-butane during the whole reaction time. Fig. 3.8 also shows that yield for TDP after 6 h-reaction showed a volcano-shaped trend with respect to Mg:Zr ratio. Among the catalysts tested, $Mg_3(VO_4)_2$/MgO-ZrO_2 (4:1) catalyst showed the best catalytic performance in the oxidative dehydrogenation of n-butane, indicating that 4:1 was the most suitable Mg:Zr ratio for $Mg_3(VO_4)_2$/MgO-ZrO_2 catalyst system.

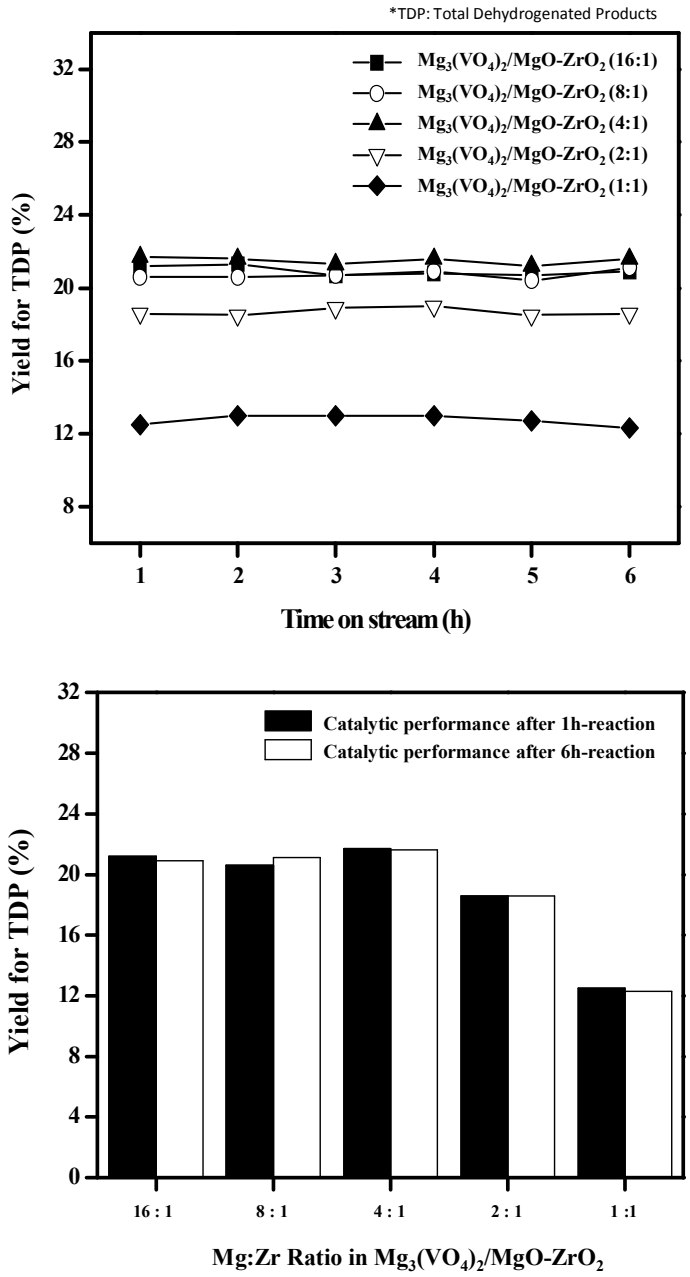

Fig. 3.8. Catalytic performance of $Mg_3(VO_4)_2$/MgO-ZrO_2 (X) catalysts.

3.2.3. Effect of Mg:Zr ratio on the catalytic performance of $Mg_3(VO_4)_2$/MgO-ZrO_2 (X) catalysts

It is known that lattice oxygen in the $Mg_3(VO_4)_2$/MgO-ZrO_2 (X) plays a key role in the oxidative dehydrogenation of n-butane, because the reaction follows the Mars-van Krevelen mechanism. It has been reported that oxygen capacity and oxygen mobility of $Mg_3(VO_4)_2$/MgO-ZrO_2 (X) served as crucial factors determining the catalytic performance in oxidative dehydrogenation of n-butane [42-48]. In order to investigate the effect of oxygen property of $Mg_3(VO_4)_2$/MgO-ZrO_2 (X) catalysts, TPRO experiments were carried out. Fig. 3.9 shows the TPRO profiles of $Mg_3(VO_4)_2$/MgO-ZrO_2 (X) (Mg:Zr ratio = 16:1, 8:1, 4:1, 2:1, and 1:1) catalysts. TPRO peak temperature and TPRO peak area reflect the oxygen mobility and the oxygen capacity, respectively [74,75]. The lower TPRO peak temperature and the larger TPRO peak area correspond to the higher oxygen mobility and the larger oxygen capacity, respectively.

Although $Mg_3(VO_4)_2$/MgO-ZrO_2 (X) (Mg:Zr ratio = 16:1, 8:1, 4:1, 2:1, and 1:1) catalysts exhibited slightly different oxygen mobility (TPRO peak temperature), all the $Mg_3(VO_4)_2$/MgO-ZrO_2 (X) catalysts showed a stable catalytic performance without catalytic deactivation during the whole reaction time. Therefore, it reasonable to expect that oxygen mobility of the catalyst was sufficiently facile for making up oxygen vacancy of the catalyst during the catalytic reaction. Thus, no correlation between catalytic activity and oxygen mobility could be established. On the other hand, oxygen capacity of the catalyst was much different depending on Mg:Zr ratio. TPRO peak area of

$Mg_3(VO_4)_2$/MgO-ZrO_2 (X) (Mg:Zr ratio = 16:1, 8:1, 4:1, 2:1, and 1:1) catalysts decreased in the order of $Mg_3(VO_4)_2$/MgO-ZrO_2 (4:1) > $Mg_3(VO_4)_2$/MgO-ZrO_2 (8:1) > $Mg_3(VO_4)_2$/MgO-ZrO_2 (16:1) > $Mg_3(VO_4)_2$/MgO-ZrO_2 (2:1) > $Mg_3(VO_4)_2$/MgO-ZrO_2 (1:1). As mentioned earlier, the larger TPRO peak area corresponds to the larger oxygen capacity. This means that a catalyst with large TPRO peak area retains a large amount of mobile oxygen in the catalyst.

We attempted to correlate the catalytic performance with the oxygen capacity of $Mg_3(VO_4)_2$/MgO-ZrO_2 (X) (Mg:Zr ratio = 16:1, 8:1, 4:1, 2:1, and 1:1) catalysts. As a result, a reliable correlation between yield for TDP after 6 h-catalytic reaction and oxygen capacity of the catalyst was observed. Fig. 3.10 shows the correlation between yield for TDP after 6 h-catalytic reaction and oxygen capacity of $Mg_3(VO_4)_2$/MgO-ZrO_2 (X) (Mg:Zr ratio = 16:1, 8:1, 4:1, 2:1, and 1:1) catalysts. Catalytic performance data were taken from Fig. 3.8. Relative oxygen capacity was defined as the ratio of TPRO peak area of the catalyst with respect to that of $Mg_3(VO_4)_2$/MgO-ZrO_2 (1:1) catalyst. The correlation clearly shows that the catalytic performance was closely related to the oxygen capacity of the catalyst in the oxidative dehydrogenation of n-butane. Yield for TDP increased with increasing oxygen capacity of the catalyst. Among the catalysts tested, $Mg_3(VO_4)_2$/MgO-ZrO_2 (4:1) catalyst with the largest oxygen capacity showed the best catalytic performance. This result was in good agreement with the previous works investigating the effect of oxygen capacity on the catalytic performance of $Mg_3(VO_4)_2$/MgO-ZrO_2 catalysts in the oxidative dehydrogenation of n-butane [74-77]. It can be concluded that the amount of lattice oxygen in the catalyst involved in the

reaction played an important role in determining the catalytic performance in the reaction.

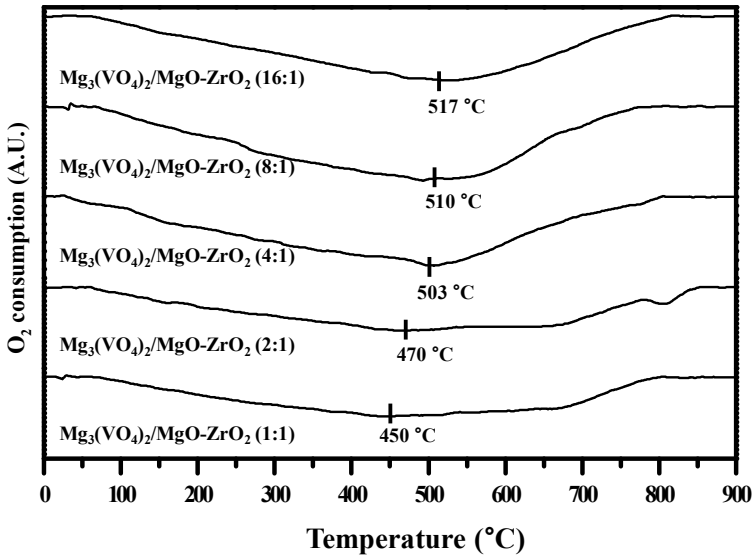

Fig. 3.9. TPRO profiles of $Mg_3(VO_4)_2$/MgO-ZrO_2 (X) (Mg:Zr = 16:1, 8:1, 4:1, 2:1, and 1:1) catalysts.

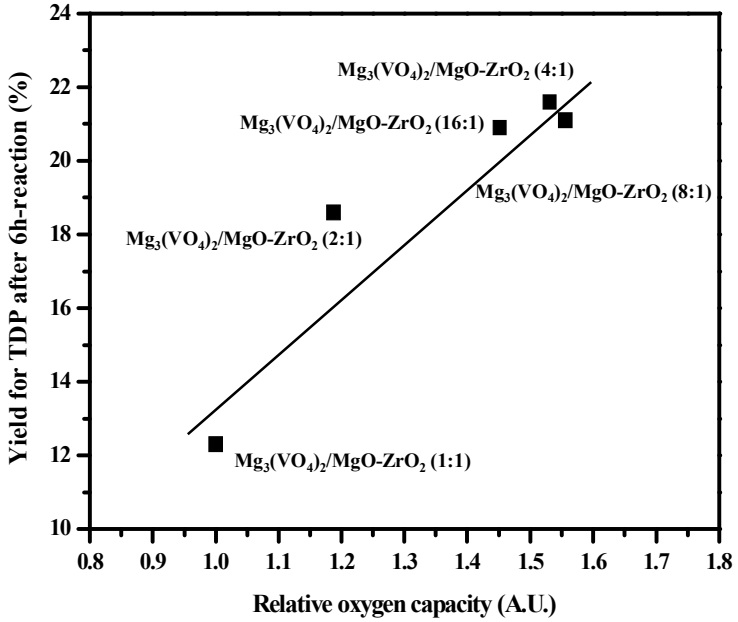

Fig. 3.10. A correlation between yield for TDP after 6 h-reaction and oxygen capacity of $Mg_3(VO_4)_2/MgO\text{-}ZrO_2$ (X) (Mg:Zr = 16:1, 8:1, 4:1, 2:1, and 1:1) catalysts.

Part 2 Direct dehydrogenation of n-butane to n-butene and 1,3-butadiene

3.3. Characterization and catalytic performance of $Pt/Sn/M/Al_2O_3$ catalysts

3.3.1. Formation of $Pt/Sn/M/Al_2O_3$ catalysts

Fig. 3.11 shows the XRD patterns of $Pt/Sn/Al_2O_3$ and $Pt/Sn/M/Al_2O_3$ (M = Zn, In, Y, Bi, and Ga) catalysts reduced at 570 °C for 3 h. No distinctive diffraction peaks were detected in the $Pt/Sn/M/Al_2O_3$ catalysts compared to $Pt/Sn/Al_2O_3$ catalyst. Only characteristic diffraction peaks corresponding to γ-Al_2O_3 were observed in all the catalysts. Any diffraction peaks of platinum and tin species were not observed, due to their small crystalline size or low concentration [78,79].

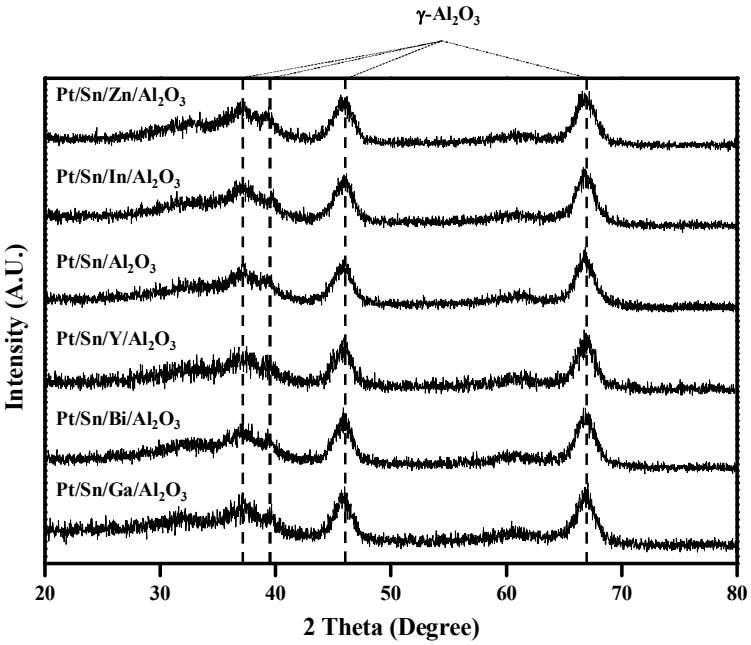

Fig. 3.11. XRD patterns of $Pt/Sn/Al_2O_3$ and $Pt/Sn/M/Al_2O_3$ (M = Zn, In, Y, Bi, and Ga) catalysts reduced at 570 ^oC for 3 h.

3.3.2. Catalytic performance of $Pt/Sn/M/Al_2O_3$ catalysts

Fig. 3.12 shows the catalytic performance of $Pt/Sn/Al_2O_3$ and $Pt/Sn/M/Al_2O_3$ (M = Zn, In, Y, Bi, and Ga) catalysts with time on stream in the direct dehydrogenation of n-butane at 550 °C. All the catalysts experienced a catalyst deactivation, which was a typical behavior of direct dehydrogenation of paraffins. However, the catalytic performance and stability strongly depended on the identity of third metal component. $Pt/Sn/Al_2O_3$, $Pt/Sn/Y/Al_2O_3$, $Pt/Sn/Bi/Al_2O_3$, and $Pt/Sn/Ga/Al_2O_3$ catalysts exhibited a sharp decrease of catalytic activity compared to $Pt/Sn/Zn/Al_2O_3$ and $Pt/Sn/In/Al_2O_3$ catalysts. Catalytic performance of $Pt/Sn/Al_2O_3$ and $Pt/Sn/M/Al_2O_3$ catalysts obtained after a 360 min-reaction is also shown in Fig. 3.12. Moreover, conversion of n-butane and selectivity for reaction products obtained after 60 min-reaction and 360 min-reaction are listed in Table 3.3. As shown in Table 3.3 isobutene, iso-butane, C1-C3 compounds (methane, ethane, ethylene, propane, propylene), and C5-C6 compounds (n-pentane, isopentane, 3-methyl-1-butene, 2-methyl-1-butene, isopentene, 1-pentene, 2-pentene, and n-hexane) were produced as by-products together with target products (1-butene, 2-butene, and 1,3-butadiene). 1-Butene and 2-butene were mainly produced via dehydrogenation of n-butane. Formation of 1- butene and 2-butene through ethylene dimerization and cracking of C5-C6 compounds was negligible. In addition, 1.3-butadiene was mainly produced by the dehydrogenation of n-butene during the reaction. Low selectivity for 1,3-butadiene was due to thermodynamic equilibrium limitation. It is believed

that C1-C3 compounds were produced by the hydrocracking while C5-C6 compounds were produced by oligomerization and polymerization of hydrocarbon species. Selectivities for C1-C3 and C5-C6 compounds were not significantly changed with the addition of third metal (M) to $Pt/Sn/Al_2O_3$. Although selectivity for 1-butene itself was not high in this work, selectivity for 1-butene was definitely increased by the addition Zn to $Pt/Sn/Al_2O_3$ catalyst. Moreover, selectivity for TDP including 2-butene was the highest over $Pt/Sn/Zn/Al_2O_3$ catalyst. Selectivities for 1-butene, 2-butene, and 1,3-butadiene were found to be 20.7%, 42.4%, and 5.2%, respectively, in the direct dehydrogenation of n-butane at 550 °C after a 360 min-reaction over $Pt/Sn/Zn/Al_2O_3$ catalyst. Furthermore, among the catalysts tested, $Pt/Sn/Zn/Al_2O_3$ catalyst exhibited the highest conversion of n-butane and the highest yield for TDP at the initial and final stage of the reaction. As expected, $Pt/Sn/Zn/Al_2O_3$ catalyst showed the lowest deactivation rate. Conversion of n-butane and yield for TDP after a 360 min-reaction decreased in the order of $Pt/Sn/Zn/Al_2O_3$ > $Pt/Sn/In/Al_2O_3$ > $Pt/Sn/Al_2O_3$ > $Pt/Sn/Y/Al_2O_3$ > $Pt/Sn/Bi/Al_2O_3$ > $Pt/Sn/Ga/Al_2O_3$. Among the catalysts tested, $Pt/Sn/Zn/Al_2O_3$ showed the best catalytic performance and stability in the direct dehydrogenation of n-butane. For comparison, direct dehydrogenation of n-butane over $ZnSn/Al_2O_3$ catalyst was also carried out. However, the catalytic performance was quite low; yield for TDP was about 0.6% and selectivity for TDP was about 6% after a 360-min reaction. Low catalytic performance of $ZnSn/Al_2O_3$ was due to the absence of active Pt metal.

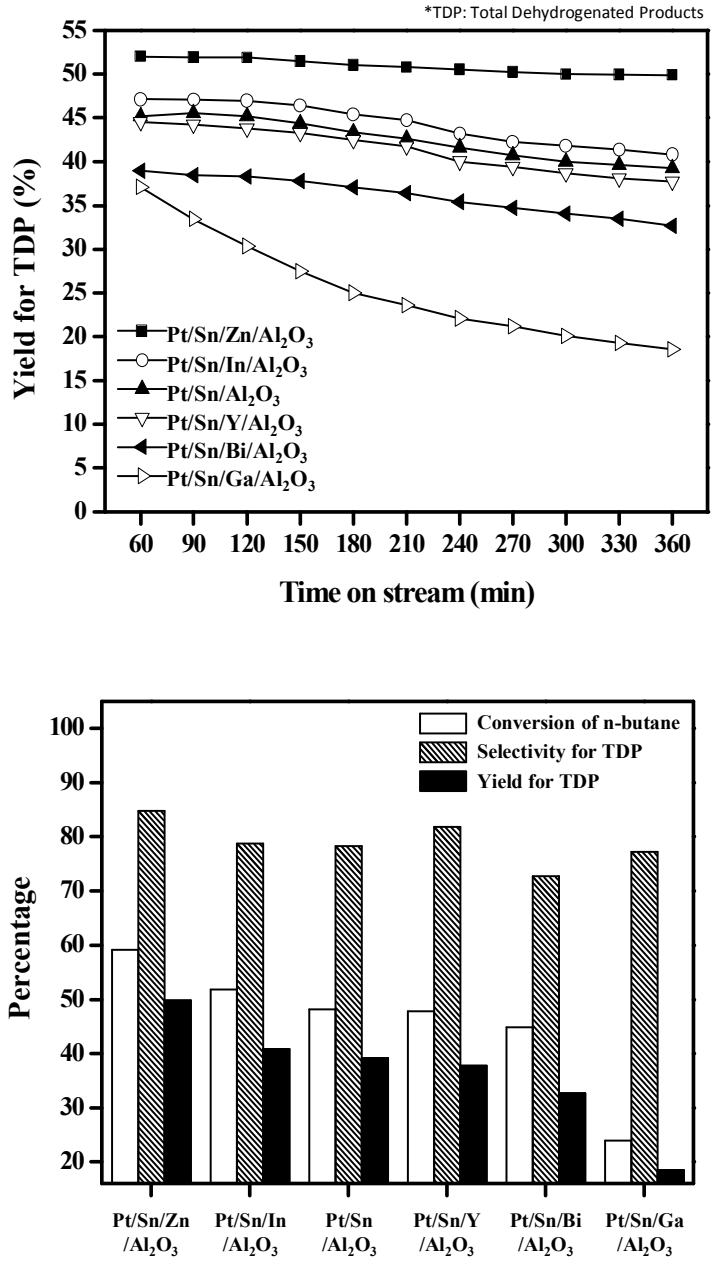

Fig. 3.12. Catalytic performance of $Pt/Sn/Al_2O_3$ and $Pt/Sn/M/Al_2O_3$ catalysts.

Table 3.3

Catalytic performance of $Pt/Sn/Al_2O_3$ and $Pt/Sn/M/Al_2O_3$ (M = Zn, In, Y, Bi, and Ga) catalysts in the direct dehydrogenation of n-butane of n-butane after a 60-min reaction and a 360 min-reaction

Catalyst	X_i (%)[a]	S_i (%)[a]						
		1-butene	2-butene	1,3-BD	i-butene	i-butane	C1-C3	C5-C6
$Pt/Sn/Zn/Al_2O_3$	76.0	20.7	42.4	5.2	13.7	12.0	5.6	0.4
$Pt/Sn/In/Al_2O_3$	69.7	21.6	30.0	6.0	24.0	9.3	8.5	0.6
$Pt/Sn/Al_2O_3$	68.9	18.7	40.3	4.6	19.5	9.1	7.0	0.8
$Pt/Sn/Y/Al_2O_3$	64.7	20.5	45.3	4.0	14.9	7.7	6.7	0.9
$Pt/Sn/Bi/Al_2O_3$	65.4	16.9	38.9	3.2	21.3	11.0	7.9	0.8
$Pt/Sn/Ga/Al_2O_3$	51.7	20.8	45.5	5.5	17.2	4.2	6.1	0.7
Catalyst	X_f (%)[b]	S_f (%)[b]						
		1-butene	2-butene	1,3-BD	i-butene	i-butane	C1-C3	C5-C6
$Pt/Sn/Zn/Al_2O_3$	59.1	24.2	54.9	5.7	7.0	1.6	5.4	1.2
$Pt/Sn/In/Al_2O_3$	51.8	22.4	49.3	7.1	14.2	1.6	4.9	0.5
$Pt/Sn/Al_2O_3$	48.2	22.3	48.9	7.1	14.6	1.6	5.0	0.5
$Pt/Sn/Y/Al_2O_3$	47.9	23.0	52.5	6.4	10.5	0.9	6.1	0.6
$Pt/Sn/Bi/Al_2O_3$	44.9	20.4	46.5	5.8	17.5	1.5	7.9	0.4
$Pt/Sn/Ga/Al_2O_3$	24.0	20.6	45.5	11.1	12.9	0.4	9.0	0.5

[a] X_i is initial conversion of n-butane and S_i is initial selectivity obtained after a 60-min reaction.

[b] X_f is final conversion of n-butane and S_f is final selectivity obtained after a 360-min reaction.

3.3.3. Metal-support interaction in the $Pt/Sn/M/Al_2O_3$ catalysts

TPR measurements were carried out to examine the interaction between metal species and support in the $Pt/Sn/Al_2O_3$ and $Pt/Sn/M/Al_2O_3$ (M = Zn, In, Y, Bi, and Ga) catalysts, as shown in Fig. 3.13. It is known that $Pt/Sn/Al_2O_3$ catalyst showed two reduction bands; a reduction band at around 250 °C is ascribed to the reduction of Pt oxide species, while a broad reduction band at around 500 °C is due to partial reduction of Sn^{4+} to Sn^{2+} and Sn^{2+} to Sn^0 [53,80]. When the third metal was added into $Pt/Sn/Al_2O_3$ catalyst, all the catalysts showed an obviously different reduction band at around 250 °C. This reduction band was attributed to the reduction of Pt oxide, a small fraction of Sn oxide, and the other metal oxide species [81]. However, the reduction band at around 500 °C was not clear due to partial reduction of tin oxide. It is suggested that Pt, Sn, and third metal (M) coexist intimately, and interaction between Pt, Sn, and M affects the spatial distribution of these components on the catalyst surface. It should be noted that the reduction peak temperature at around 250 °C was different depending on the identity of third metal, indicating that the third metal significantly affected the metal-support interaction in our catalyst system. The reduction peak temperature decreased in the order of $Pt/Sn/Zn/Al_2O_3$ > $Pt/Sn/In/Al_2O_3$ > $Pt/Sn/Al_2O_3$ > $Pt/Sn/Y/Al_2O_3$ > $Pt/Sn/Bi/Al_2O_3$ > $Pt/Sn/Ga/Al_2O_3$. It is believed that platinum-alumina interaction and tin-alumina interaction increased by the addition of Zn to $Pt/Sn/Al_2O_3$ catalyst due to favorable spatial distribution of metal components. This trend was well consistent with the trend of catalytic activity (Fig. 3.12).

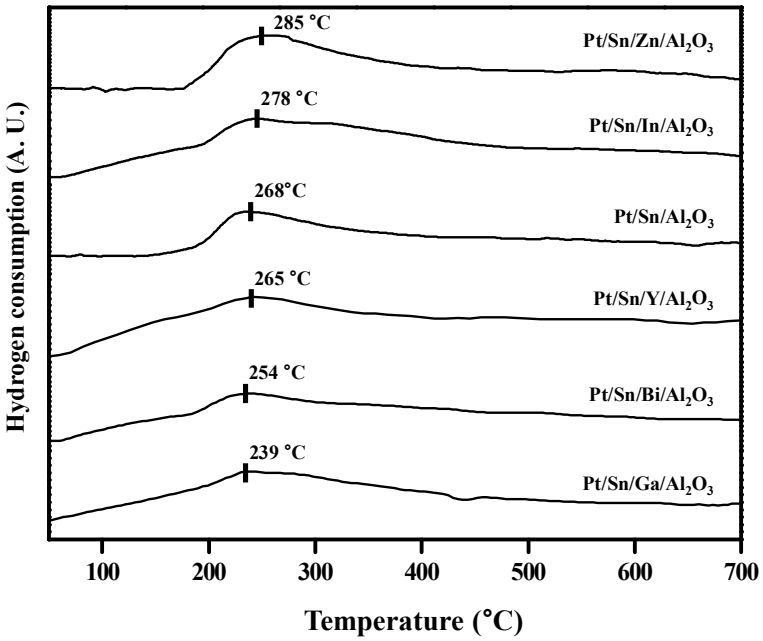

Fig. 3.13. TPR profiles of $Pt/Sn/Al_2O_3$ and $Pt/Sn/M/Al_2O_3$ catalysts.

3.3.4. Pt dispersion and Pt surface area in the reduced $Pt/Sn/M/Al_2O_3$ catalysts

Hydrogen chemisorption measurements were conducted to determine Pt dispersion and Pt surface area in the reduced $Pt/Sn/Al_2O_3$ and $Pt/Sn/M/Al_2O_3$ (M = Zn, In, Y, Bi, and Ga) catalysts. Hydrogen chemisorption results for the reduced catalysts are listed in Table 3.4. The amount of hydrogen uptake on the reduced catalysts decreased in the order of $Pt/Sn/Zn/Al_2O_3$ > $Pt/Sn/In/Al_2O_3$ > $Pt/Sn/Al_2O_3$ > $Pt/Sn/Y/Al_2O_3$ > $Pt/Sn/Bi/Al_2O_3$ > $Pt/Sn/Ga/Al_2O_3$. As a consequence, Pt dispersion and Pt surface area decreased in the order of $Pt/Sn/Zn/Al_2O_3$ > $Pt/Sn/In/Al_2O_3$ > $Pt/Sn/Al_2O_3$ > $Pt/Sn/Y/Al_2O_3$ > $Pt/Sn/Bi/Al_2O_3$ > $Pt/Sn/Ga/Al_2O_3$. Pt particle size increased in the order of $Pt/Sn/Zn/Al_2O_3$ < $Pt/Sn/In/Al_2O_3$ < $Pt/Sn/Al_2O_3$ < $Pt/Sn/Y/Al_2O_3$ < $Pt/Sn/Bi/Al_2O_3$ < $Pt/Sn/Ga/Al_2O_3$. These trends were well consistent with the trends of catalytic activity (Fig. 3.12) and TPR results (Fig. 3.13). When the metal-support interaction was strong, Pt species were well dispersed on the support and Pt particle size decreased. That is, strong surface interaction retarded agglomeration of Pt particles and increased Pt surface area by decreasing Pt particle size. $Pt/Sn/Zn/Al_2O_3$ and $Pt/Sn/In/Al_2O_3$ catalysts showed high Pt dispersion because chemical interactions between Pt, Sn, and Zn (or In) affected either the degree of Pt sintering during calcination or the properties of surface of active metal [82]. It is believed that zinc served as an efficient spacer to reduce the size of platinum ensemble as tin acted as a spacer in the Pt-Sn catalyst [83,84].

Table 3.4

Hydrogen chemisorption results for reduced $Pt/Sn/Al_2O_3$ and $Pt/Sn/M/Al_2O_3$ (M = Zn, In, Y, Bi, and Ga) catalysts

Catalyst	Pt dispersion (%)[a]	Pt surface area (m^2/g)[a]	Average Pt particle size (nm)[a]
$Pt/Sn/Zn/Al_2O_3$	47.2	116.4	2.4
$Pt/Sn/In/Al_2O_3$	37.4	92.4	3.0
$Pt/Sn/Al_2O_3$	30.0	73.8	3.8
$Pt/Sn/Y/Al_2O_3$	29.4	69.4	3.9
$Pt/Sn/Bi/Al_2O_3$	21.6	53.6	5.2
$Pt/Sn/Ga/Al_2O_3$	20.0	46.8	5.3

[a] Calculated by assuming a stoichiometry factor of H/Pt =1.

3.3.5. Electronic effect in the reduced $Pt/Sn/M/Al_2O_3$ catalysts

To investigate the chemical state of metal components, XPS analyses were carried out. XPS spectra of Sn $3d_{5/2}$ levels for the reduced catalysts are shown in Fig. 3.14, and the measured binding energies of Pt $4f_{7/2}$ and Sn $3d_{5/2}$ and surface atomic ratio are summarized in Table 3.5. All the catalysts showed binding energy of single Pt $4f_{7/2}$ component at 71.7-72.3 eV, indicating the presence of zerovalent platinum [85]. In general, Sn $3d_{5/2}$ peak can be divided into zerovalent tin, alloyed tin, oxidized tin and chlorinated tin [86]. As shown in Fig. 3.14, however, only two Sn $3d_{5/2}$ components were observed in our catalyst system; the component at lower binding energy of 485.3-486.2 eV corresponded to alloyed tin, while that at higher binding energy of 487.1-487.6 eV was oxidized tin (II, IV) [87]. Any peaks related to zerovalent tin and chlorinated tin were not detected.

When the third metal was added into $Pt/Sn/Al_2O_3$ catalyst, binding energy of each component was changed. It can be inferred that Pt was alloyed with Sn or electronically modified by the third metal. In case of $Pt/Sn/Zn/Al_2O_3$ and $Pt/Sn/In/Al_2O_3$ catalysts, which showed an excellent catalytic activity, high surface atomic ratio of Pt/Al and high percentage of oxidized tin were observed. In case of $Pt/Sn/Al_2O_3$ and $Pt/Sn/Ga/Al_2O_3$ catalysts, however, the percentage of alloyed tin species was higher than that of oxidized tin species. It was reported that the promoter such as zinc and indium can decrease the surface Pt ensembles by geometric effect, which leads to the increased Pt dispersion and reaction activity, since the desired

dehydrogenation reaction can proceed on small ensembles of surface platinum atoms [80].

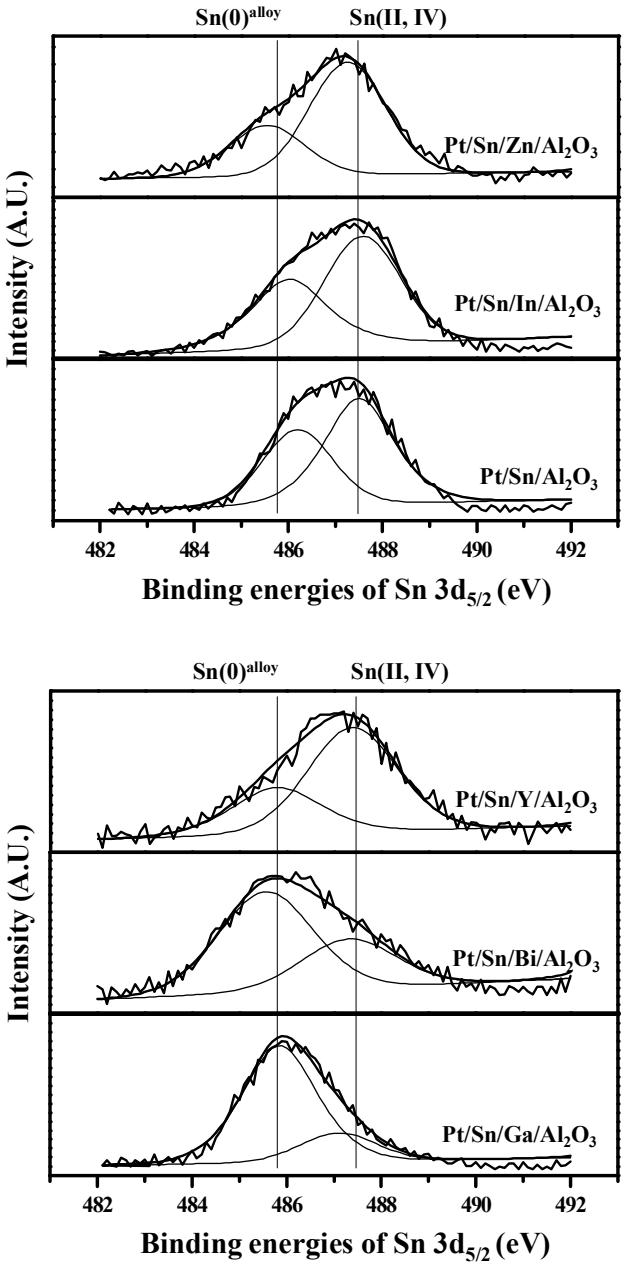

Fig. 3.14. XPS spectra of Sn $3d_{5/2}$ of $Pt/Sn/Al_2O_3$ and $Pt/Sn/M/Al_2O_3$ catalysts reduced at 570 ^oC for 3 h.

Table 3.5

Binding energies of Pt $4f_{7/2}$ and Sn $3d_{5/2}$ and surface atomic ratio of $Pt/Sn/Al_2O_3$ and $Pt/Sn/M/Al_2O_3$ (M = Zn, In, Y, Bi, and Ga) catalysts

Catalyst	Binding energy of Pt $4f_{7/2}$ (eV)	Binding energy of Sn $3d_{5/2}$ (eV)	Surface atomic ratio Pt/Al
$Pt/Sn/Zn/Al_2O_3$	72.3	487.3 485.3	0.0057
$Pt/Sn/In/Al_2O_3$	72.0	487.6 486.0	0.0057
$Pt/Sn/Al_2O_3$	71.9	487.5 486.2	0.0045
$Pt/Sn/Y/Al_2O_3$	71.9	487.4 485.8	0.0053
$Pt/Sn/Bi/Al_2O_3$	71.9	487.3 485.6	0.0037
$Pt/Sn/Ga/Al_2O_3$	71.7	487.1 485.9	0.0037

3.3.6. Correlations between catalytic performance and catalytic properties

Fig. 3.15 shows the correlations between catalytic performance and catalytic properties. Yield for TDP increased with increasing TPR peak temperature and with increasing Pt surface area. The correlations clearly showed that metal-support interaction and Pt surface area played key roles in determining the catalytic performance of $Pt/Sn/M/Al_2O_3$ catalysts. Among the catalysts tested, $Pt/Sn/Zn/Al_2O_3$ catalyst, which retained the strongest metal-support interaction and the highest Pt surface area, exhibited the best catalytic performance in the direct dehydrogenation of n-butane.

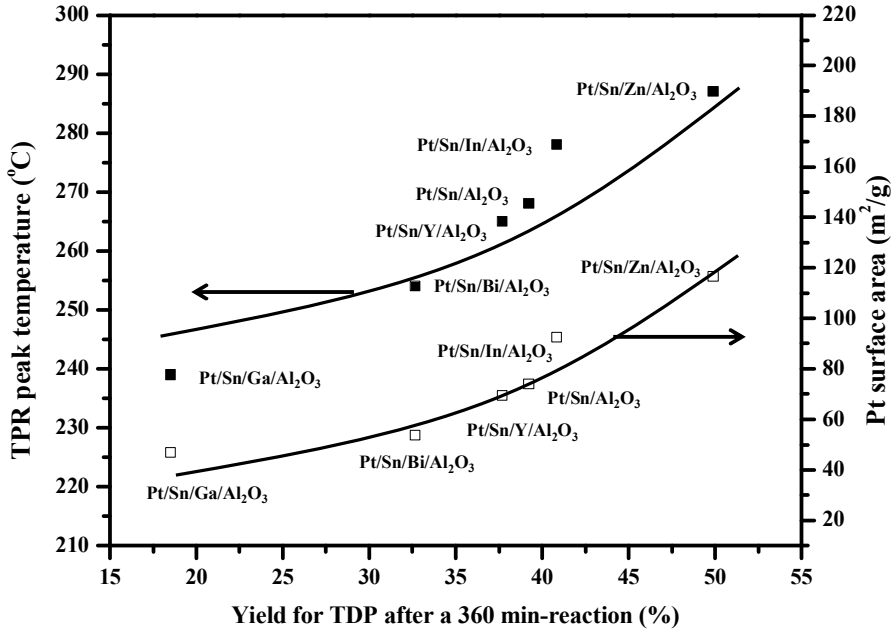

Fig. 3.15. Correlations between yield for TDP after a 360 min-reaction and TPR peak temperature, and between yield for TDP after a 360 min-reaction and Pt surface area.

3.4. Characterization and catalytic performance of $Pt/Sn/Zn/Al_2O_3$ catalysts

3.4.1. Formation of $Pt/Sn/XZn/Al_2O_3$ catalysts

Fig. 3.16 shows the XRD patterns of $Pt/Sn/XZn/Al_2O_3$ (X = 0, 0.25, 0.5, 0.75, and 1.0 wt%) catalysts reduced at 570 ^oC for 3 h. No distinctive diffraction peaks for metal species were detected in the $Pt/Sn/XZn/Al_2O_3$ (X = 0-1.0 wt%) catalysts. Instead, characteristic diffraction peaks corresponding to γ-Al_2O_3 were only observed. This indicates that metal species were finely dispersed on alumina support [78,79].

Textural properties of $Pt/Sn/XZn/Al_2O_3$ catalysts were examined by nitrogen adsorption-desorption isotherm measurements. Fig. 3.17 shows the nitrogen adsorption-desorption isotherms of $Pt/Sn/XZn/Al_2O_3$ catalysts reduced at 570 ^oC for 3 h. It was observed that all the catalysts exhibited IV-type isotherm with H3-type hysteresis loop, indicating the existence of mesopores. Detailed physicochemical properties of $Pt/Sn/XZn/Al_2O_3$ catalysts are summarized in Table 3.6. BET surface area of the catalysts decreased with increasing Zn content. This might be due to the pore blockage by Zn with increasing Zn content. As listed in Table 3.6, atomic ratios of constituent metal components were in good agreement with the designed values, indicating that all the catalysts were successfully prepared as attempted in this work.

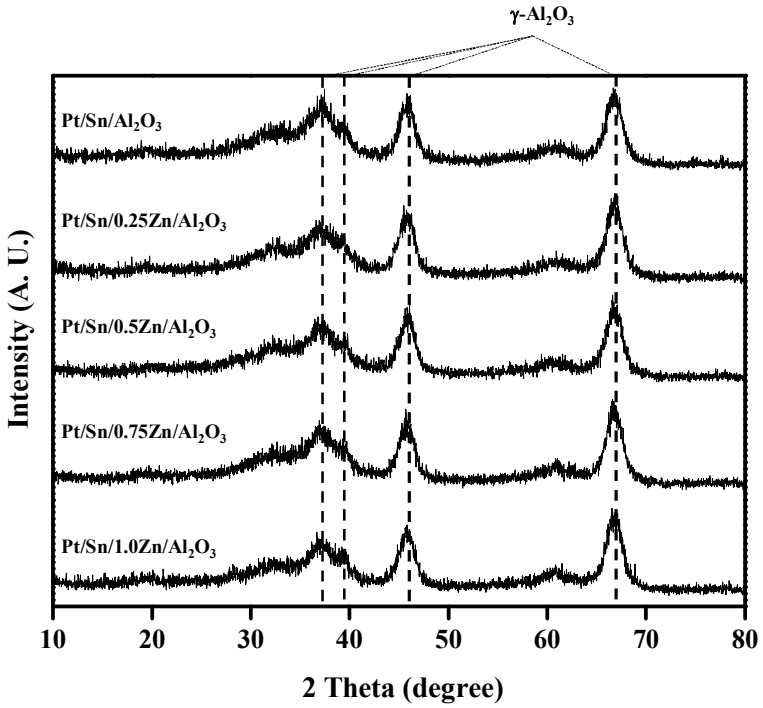

Fig. 3.16. XRD patterns of $Pt/Sn/XZn/Al_2O_3$ catalysts reduced at 570 ^oC for 3 h.

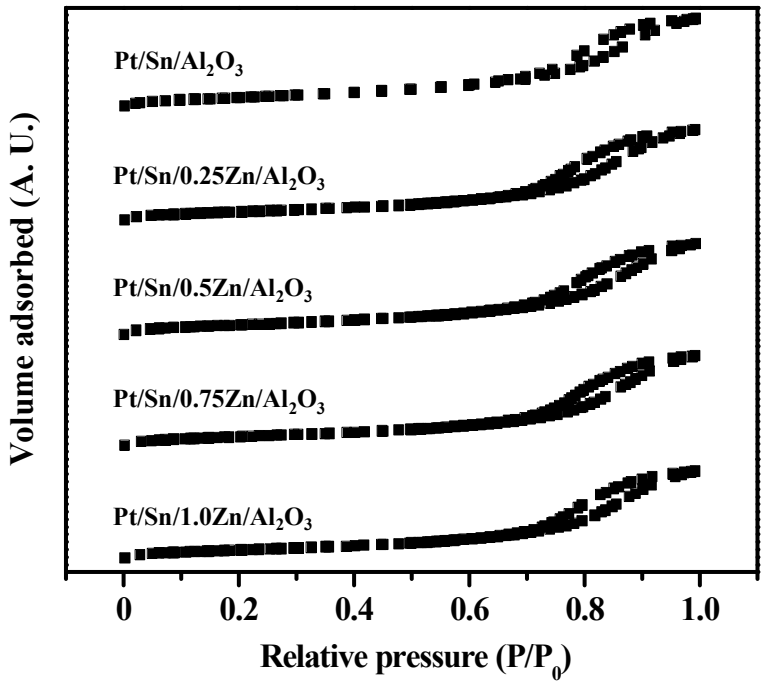

Fig. 3.17. Nitrogen adsorption-desorption isotherms of $Pt/Sn/XZn/Al_2O_3$ catalysts reduced at 570 ^oC for 3 h.

Table 3.6

Atomic ratios and BET surface areas of $Pt/Sn/XZn/Al_2O_3$ catalysts (X = 0, 0.25, 0.5, 0.75, and 1.0 wt%) reduced at 570 ^oC for 3 h

Catalyst	Atomic ratio			BET surface area (m^2/g)[b]
	Pt (wt%)[a]	Sn (wt%)[a]	Zn (wt%)[a]	
$Pt/Sn/Al_2O_3$	0.96	1.04	-	185
$Pt/Sn/0.25Zn/Al_2O_3$	0.96	1.04	0.23	180
$Pt/Sn/0.5Zn/Al_2O_3$	0.94	1.06	0.52	179
$Pt/Sn/0.75Zn/Al_2O_3$	1.03	1.05	0.74	173
$Pt/Sn/1.0Zn/Al_2O_3$	1.03	0.99	1.10	169

[a] Determined by ICP-AES measurement.

[b] Calculated by the BET equation.

3.4.2. Catalytic performance of Pt/Sn/XZn/Al_2O_3 catalysts

Fig. 3.18 shows the yield for TDP of Pt/Sn/XZn/Al_2O_3 (X = 0, 0.25, 0.5, 0.75, and 1.0 wt%) catalysts after 60 min-reaction and 360 min-reaction in the direct dehydrogenation of n-butane. Yield for TDP strongly depended on zinc content. It is noteworthy that Pt/Sn/0.5Zn/Al_2O_3 catalyst showed a slight catalyst deactivation while the other catalysts experienced a severe catalyst deactivation. This indicates that Pt/Sn/0.5Zn/Al_2O_3 catalyst with an appropriate amount of zinc showed an improved catalytic stability in the direct dehydrogenation of n-butane. Fig. 3.18 also shows the catalytic performance of Pt/Sn/XZn/Al_2O_3 (X = 0, 0.25, 0.5, 0.75, and 1.0 wt%) catalysts in the direct dehydrogenation of n-butane at 550 ^oC after a 360 min-reaction, plotted as a function of zinc content. In the direct dehydrogenation of n-butane over Pt/Sn/XZn/Al_2O_3 catalysts, iso-butene, iso-butane, and C1-C3 compounds (methane, ethane, ethylene, propane, propylene) were also produced as by-products together with target products (1-butene, 2-butene, and 1,3-butadiene). Selectivity for TDP was almost constant (ca. 84 %). Conversion of n-butane and yield for TDP exhibited volcano-shaped curves with respect to zinc content. Conversion of n-butane and yield for TDP after a 360 min-reaction decreased in the order of Pt/Sn/0.5Zn/Al_2O_3 > Pt/Sn/0.75Zn/Al_2O_3 > Pt/Sn/0.25Zn/Al_2O_3 > Pt/Sn/1.0Zn/Al_2O_3 > Pt/Sn/Al_2O_3. It is interesting to note that the catalytic activity over Pt/Sn/Zn/Al_2O_3 catalysts was higher than that over Pt/Sn/Al_2O_3 catalyst. This result indicates that the addition of zinc to Pt/Sn/Al_2O_3 catalyst was favorable for enhancing the catalytic performance of Pt/Sn/Al_2O_3 catalyst in the direct dehydrogenation of

n-butane. Among the catalysts tested, Pt/Sn/0.5Zn/Al_2O_3 catalyst showed the best catalytic performance.

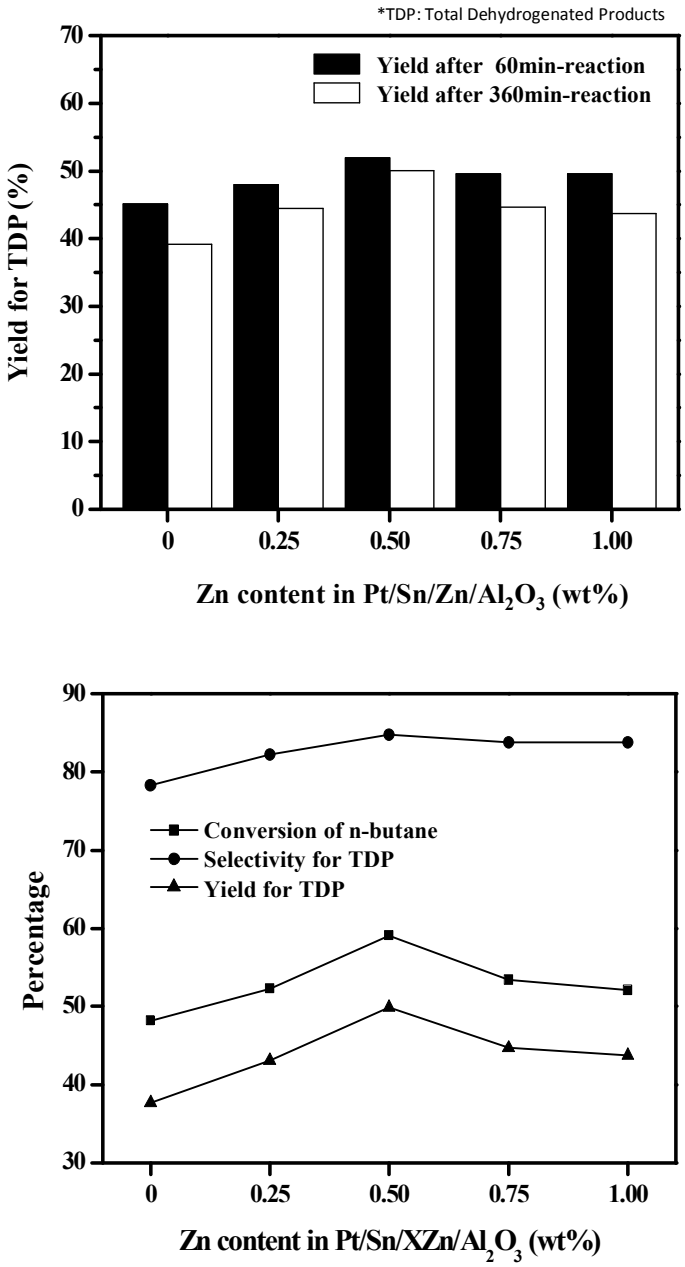

Fig. 3.18. Catalytic performance of $Pt/Sn/XZn/Al_2O_3$ catalysts.

3.4.3. Metal-support interaction in the $Pt/Sn/XZn/Al_2O_3$ catalysts

TPR measurements were carried out to examine the interaction between metal species and support in the $Pt/Sn/XZn/Al_2O_3$ (X = 0, 0.25, 0.5, 0.75, and 1.0 wt%) catalysts, as shown in Fig. 3.19. It is known that $Pt/Sn/Al_2O_3$ catalyst showed two reduction bands; a reduction band at around 250 ^oC is ascribed to the reduction of Pt oxide species, while a broad reduction band at around 500 ^oC is due to the partial reduction of tin oxide species [53,80,81]. When zinc is added into $Pt/Sn/Al_2O_3$ catalyst, $Pt/Sn/XZn/Al_2O_3$ catalysts showed an obviously different reduction band within the range of 260-290 ^oC. This reduction band might be assigned to the reduction of Pt oxide, a small fraction of Sn oxide, and zinc oxide species. However, the reduction band at around 500 ^oC was not clear in our $Pt/Sn/XZn/Al_2O_3$ catalysts. In the $Pt/Sn/XZn/Al_2O_3$ (X = 0, 0.25, and 0.5 wt%) catalysts, the reduction peak temperature increased with increasing zinc content. On the other hand, the reduction peak temperature decreased with increasing zinc content in the $Pt/Sn/XZn/Al_2O_3$ (X = 0.5, 0.75, and 1.0 wt%) catalysts. In summary, the major reduction peak temperature within the range of 260-290 ^oC showed a volcano-shaped trend with respect to zinc content. The reduction peak temperature of the catalysts decreased in the order of $Pt/Sn/0.5Zn/Al_2O_3$ > $Pt/Sn/0.75Zn/Al_2O_3$ > $Pt/Sn/0.25Zn/Al_2O_3$ > $Pt/Sn/1.0Zn/Al_2O_3$ > $Pt/Sn/Al_2O_3$. This trend was well consistent with the trend of catalytic activity (Fig. 3.18).

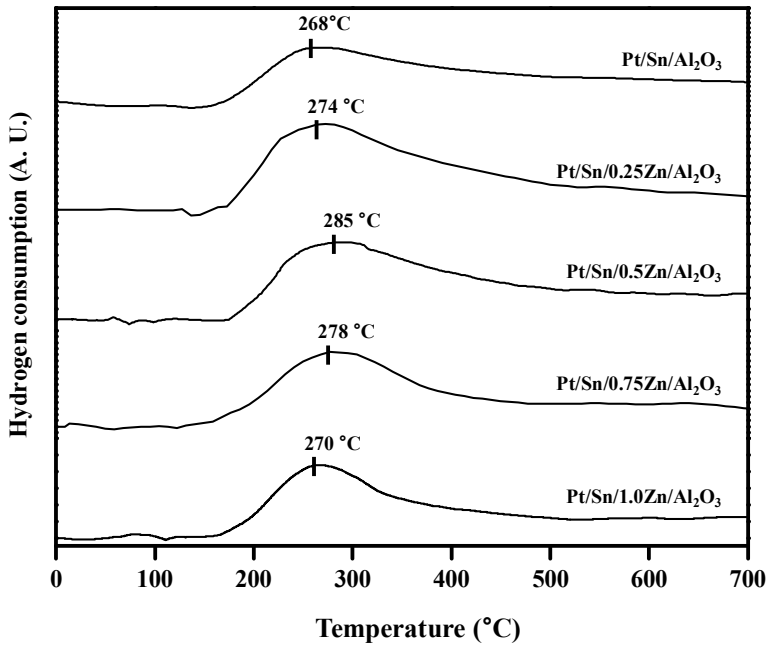

Fig. 3.19. TPR profiles of $Pt/Sn/XZn/Al_2O_3$ catalysts.

3.4.4. Pt dispersion and Pt surface area in the reduced Pt/Sn/XZn/Al_2O_3 catalysts

Hydrogen chemisorption measurements were conducted to determine the Pt dispersion and Pt surface area of the reduced Pt/Sn/XZn/Al_2O_3 (X = 0, 0.25, 0.5, 0.75, and 1.0 wt%) catalysts. Hydrogen chemisorption results for the reduced catalysts are listed in Table 3.7. The amount of hydrogen uptake on the reduced catalysts decreased in the order of Pt/Sn/0.5Zn/Al_2O_3 > Pt/Sn/0.75Zn/Al_2O_3 > Pt/Sn/0.25Zn/Al_2O_3 > Pt/Sn/1.0Zn/Al_2O_3 > Pt/Sn/Al_2O_3. As a consequence, Pt dispersion and Pt surface area decreased in the order of Pt/Sn/0.5Zn/Al_2O_3 > Pt/Sn/0.75Zn/Al_2O_3 > Pt/Sn/0.25Zn/Al_2O_3 > Pt/Sn/1.0Zn/Al_2O_3 > Pt/Sn/Al_2O_3. Pt particle size increased in the order of Pt/Sn/0.5Zn/Al_2O_3 < Pt/Sn/0.75Zn/Al_2O_3 < Pt/Sn/0.25Zn/Al_2O_3 < Pt/Sn/1.0Zn/Al_2O_3 < Pt/Sn/Al_2O_3. These trends were well consistent with the trends of catalytic activity (Fig. 3.18) and TPR results (Fig. 3.19). When the metal-support interaction was strong, Pt species were well dispersed on the support and Pt surface area increased by decreasing Pt particle size. In other words, the addition of certain amount of zinc increased Pt dispersion and Pt surface area. The highest Pt dispersion and Pt surface area was observed over Pt/Sn/0.5Zn/Al_2O_3 catalyst. This implies that the presence of certain amount of zinc in the vicinity of Pt particles can lead to a decrease in the number of accessible Pt sites, which is favorable for the improvement of metallic Pt dispersion [82]. That is, an optimal amount of zinc served as an efficient spacer to reduce the size of platinum ensembles as tin acted as a spacer in the

Pt-Sn catalyst [83,84].

Table 3.7

Hydrogen chemisorption results for reduced Pt/Sn/XZn/Al_2O_3 (X = 0, 0.25, 0.5, 0.75, and 1.0 wt%) catalysts

Catalyst	Pt dispersion (%)[a]	Pt surface area (m^2/g)[a]	Average Pt particle size (nm)[a]
Pt/Sn/Al_2O_3	30.0	73.8	3.8
Pt/Sn/0.25Zn/Al_2O_3	33.8	83.6	3.3
Pt/Sn/0.5Zn/Al_2O_3	47.2	116.4	2.4
Pt/Sn/0.75Zn/Al_2O_3	43.2	106.4	2.6
Pt/Sn/1.0Zn/Al_2O_3	32.0	80.4	3.5

[a] Calculated by assuming a stoichiometry factor of H/Pt =1.

3.4.5. Electronic effect in the reduced Pt/Sn/XZn/Al_2O_3 catalysts

To investigate the chemical state of metal components, X-ray photoelectron spectroscopy (XPS) was carried out. XPS spectra of Zn $2p_{3/2}$ levels for the reduced catalysts are shown in Fig. 3.20, and the measured binding energies of Pt $4f_{7/2}$, Sn $3d_{5/2}$, and Zn $2p_{3/2}$ are summarized in Table 3.8. All the catalysts showed binding energy of single Pt $4f_{7/2}$ component at 71.7-72.3 eV, indicating the presence of zerovalent platinum [85]. The Sn $3d_{5/2}$ peak was decomposed into two components. The component at lower binding energy 485.3-486.2 eV, which corresponds to alloyed tin, and that located at binding energy 487.1-487.6 eV could be assigned to oxidized species of tin (II, IV) [86-87]. As shown in Fig. 3.20, XPS spectrum of Zn $2p_{3/2}$ level for each reduced catalyst is different. In case of Pt/Sn/XZn/Al_2O_3 (X = 0.25 and 0.5) catalysts, Zn almost exists as ZnO species. When the amount of Zn is excess, however, Zn exists as metallic Zn and ZnO species. It is inferred that ZnO can be reduced to metallic zinc, which results in the formation of PtZn alloy. As Pt-Zn alloy is formed, alloyed Zn atoms can increase the electron density of Pt sites and binding energy of Pt $4f_{7/2}$ decreases due to electropositive nature of Zn [88]. Thus, this modification of Pt electronic character leads to decrease in hydrogen adsorption strength and the PtZn alloy operate as an inactive phase for hydrogen chemisorption and dehydrogenation of paraffins [54]. This may be the reason for the decrease of the Pt dispersion and the catalytic performance, when the amount of zinc is excess. Based on these results, schematic model of Pt/Sn/Zn/Al_2O_3 catalysts is proposed in Fig. 3.21.

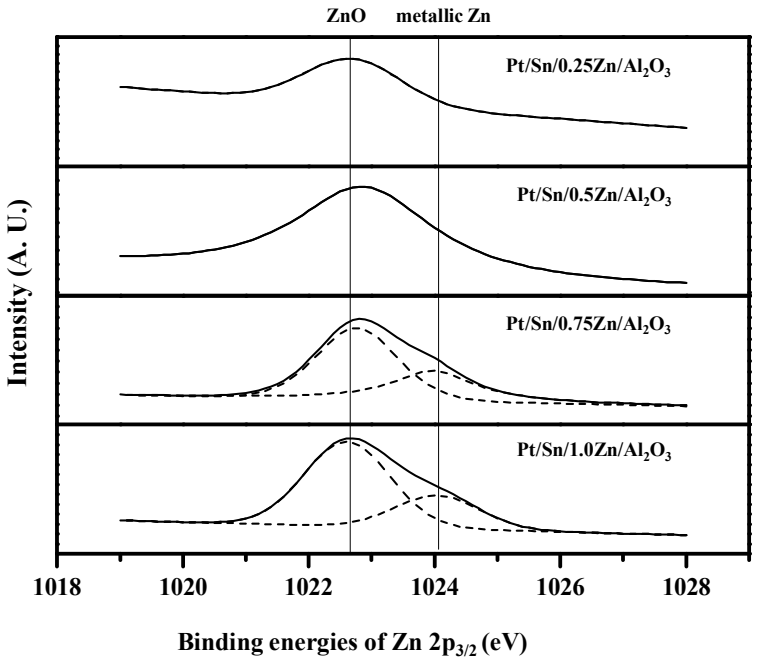

Fig. 3.20. XPS spectra of Zn $2p_{3/2}$ level of Pt/Sn/XZn/Al_2O_3 catalysts reduced at 570 ^oC for 3 h.

Table 3.8

Binding energies of Pt $4f_{7/2}$, Sn $3d_{5/2}$, and Zn $2p_{3/2}$ of Pt/Sn/XZn/Al_2O_3 catalysts

Catalyst	Binding energy of Pt $4f_{7/2}$ (eV)	Binding energy of Sn $3d_{5/2}$ (eV)	Binding energy of Zn $2p_{3/2}$ (eV)
Pt/Sn/Al_2O_3	72.1	487.1 486.2	-
Pt/Sn/0.25Zn/Al_2O_3	72.1	487.1 486.1	1022.7
Pt/Sn/0.5Zn/Al_2O_3	72.0	487.0 486.6	1022.6
Pt/Sn/0.75Zn/Al_2O_3	71.7	488.1 486.5	1024.0 1022.8
Pt/Sn/1.0Zn/Al_2O_3	71.7	487.4 486.2	1024.0 1022.6

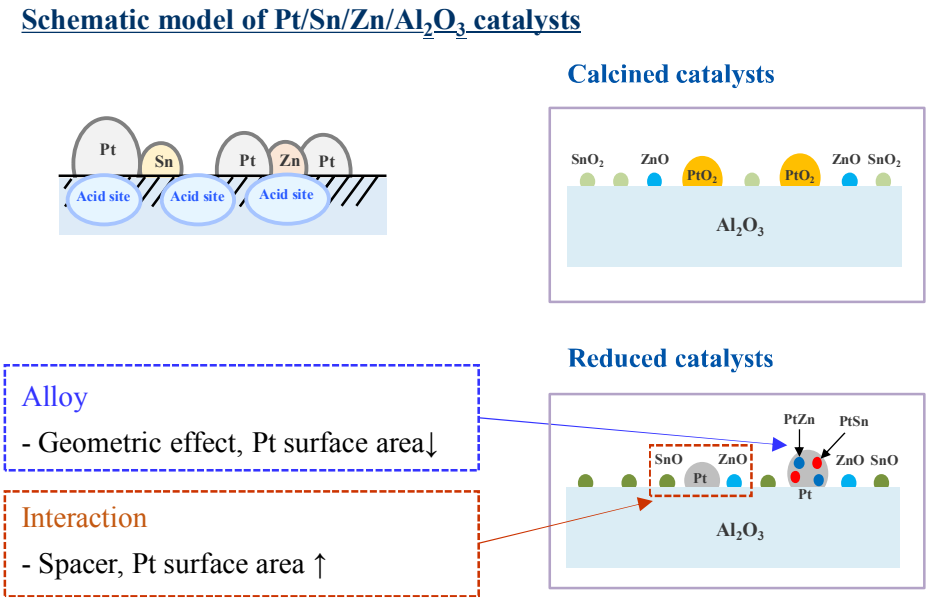

Fig. 3.21. Schematic model of $Pt/Sn/Zn/Al_2O_3$ catalysts.

3.4.6. Correlation between catalytic performance and catalytic properties

Fig. 3.22 shows the correlations between catalytic performance and catalytic properties. Yield for TDP increased with increasing TPR peak temperature (with increasing metal-support interaction) and with increasing Pt surface area. The correlations clearly show that metal-support interaction and Pt surface area served as important factors determining the catalytic performance of $Pt/Sn/XZn/Al_2O_3$ catalysts. Among the catalysts tested, $Pt/Sn/0.5Zn/Al_2O_3$ catalyst, which retained the strongest metal-support interaction and the highest Pt surface area, exhibited the best catalytic performance in the direct dehydrogenation of n-butane. Suitable addition of Zn (0.5 wt%) can reduce the size of the platinum ensembles by geometric effect, thus increasing the Pt surface area. However, when the content of Zn is excessive, the character of active metal has been modified by the formation of PtZn alloy and the decrease of Pt surface area is observed.

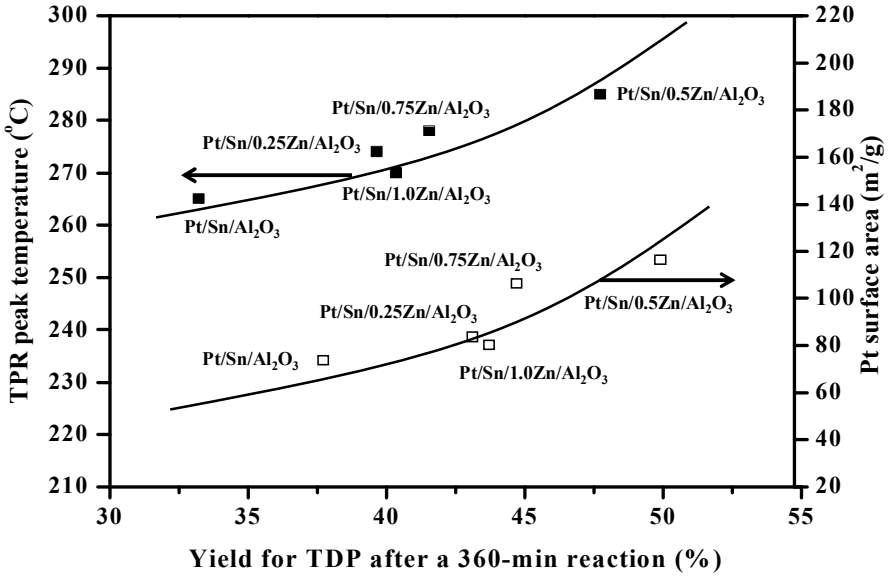

Fig. 3.22. Correlations between yield for TDP after a 360 min-reaction and TPR peak temperature, and between yield for TDP after a 360 min-reaction and Pt surface area.

3.5. Characterization and catalytic performance of $Pt/Sn/Al_2O_3$ (X) catalysts prepared by various preparation methods

3.5.1. Formation of $Pt/Sn/Al_2O_3$ (X) catalysts

Successful formation of $Pt/Sn/Al_2O_3$ (X) catalysts was confirmed by XRD and ICP-AES measurements. Fig. 3.23 shows the XRD patterns of reduced $Pt/Sn/Al_2O_3$ (X) catalysts. Crystalline phase of Al_2O_3 was identified using JCPDS. As shown in Fig. 3.23, characteristic diffraction peaks of γ-Al_2O_3 were observed in all the $Pt/Sn/Al_2O_3$ (X) catalysts. XRD peaks corresponding to Pt and Sn were not detected, indicating that Pt and Sn species were finely dispersed on the support. This result was well consistent with the previous works in a sense that γ-Al_2O_3 peaks were only detected in the XRD patterns of $Pt/Sn/Al_2O_3$ catalysts with low Pt and Sn contents [78,79]. Pt and Sn contents in the $Pt/Sn/Al_2O_3$ (X) catalysts are summarized in Table 3.9. The measured Pt and Sn contents were in good agreement with the designed values. These results indicate that $Pt/Sn/Al_2O_3$ (X) catalysts were successfully prepared in this work. Physicochemical properties of the catalysts are also summarized in Table 3.9. BET surface area, pore volume of $Pt/Sn/Al_2O_3$ (X) catalysts decreased in the order of $Pt/Sn/Al_2O_3$ (ES) > $Pt/Sn/Al_2O_3$ (AS) > $Pt/Sn/Al_2O_3$ (P) > $Pt/Sn/Al_2O_3$ (C). Among the catalysts examined, $Pt/Sn/Al_2O_3$ (ES) catalyst retained the highest surface area and the

largest pore volume. From these results, it is inferred that the preparation method of support strongly affects the physicochemical properties of $Pt/Sn/Al_2O_3$ (X) catalysts.

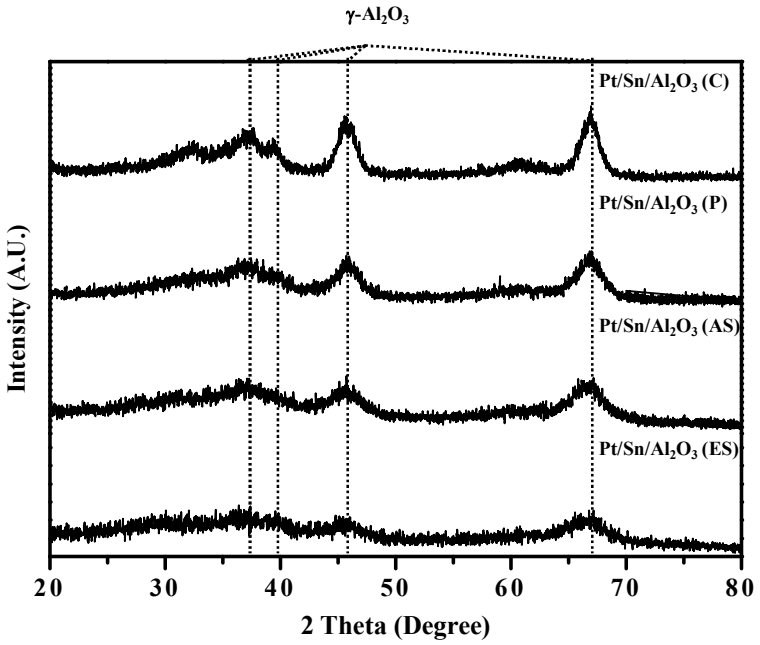

Fig. 3.23. XRD patterns of $Pt/Sn/Al_2O_3$ (X) catalysts reduced at 570 ^oC for 3 h.

Table 3.9

Metal content, BET surface area, pore volume, and average pore diameter of $Pt/Sn/Al_2O_3$ (X) catalysts

Catalyst	Pt content (wt%)[a]	Sn content (wt%)[a]	BET surface area (m^2/g)[b]	Pore volume (cm^3/g)[c]	Average pore diameter (nm)[d]
$Pt/Sn/Al_2O_3$ (C)	1.0	1.1	185	0.48	10.4
$Pt/Sn/Al_2O_3$ (P)	1.0	1.1	190	0.35	8.2
$Pt/Sn/Al_2O_3$ (AS)	1.0	1.1	233	0.50	7.2
$Pt/Sn/Al_2O_3$ (ES)	1.0	1.1	275	0.55	7.2

[a] Determined by ICP-AES analyses.

[b] Calculated by the BET equation.

[c] BJH desorption pore volume.

[d] BJH desorption average pore diameter.

3.5.2. Catalytic performance of $Pt/Sn/Al_2O_3$ (X) catalysts

Fig. 3.24 shows the catalytic performance of $Pt/Sn/Al_2O_3$ (X) catalysts with time on stream in the direct dehydrogenation of n-butane at 550 °C. All the $Pt/Sn/Al_2O_3$ (X) catalysts exhibited a slight deactivation during the direct dehydrogenation reaction. However, the catalytic performance of $Pt/Sn/Al_2O_3$ (X) catalysts was strongly influenced by the preparation method of support. Detailed catalytic performance of $Pt/Sn/Al_2O_3$ (X) catalysts obtained after a 360 min-reaction is also shown in Fig. 3.24. As shown in Fig 3.24, yield for TDP (total dehydrogenation products, n-butenes and 1,3-butadiene) after a 360 min-reaction decreased in the order of $Pt/Sn/Al_2O_3$ (ES) > $Pt/Sn/Al_2O_3$ (AS) > $Pt/Sn/Al_2O_3$ (P) > $Pt/Sn/Al_2O_3$ (C). Among the catalysts tested, $Pt/Sn/Al_2O_3$ (ES) catalyst showed the best catalytic performance in terms of yield for TDP in the direct dehydrogenation of n-butane.

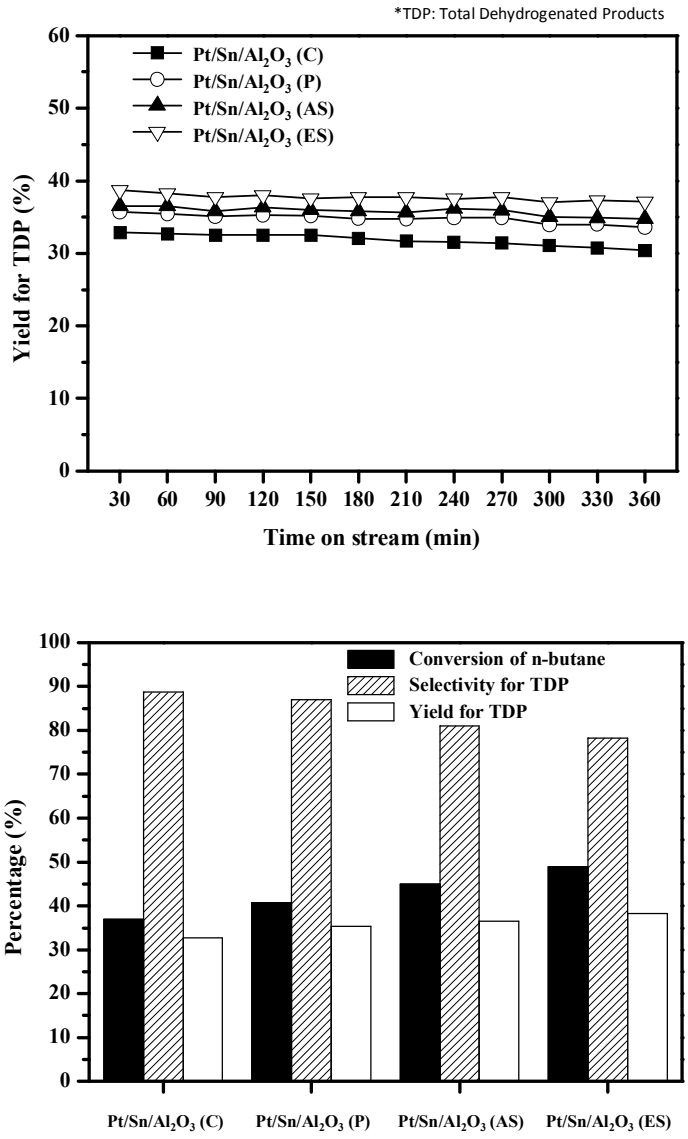

Fig. 3.24. Catalytic performance of $Pt/Sn/Zn/Al_2O_3$ (X) catalysts.

3.5.3. TPR results of $Pt/Sn/Al_2O_3$ (X) catalysts

TPR measurements were carried out to investigate the reduction behavior of metal species and to examine the interaction between metal species and support in the $Pt/Sn/Al_2O_3$ (X) catalysts. Fig. 3.25 shows the TPR profiles of $Pt/Sn/Al_2O_3$ (X) catalysts. All the $Pt/Sn/Al_2O_3$ (X) catalysts exhibited a broad reduction bands at around 260~280 ^oC with a shoulder at around 400 ^oC. The major reduction band appearing at low temperature was attributed to the reduction of Pt oxide species interacted with alumina, while the minor shoulder appearing at high temperature was due to the partial reduction of Sn^{4+} to Sn^{2+} and Sn^{2+} to Sn^0 [53,80,81].

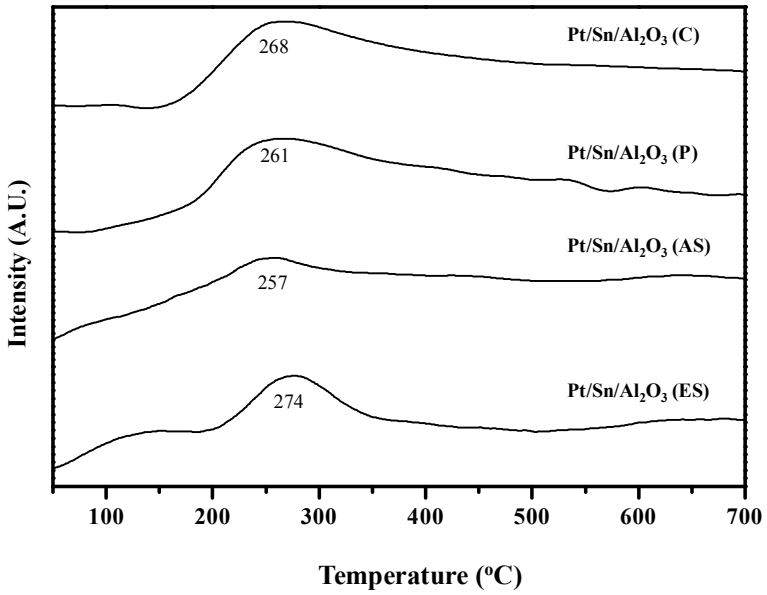

Fig. 3.25. TPR profiles of $Pt/Sn/Al_2O_3$ (X) catalysts.

3.5.4. Pt dispersion and Pt surface area of $Pt/Sn/Al_2O_3$ (X) catalysts

CO chemisorption measurements were conducted in order to determine the platinum dispersion and platinum surface area in the $Pt/Sn/Al_2O_3$ (X) catalysts. CO chemisorption results for reduced $Pt/Sn/Al_2O_3$ (X) catalysts are listed in Table 3.10. The platinum dispersion and platinum surface area of $Pt/Sn/Al_2O_3$ (X) catalysts decreased in the order of $Pt/Sn/Al_2O_3$ (ES) > $Pt/Sn/Al_2O_3$ (AS) > $Pt/Sn/Al_2O_3$ (P) > $Pt/Sn/Al_2O_3$ (C). Platinum particle size of the catalysts increased in the order of $Pt/Sn/Al_2O_3$ (ES) < $Pt/Sn/Al_2O_3$ (AS) < $Pt/Sn/Al_2O_3$ (P) < $Pt/Sn/Al_2O_3$ (C). Among the catalysts examined, $Pt/Sn/Al_2O_3$ (ES) catalyst exhibited the highest platinum dispersion, the highest platinum surface area, and the smallest platinum particle size. This might be due to the highest surface area and the largest pore volume of $Pt/Sn/Al_2O_3$ (ES) catalyst (Table 3.9), which effectively suppressed the aggregation of platinum species during the impregnation step.

Table 3.10

CO chemisorption results for reduced $Pt/Sn/Al_2O_3$ (X) catalysts

Catalyst	Pt dispersion (%)[a]	Pt surface area (m^2/g)[a]	Average Pt particle size (nm)[a]
$Pt/Sn/Al_2O_3$ (C)	44.0	108.6	2.6
$Pt/Sn/Al_2O_3$ (P)	50.6	125.0	2.2
$Pt/Sn/Al_2O_3$ (AS)	55.6	137.4	2.0
$Pt/Sn/Al_2O_3$ (ES)	65.3	161.3	1.7

[a] Calculated by assuming a stoichiometry factor of CO/Pt =1.

3.5.5. Correlation between catalytic performance and Pt surface area

Fig. 3.26 shows the correlation between platinum surface area and catalytic performance in the direct dehydrogenation of n-butane. It is interesting to note that yield for TDP increased with increasing platinum surface area. Although platinum surface area of the catalyst is not the sole factor determining the catalytic performance in the direct dehydrogenation of n-butane, it can serve as an important correlating parameter for the catalytic performance in the direct dehydrogenation of n-butane. Among the catalysts tested, $Pt/Sn/Al_2O_3$ (ES) catalyst with the highest platinum surface area showed the best catalytic performance in the direct dehydrogenation of n-butane.

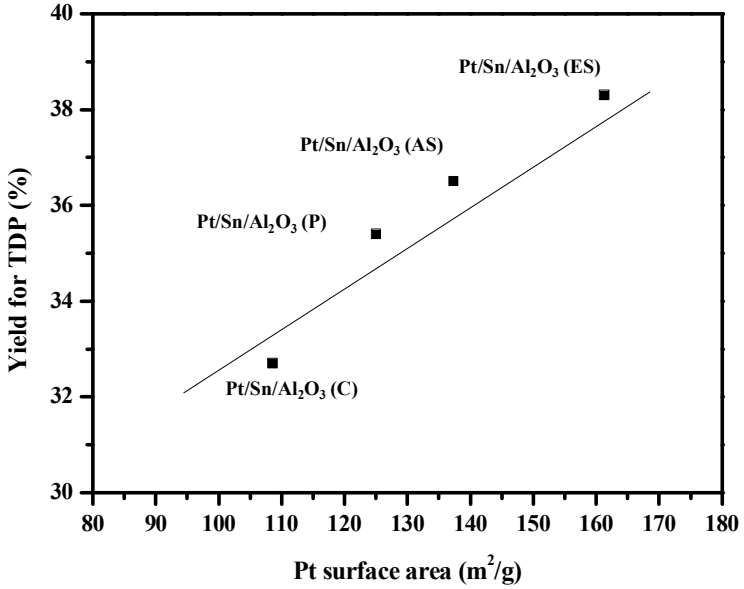

Fig. 3.26. A correlation between yield for TDP after 360 min-reaction and Pt surface area of $Pt/Sn/Al_2O_3$ (X) catalysts.

3.6. Characterization and catalytic performance of $Pt/Sn/Al_2O_3$-X prepared by an epoxide-driven sol-gel method and a sequential impregnation method

3.6.1. Physicochemical properties of $Pt/Sn/Al_2O_3$-X catalysts

Textural properties of $Pt/Sn/Al_2O_3$-X catalysts were examined by nitrogen adsorption-desorption isotherm measurements. Fig. 3.27 shows the nitrogen adsorption-desorption isotherms of $Pt/Sn/Al_2O_3$-X catalysts. $Pt/Sn/Al_2O_3$-X (X = 600, 700, 800, 900, and 1000) catalysts exhibited IV-type isotherms with H2-type hysteresis loops, indicating the existence of well-developed framework mesopores [89,90]. It is interesting to note that hysteresis loops of $Pt/Sn/Al_2O_3$-X catalysts shifted to the higher relative pressure with increasing calcination temperature of alumina. It was also observed that average pore size of $Pt/Sn/Al_2O_3$-X (X = 600, 700, 800, 900, and 1000) catalysts increased with increasing calcination temperature of alumina, as shown in Fig. 3.27. Typically, alumina particles are strongly bonded to others by hydrogen bond between Al-OH groups. With increasing calcination temperature, these Al-OH groups are removed, resulting in an increase of average pore size [91-93]. On the other hand, nitrogen adsorption-desorption isotherm of $Pt/Sn/Al_2O_3$-1100 catalyst was quite different from that of $Pt/Sn/Al_2O_3$-X (X = 600, 700, 800, 900, and 1000) catalysts. Hysteresis loop and pore size distribution were not observable in the $Pt/Sn/Al_2O_3$-1100 catalyst.

Detailed physicochemical of $Pt/Sn/Al_2O_3$-X catalysts are summarized in Table 3.11. BET surface area and pore volume of $Pt/Sn/Al_2O_3$-X catalysts decreased with increasing calcination temperature of alumina, while average pore size of $Pt/Sn/Al_2O_3$-X catalysts increased with increasing calcination temperature of alumina. The measured Pt and Sn contents were in good agreement with the designed values. These results indicate that $Pt/Sn/Al_2O_3$-X catalysts were successfully prepared in this work.

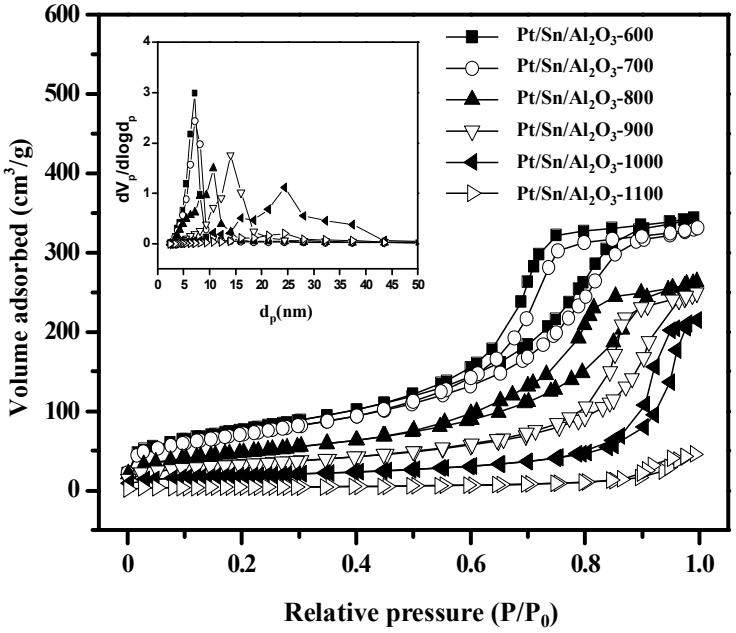

Fig. 3.27. Nitrogen adsorption-desorption isotherms and pore size distribution of $Pt/Sn/Al_2O_3$-X catalysts.

Table 3.11

Metal content, BET surface area, pore volume, and average pore diameter of $Pt/Sn/Al_2O_3$-X catalysts

Catalyst	Pt content (wt%)[a]	Sn content (wt%)[a]	BET surface area (m^2/g)[b]	Pore volume (cm^3/g)[c]	Average pore diameter (nm)[d]
$Pt/Sn/Al_2O_3$-600	0.9	1.2	275	0.55	7.18
$Pt/Sn/Al_2O_3$-700	0.9	1.1	254	0.52	7.18
$Pt/Sn/Al_2O_3$-800	0.9	1.1	172	0.41	10.7
$Pt/Sn/Al_2O_3$-900	0.9	1.1	115	0.38	14.0
$Pt/Sn/Al_2O_3$-1000	1.0	1.1	64	0.32	24.4
$Pt/Sn/Al_2O_3$-1100	1.0	1.2	1	-[e]	-[e]

[a] Determined by ICP-AES analyses.

[b] Calculated by the BET equation.

[c] BJH desorption pore volume.

[d] BJH desorption average pore diameter.

[e] Not measureable due to very small pore volume.

3.6.2. Crystalline structure of reduced $Pt/Sn/Al_2O_3$-X catalysts

Crystalline phases of reduced $Pt/Sn/Al_2O_3$-X catalysts were examined by XRD measurements as shown in Fig. 3.28. $Pt/Sn/Al_2O_3$-X (X = 600 and 700) catalysts showed the characteristic diffraction peaks of γ-alumina. $Pt/Sn/Al_2O_3$-X (X = 800 and 900) catalysts retained the mixed phase of γ-alumina and θ-alumina, indicating that $Pt/Sn/Al_2O_3$-X (X = 800 and 900) catalysts were in the transition state between γ-alumina and θ-alumina. $Pt/Sn/Al_2O_3$-1000 catalyst showed the mixed phase of θ-alumina and α-alumina, indicating that $Pt/Sn/Al_2O_3$-1000 catalyst was in the middle of phase transformation from θ-alumina to α-alumina. On the other hand, $Pt/Sn/Al_2O_3$-1100 catalyst exhibited the diffraction patterns of α-alumina. These results were well consistent with the previous results reporting that phase transformation of transition alumina occured in the sequence of γ→δ→θ→α within temperature of 600-1100 ^oC [92-95].

It is noticeable that no characteristic diffraction peaks corresponding to platinum and tin were observed in the $Pt/Sn/Al_2O_3$-X (X = 600, 700, 800, and 900) catalysts. This result indicates that platinum and tin species were less crystallized or finely dispersed on the surface of $Pt/Sn/Al_2O_3$-X (X = 600, 700, 800, and 900) catalysts. On the other hand, $Pt/Sn/Al_2O_3$-X (X = 1000 and 1100) catalysts showed the additional diffraction peaks of platinum-tin compounds. Thus, it is reasonable to expect that platinum-tin compounds were more crystallized or alloyed in the $Pt/Sn/Al_2O_3$-X (X = 1000 and 1100) catalysts due to low surface area and small pore volume of θ-alumina and/or

α-alumina [96].

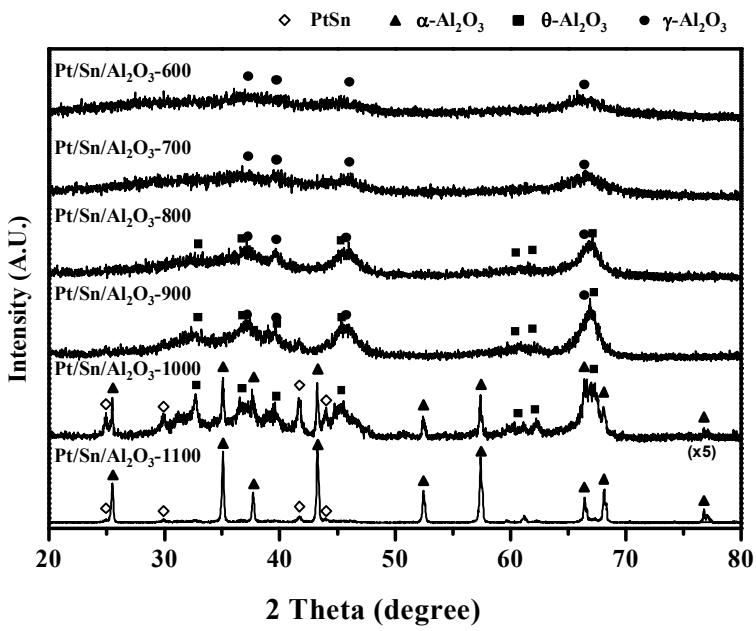

Fig. 3.28. XRD patterns of reduced $Pt/Sn/Al_2O_3$-X catalysts.

3.6.3. TPR results of $Pt/Sn/Al_2O_3$-X catalysts

TPR measurements were carried out to investigate the interaction between metal species and support and to examine the reduction behavior of metal species in the $Pt/Sn/Al_2O_3$-X catalysts. Fig. 3.29 shows the TPR profiles of $Pt/Sn/Al_2O_3$-X catalysts. $Pt/Sn/Al_2O_3$-X (X = 600, 700, 800, and 900) catalysts exhibited a broad reduction band at around 270-300 ^oC with a shoulder at around 400 ^oC. The major reduction band appearing at low temperature was attributed to the reduction of Pt oxide species interacted with alumina, while the minor shoulder appearing at high temperature was due to the partial reduction of Sn^{4+} to Sn^{2+} and/or Sn^{2+} to Sn^0 [80,97,98]. On the other hand, $Pt/Sn/Al_2O_3$-X (X = 1000 and 1100) catalysts showed two reduction bands at around 300 ^oC and 445 ^oC. Low-temperature reduction peak was attributed to the reduction of Pt oxide species, while high-temperature reduction peak was ascribed to the reduction of Sn^{2+} to Sn^0 strongly interacted with alumina support [96-98]. It was found that the reduction temperature of Pt species shifted toward higher temperature and the amount of hydrogen consumption decreased with increasing calcination temperature of alumina, suggesting that the interaction between Pt and support became strong and the reduction of Pt species became more difficult with increasing calcination temperature of alumina. This is because the sintering of Pt particles was remarkable with increasing calcination temperature of alumina, which decreased the amount of hydrogen consumption [99]. $Pt/Sn/Al_2O_3$-X (X = 1000 and 1100) catalysts showed large reduction peaks of Sn species,

indicating that much amount of Sn species was reduced in a form of zerovalent tin or metallic tin of platinum-tin compound. These results were well consistent with the XRD results (Fig. 3.28).

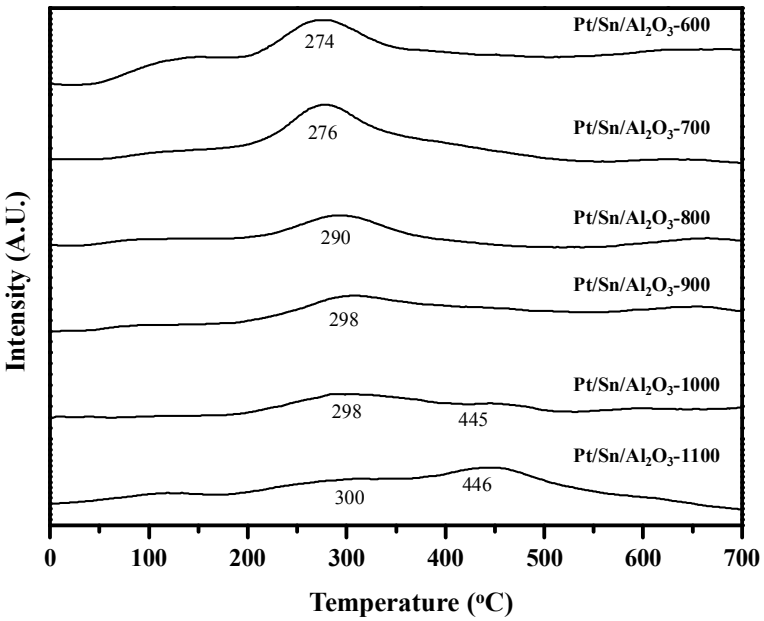

Fig. 3.29. TPR profiles of $Pt/Sn/Al_2O_3$-X catalysts.

3.6.4. Catalytic performance of $Pt/Sn/Al_2O_3$-X catalysts

Fig. 3.30 shows the yield for TDP over $Pt/Sn/Al_2O_3$-X catalysts with time on stream in the direct dehydrogenation of n-butane at 550 °C. All the $Pt/Sn/Al_2O_3$-X catalysts exhibited a slight deactivation during the direct dehydrogenation reaction. The yield for TDP over $Pt/Sn/Al_2O_3$-X catalysts strongly depended on the calcination temperature of alumina. Detailed catalytic performance of $Pt/Sn/Al_2O_3$-X catalysts obtained after a 60 min-reaction is also shown in Fig. 3.30. It was found that conversion of n-butane decreased with increasing calcination temperature of alumina, while selectivity for TDP increased with increasing calcination temperature of alumina. As a consequence, yield for TDP showed a volcano-shaped trend with respect to calcination temperature of alumina. Among the catalyst tested, $Pt/Sn/Al_2O_3$-700 catalyst showed the best catalytic performance in terms of yield for TDP.

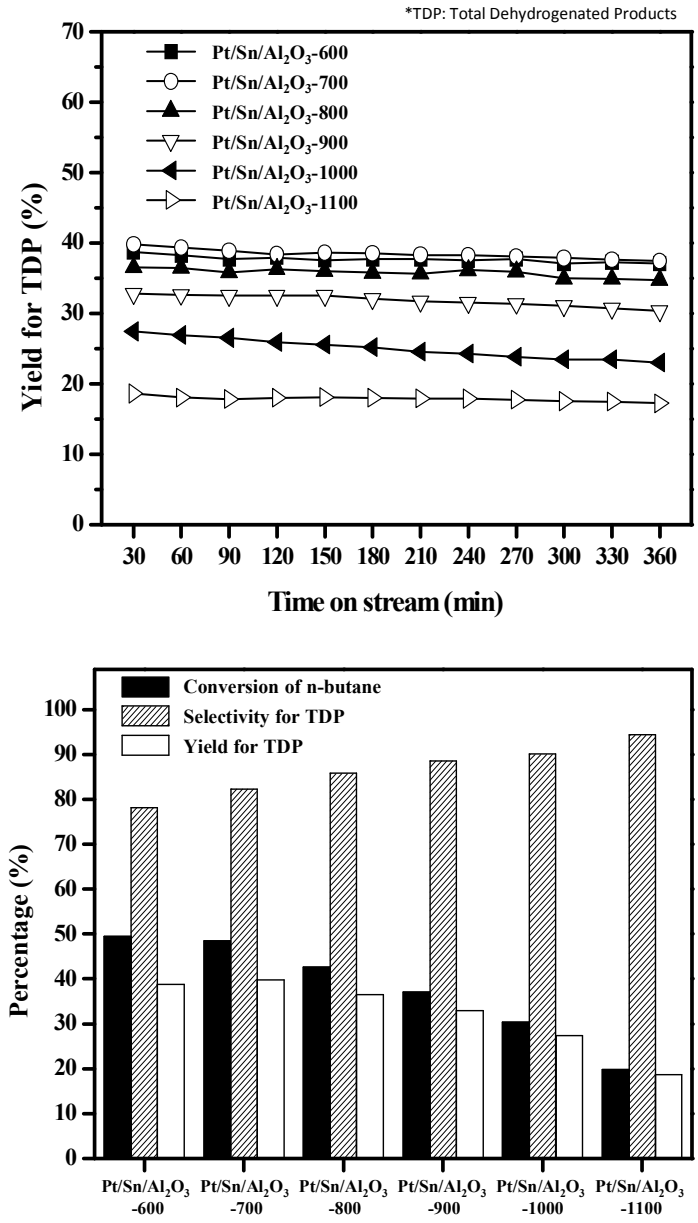

Fig. 3.30. Catalytic performance of $Pt/Sn/Al_2O_3$-X catalysts.

3.6.5. Platinum and acid sites of $Pt/Sn/Al_2O_3$-X catalysts

To determine the platinum dispersion and platinum surface area in the $Pt/Sn/Al_2O_3$-X catalysts, CO chemisorption measurements were conducted. CO chemisorption results for reduced $Pt/Sn/Al_2O_3$-X catalysts are listed in Table 3.12. It was found that platinum dispersion and platinum surface area of $Pt/Sn/Al_2O_3$-X catalysts decreased with increasing calcination temperature of alumina, while platinum particle size of the catalysts increased with increasing calcination temperature of alumina. This result was closely related to the trends of BET surface area and pore volume of $Pt/Sn/Al_2O_3$-X catalysts (Table 3.11) with regard to calcination temperature of alumina. Fig. 3.31 shows the HR-TEM images of $Pt/Sn/Al_2O_3$-X catalysts reduced at 570 ^oC. $Pt/Sn/Al_2O_3$-600 catalyst showed small platinum and tin species (less than 5 nm), while $Pt/Sn/Al_2O_3$-1100 catalyst retained large platinum-tin aggregates (more than 30 nm). HR-TEM images also support that platinum species were more finely dispersed with decreasing calcination temperature of alumina in the $Pt/Sn/Al_2O_3$-X catalysts.

In order to investigate the effect of calcination temperature of alumina on the acidity of $Pt/Sn/Al_2O_3$-X catalysts, NH_3-TPD experiments were conducted. Fig. 3.32 shows the NH_3-TPD profiles of reduced $Pt/Sn/Al_2O_3$-X catalysts. Acidity of $Pt/Sn/Al_2O_3$-X catalysts calculated from TPD peak area is summarized in Table 3.13. Acidity of the catalysts was strongly influenced by calcination temperature of alumina. That is, acidity of $Pt/Sn/Al_2O_3$-X catalysts decreased with increasing calcination temperature of alumina.

Table 3.12

CO chemisorption results for $Pt/Sn/Al_2O_3$-X catalysts reduced at 570 ^oC for 3 h

Catalyst	Pt dispersion (%)[a]	Pt surface area (m^2/g)[a]	Pt partice size (nm)[a]
$Pt/Sn/Al_2O_3$-600	65.3	161.3	1.7
$Pt/Sn/Al_2O_3$-700	63.9	157.9	1.7
$Pt/Sn/Al_2O_3$-800	32.3	79.8	3.5
$Pt/Sn/Al_2O_3$-900	7.4	18.2	15.3
$Pt/Sn/Al_2O_3$-1000	5.2	12.9	21.6
$Pt/Sn/Al_2O_3$-1100	2.9	7.4	37.9

[a] Calculated by assuming stoichiometry factor of CO/Pt =1.

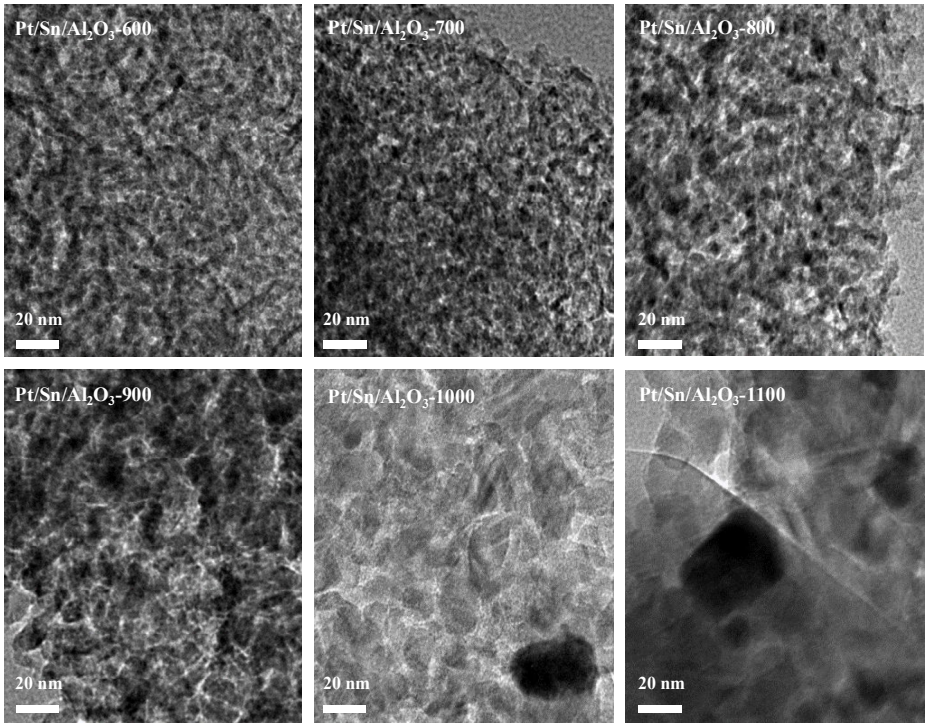

Fig. 3.31. HR-TEM image of reduced $Pt/Sn/Al_2O_3$-X catalysts.

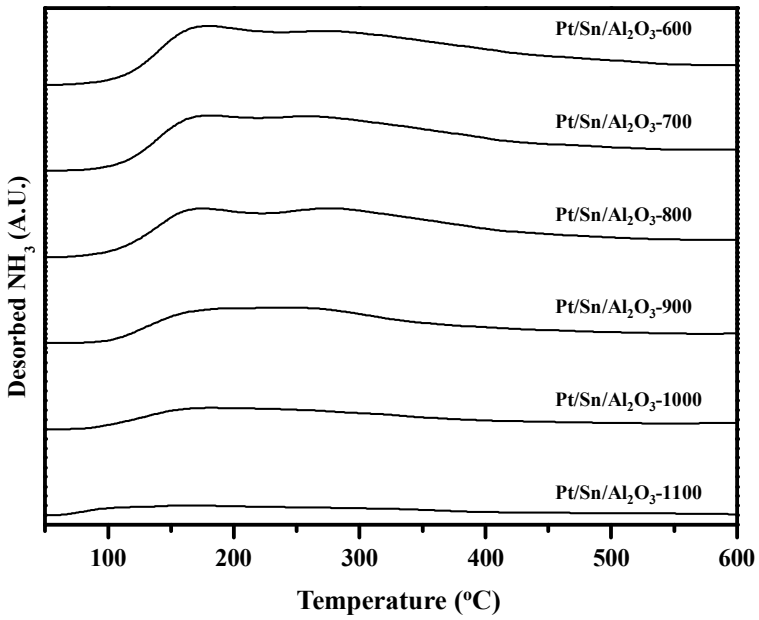

Fig. 3.32. NH_3-TPD profiles of $Pt/Sn/Al_2O_3$-X catalysts.

Table 3.13

Acidity of $Pt/Sn/Al_2O_3$-X catalysts reduced at 570 ^oC for 3 h

Catalyst	Acidity (mmol/g-catalyst)
$Pt/Sn/Al_2O_3$-600	0.951
$Pt/Sn/Al_2O_3$-700	0.917
$Pt/Sn/Al_2O_3$-800	0.840
$Pt/Sn/Al_2O_3$-900	0.514
$Pt/Sn/Al_2O_3$-1000	0.321
$Pt/Sn/Al_2O_3$-1100	0.151

3.6.6. Effect of platinum surface area and acidity on catalytic performance

As described earlier, platinum surface area of the catalyst is one of the crucial factors determining the catalytic performance in the direct dehydrogenation of n-butane. Thus, an attempt has been made to correlate platinum surface area with catalytic performance of $Pt/Sn/Al_2O_3$-X catalysts. Fig. 3.33 (a) shows the correlation between platinum surface area and conversion of n-butane over $Pt/Sn/Al_2O_3$-X catalysts. Conversion of n-butane increased with increasing platinum surface area of the catalyst. It is generally accepted that dehydrogenation activity of the catalyst increases with increasing platinum surface area of the catalyst [49,100]. Therefore, the decrease of n-butane conversion over $Pt/Sn/Al_2O_3$-X catalysts with increasing calcination temperature of alumina was mainly due to the decrease of platinum surface area of the catalyst. It is known that selectivity for TDP is influenced by acidity of the catalyst, as shown in Fig. 1.5. Fig. 3.33 (b) shows the correlation between acidity and selectivity for TDP. The correlation clearly shows that selectivity for TDP decreased with increasing acidity of the catalyst. It was reported that the increased selectivity for TDP with decreasing acidity of $Pt/Sn/Al_2O_3$-X catalysts was attributed to the decrease of side reactions such as coke formation, isomerization, and cracking reaction [49,101].

From these results, it can be summarized that conversion of n-butane and selectivity for TDP over $Pt/Sn/Al_2O_3$-X catalysts were closely related to

platinum surface area and acidity of the catalyst, respectively (Fig. 3.33). In this work, yield for TDP was obtained by multiplying conversion of n-butane and selectivity for TDP. As a result, maximum catalytic performance in terms of yield for TDP could be obtained over $Pt/Sn/Al_2O_3$-700 catalyst (Fig. 3.30). Based on these results, schematic model of $Pt/Sn/Al_2O_3$-X catalysts is proposed in Fig. 3.34.

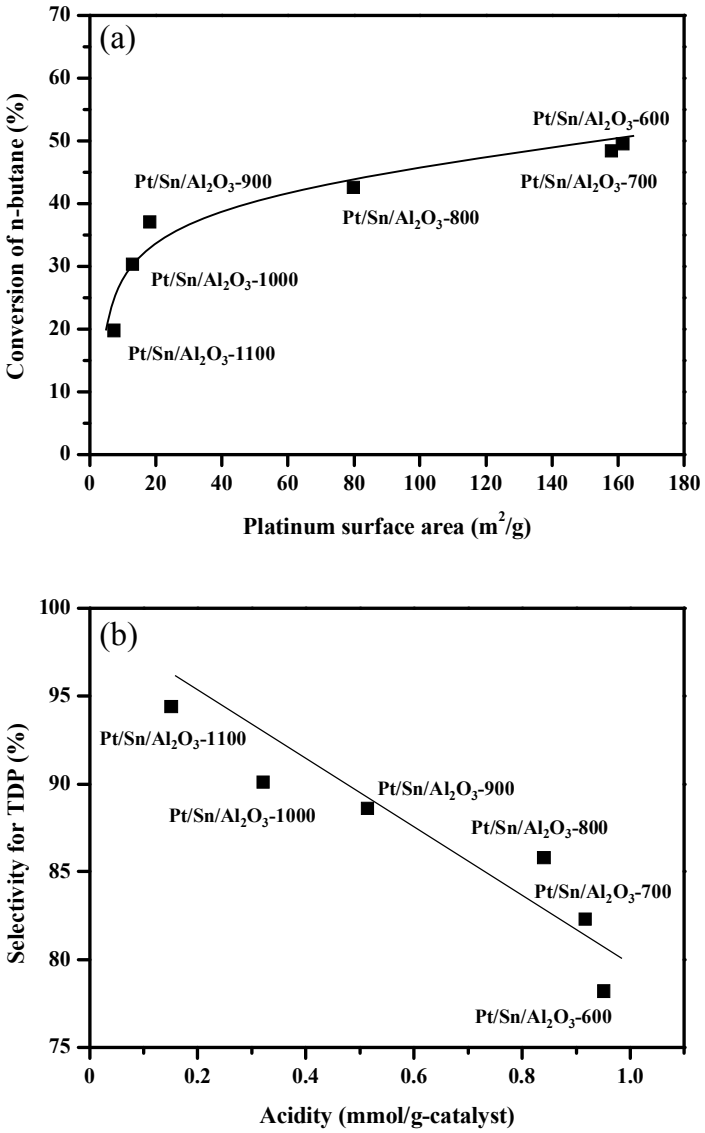

Fig. 3.33. (a) Correlation between platinum surface area and conversion of n-butane and (b) correlation between acidity and selectivity for TDP over $Pt/Sn/Al_2O_3$-X catalysts.

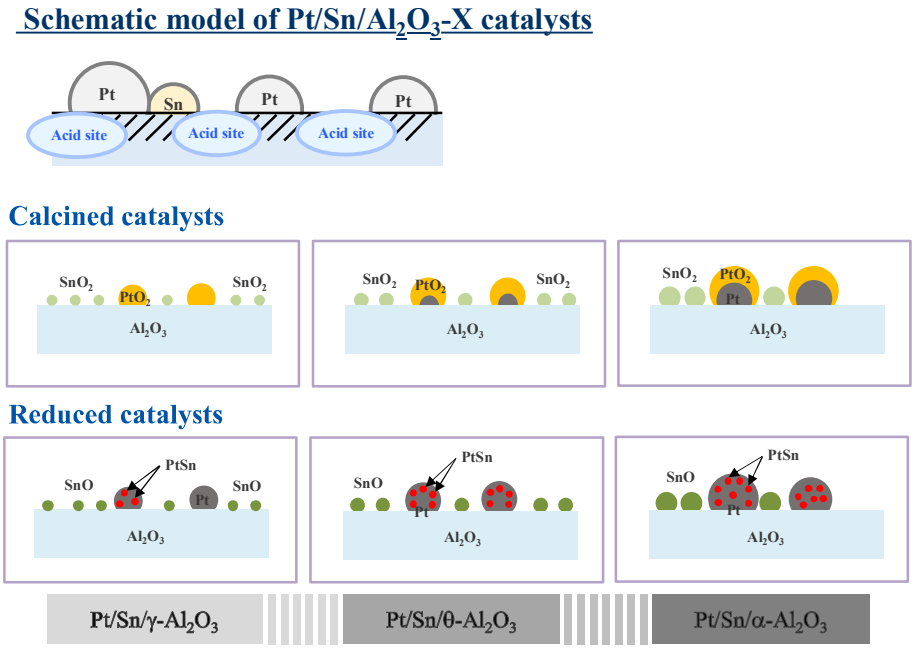

Fig. 3.34. Schematic model of $Pt/Sn/Al_2O_3$-X catalysts.

Chapter 4. Conclusions

Part 1 Oxidative dehydrogenation of n-butane to n-butene and 1,3-butadiene

Various $Mg_3(VO_4)_2/MgO\text{-}ZrO_2$ catalysts were prepared by a citric acid sol-gel method and a wet impregnation method, were applied to the oxidative dehydrogenation of n-butane to n-butene and 1,3-butadiene.

X-$Mg_3(VO_4)_2/MgO\text{-}ZrO_2$ catalysts with a variation of V content (X = 6.6, 9.9, 12.8, 15.2, and 19.1 wt%) were prepared by a citric acid sol-gel method and a wet impregnation method for use in the oxidative dehydrogenation of n-butane. Catalytic performance of X-$Mg_3(VO_4)_2/MgO\text{-}ZrO_2$ catalysts was strongly dependent on vanadium content. Catalytic performance of X-$Mg_3(VO_4)_2/MgO\text{-}ZrO_2$ catalysts decreased in the order of 12.8-$Mg_3(VO_4)_2/MgO\text{-}ZrO_2$ > 9.9-$Mg_3(VO_4)_2/MgO\text{-}ZrO_2$ > 6.6-$Mg_3(VO_4)_2/MgO\text{-}ZrO_2$ > 15.2-$Mg_3(VO_4)_2/MgO\text{-}ZrO_2$ > 19.1-$Mg_3(VO_4)_2/MgO\text{-}ZrO_2$. The catalytic activity of 15.2-$(VO_4)_2/MgO\text{-}ZrO_2$ and 19.1-$Mg_3(VO_4)_2/MgO\text{-}ZrO_2$ catalysts decreased with increasing reaction time, while 6.6-$Mg_3(VO_4)_2/MgO\text{-}ZrO_2$, 9.9-$Mg_3(VO_4)_2/MgO\text{-}ZrO_2$, and 12.8-$Mg_3(VO_4)_2/MgO\text{-}ZrO_2$ catalysts exhibited a stable catalytic performance during the whole reaction time. Temperature-programmed reoxidation (TPRO) measurements revealed that the catalytic performance in the oxidative dehydrogenation of n-butane was closely related to the oxygen

capacity and oxygen mobility of the catalysts. Stable catalytic performance of X-$Mg_3(VO_4)_2$/MgO-ZrO_2 (X = 6.6, 9.9, and 12.8) catalysts was attributed to their sufficient oxygen mobility, while X-$Mg_3(VO4)_2$/MgO-ZrO_2 (X = 15.2 and 19.1) catalysts with low oxygen mobility suffered from a catalyst deactivation. Furthermore, catalytic performance of catalysts increased with increasing oxygen capacity of the catalyst. It was revealed that oxygen capacity and oxygen mobility of the catalyst were closely related to the catalytic performance and the catalyst stability, respectively, in the oxidative dehydrogenation of n-butane. Among the catalysts tested, 12.8-$Mg_3(VO_4)_2$/MgO-ZrO_2 catalyst with the largest oxygen capacity showed the best catalytic performance in terms of yield for TDP.

$Mg_3(VO_4)_2$/MgO-ZrO_2 (X) catalysts with different Mg:Zr ratio (X = 16:1, 8:1, 4:1, 2:1, and 1:1) were prepared by a citric acid sol-gel method and a wet impregnation method for use in the oxidative dehydrogenation of n-butane. Catalytic performance of $Mg_3(VO_4)_2$/MgO-ZrO_2 (X) catalysts was strongly dependent on Mg:Zr ratio. It was observed that all the catalysts showed a stable catalytic performance in the oxidative dehydrogenation of n-butane during the whole reaction time. Catalytic performance of $Mg_3(VO_4)_2$/MgO-ZrO_2 (X) catalysts in the oxidative dehydrogenation of n-butane showed a volcano-shaped trend with respect to Mg:Zr ratio. TPRO measurements revealed that the oxygen capacity of the $Mg_3(VO_4)_2$/MgO-ZrO_2 (X) catalysts showed a volcano-shaped trend. The catalytic performance of $Mg_3(VO_4)_2$/MgO-ZrO_2 (X) catalysts increased with increasing the oxygen capacity in the catalysts. Among the catalysts tested, $Mg_3(VO_4)_2$/MgO-ZrO_2 (4:1) catalyst showed the best catalytic performance in the oxidative

dehydrogenation of n-butane, indicating that 4:1 was the most suitable Mg:Zr ratio for $Mg_3(VO_4)_2$/MgO-ZrO_2 catalyst system.

Part 2 Direct dehydrogenation of n-butane to n-butene and 1,3-butadiene

Various platinum-tin catalysts, including $Pt/Sn/M/Al_2O_3$ (M = Zn, In, Y, Bi, and Ga), a series of $Pt/Sn/Zn/Al_2O_3$ catalysts with a variation of Zn content (X = 0, 0.25, 0.5, 0.75, 1.0), $Pt/Sn/Al_2O_3$ (various Al_2O_3 support preparation method), and $Pt/Sn/Al_2O_3$ (different Al_2O_3 support calcination temperature), were prepared by a sequential impregnation method. They were applied to the direct dehydrogenation of n-butane to n-butene and 1,3-butadiene.

A series of $Pt/Sn/M/Al_2O$ catalysts with different third metal (M = Zn, In, Y, Bi, and Ga) were prepared by a sequential impregnation method for use in the direct dehydrogenation of n-butane to n-butene and 1,3-butadiene. It was found that chemical and electronic properties of the catalysts were affected by the addition of third metal (M). Yield for TDP decreased in order of $Pt/Sn/Zn/Al_2O_3$ > $Pt/Sn/In/Al_2O_3$ > $Pt/Sn/Al_2O_3$ > $Pt/Sn/Y/Al_2O_3$ > $Pt/Sn/Bi/Al_2O_3$ > $Pt/Sn/Ga/Al_2O_3$. Metal-support interaction and Pt surface area played important roles in determining the catalytic performance. Yield for TDP increased with increasing metal-support interaction and Pt surface area of the catalyst. Among the catalysts tested, $Pt/Sn/Zn/Al_2O_3$ catalyst, which retained the strongest metal-support interaction and the highest Pt surface area, showed the best catalytic performance and stability in the direct dehydrogenation of n-butane.

A series of $Pt/Sn/XZn/Al_2O_3$ catalysts with different zinc content (X = 0,

0.25, 0.5, 0.75, and 1.0 wt%) were prepared by a sequential impregnation method for use in the direct dehydrogenation of n-butane. Conversion of n-butane and yield for TDP after a 360 min-reaction showed volcano-shaped trends with respect to zinc content. Conversion of n-butane and yield for TDP after a 360 min-reaction decreased in the order of $Pt/Sn/0.5Zn/Al_2O_3$ > $Pt/Sn/0.75Zn/Al_2O_3$ > $Pt/Sn/0.25Zn/Al_2O_3$ > $Pt/Sn/1.0Zn/Al_2O_3$ > $Pt/Sn/Al_2O_3$. This indicates that an optimal zinc content was required for maximum production of n-butene and 1,3-butadiene. The catalytic performance of $Pt/Sn/XZn/Al_2O_3$ catalysts was closely related to the metal-support interaction and Pt surface area. Yield for TDP increased with increasing TPR peak temperature (with increasing metal-support interaction) and with increasing Pt surface area. Among the catalysts tested, $Pt/Sn/0.5Zn/Al_2O_3$ catalyst, which retained the strongest metal-support interaction and the highest Pt surface area, showed the best catalytic performance in terms of conversion of n-butane and yield for TDP.

Al_2O_3 (X) supports were prepared by precipitation method (Al_2O_3 (P)), alkoxide-based sol-gel method (Al_2O_3 (AS)), and epoxide-driven sol-gel method (Al_2O_3 (ES)). For comparison, a commercially available Al_2O_3 (Alfa Aesar) was used as a support (denoted as Al_2O_3 (C)). $Pt/Sn/Al_2O_3$ (X) catalysts were then prepared by a sequential impregnation method for use in the direct dehydrogenation of n-butane to n-butene and 1,3-butadiene. BET surface area, pore volume of $Pt/Sn/Al_2O_3$ (X) catalysts decreased in the order of $Pt/Sn/Al_2O_3$ (ES) > $Pt/Sn/Al_2O_3$ (AS) > $Pt/Sn/Al_2O_3$ (P) > $Pt/Sn/Al_2O_3$ (C). It was found that the platinum dispersion and platinum surface area of $Pt/Sn/Al_2O_3$ (X) catalysts decreased in the order of $Pt/Sn/Al_2O_3$ (ES) >

$Pt/Sn/Al_2O_3$ (AS) > $Pt/Sn/Al_2O_3$ (P) > $Pt/Sn/Al_2O_3$ (C). This might be due to the highest surface area and the largest pore volume of $Pt/Sn/Al_2O_3$ (ES) catalyst, which effectively suppressed the aggregation of platinum species during the impregnation step. In the direct dehydrogenation of n-butane, the catalytic performance of $Pt/Sn/Al_2O_3$ (X) catalysts increased with increasing platinum surface area in the catalysts. Among the catalysts tested, $Pt/Sn/Al_2O_3$ (ES) catalyst with the highest platinum surface area showed the best catalytic performance in the direct dehydrogenation of n-butane.

Al_2O_3-X supports prepared by a sol-gel method were calcined at various temperatures, and $Pt/Sn/Al_2O_3$-X catalysts were then prepared by a sequential impregnation method for use in the direct dehydrogenation of n-butane. It was revealed that platinum surface area and acidity of $Pt/Sn/Al_2O_3$-X catalysts were strongly influenced by the calcination temperature of alumina. Platinum surface area and acidity of $Pt/Sn/Al_2O_3$-X catalysts decreased with increasing calcination temperature of alumina. It was also revealed that catalytic performance of $Pt/Sn/Al_2O_3$-X catalysts was strongly influenced by platinum surface area and acidity of the catalyst. Conversion of n-butane increased with increasing platinum surface area of the catalyst, while selectivity for TDP decreased with increasing acidity of the catalyst. Among the catalysts tested, $Pt/Sn/Al_2O_3$-700 catalyst showed the best catalytic performance in terms of yield for TDP. Thus, an optimal calcination temperature of alumina was required for maximum production of n-butenes and 1,3-butadiene.

Bibliography

[1] L. Rodriguez, D. Romero, D. Rodriguez, J. Sanchez, F. Dominguez, G. Arteaga, "Dehydrogenation of n-buatne over Pd-Ga/Al_2O_3 catalysts", *Appl. Catal. A: Gen.* **373** (2010) 66.

[2] S.A. Bocanegra, A.A. Castro, O.A. Scelza, S.R. de Miguel, "Characterization and catalytic behavior in the n-butane dehydrogenation of trimetallic InPtSn/$MgAl_2O_4$ catalysts", *Appl. Catal. A: Gen.* **333** (2007) 49.

[3] S.D. Jackson, S. Rugmini, P.C. Stair, Z. Wu, "A comparison of catalyst deactivation of vanadia catalysts used for alkane dehydrogenation", *Chem. Eng. J.* **120** (2006) 127.

[4] J.-C. Liu, B.-X, Shen, D.-Q. Wang, J.-H. Dong, "Separating group compositions in naphtha by adsorption and solvent extraction to improve olefin yields of steam cracking process", *J. Pet. Sci. Eng.* **66** (2009) 156.

[5] K. Keyvanloo, J. Towfighi, S.M. Sadrameli, A. Mohamadalizadeh, "Investigating the effect of key factors, their interactions and optimization of naphtha steam cracking by statistical design of experiments", *J. Anal. Appl. Pyrolysis* **87** (2010) 224.

[6] E.V. Makshina, W. Janssens, B.F. Sels, P.A. Jacobs, "Catalytic study of the conversion of ethanol into 1,3-butadiene", *Catal. Today* **198** (2012) 338.

[7] H.-J. Chae, T.-W. Kim, Y.-K. Moon, H.-K. Kim, K.-E. Jeong, C.-U. Kim, S.-Y. Jeong, "Butadiene production from bioethanol and acetaldehyde over tantalum oxide-supported ordered mesoporous silica catalysts", *Appl. Catal. B: Environ.* **150** (2014) 596.

[8] B.M. Weckhuysen, R.A. Schoonheydt, "Alkane dehydrogenation over supported chromium oxide catalysts", *Catal. Today* **51** (1999) 223.

[9] T. Waku, J.A. Biscardi, E. Iglesia, "Catalytic dehydrogenation of alkanes on Pt/Na-[Fe]ZSM5 and staged O_2 introduction for selective H_2 removal", *J. Catal.* **222** (2004) 481.

[10] T.F. Narbeshuber, A. Brait, K. Seshan, J.A. Lercher, "Dehydrogenation of light alkanes over zeolites", *J. Catal.* **172** (1997) 127.

[11] A.D. Ballarini, C.G. Ricci, S.R. de Miguel, O.A. Scelza, "Use of Al_2O_3-SnO_2 as a support of Pt for selective dehydrogenation of light paraffins", *Catal. Today* **133** (2008) 28.

[12] X. Liu, B. Frank, W. Zhang, T.P. Cotter, R. Schlogl, D.S. Su, "Carbon-catalyzed oxidative dehydrogenation of n-butane: selective site formation during sp^3-to-sp^2 lattice rearrangement", *Angew. Chem. Int. Ed.* **50** (2011) 3318.

[13] M. Setnicka, R. Bulanek, L. Capek, P. Cicmanec, "n-Butane oxidative dehydrogenation over VO_X-HMS catalyst", *J. Mol. Catal. A: Chem.* **344** (2011) 1.

[14] G. Rajua, B.M. Reddya, B. Abhishek, Y.-H. Mo, S.-E. Park, "Synthesis of C4 olefins from n-butane over a novel VO_x/SnO_2-ZrO_2 catalyst using CO_2 as soft oxidant", *Appl. Catal. A: Gen.* **423** (2012) 168.

[15] S. Veldurthi, C.-H. Shin, O.-S. Joo, K.-D. Jung, "Promotional effects of Cu on Pt/Al_2O_3 and Pd/Al_2O_3 catalysts during n-butane dehydrogenation", *Catal. Today* **185** (2012) 88.

[16] R. Bulaneka, A. Kaluzova, M. Setnicka, A. Zukal, P. Cicmanec, J. Mayerova, "Study of vanadium based mesoporous silicas for oxidative dehydrogenation of propane and n-butane", *Catal. Today* **179** (2012) 149.

[17] C. Wang, J.-G. Chen, T. Xing, Z.-T. Liu, Z.-W. Liu, J. Jiang, J. Lu, "Vanadium oxide supported on titanosilicates for the oxidative dehydrogenation of n-butane", *Ind. Eng. Chem. Res.* **54** (2015) 3602.

[18] N. Madaan, R. Haufe, N.R. Shiju, G. Rothenberg, "Oxidative dehydrogenation of n-butane: activity and kinetics over VO_x/Al_2O_3

catalysts", *Top. Catal.* **57** (2014) 1400.

[19] B.M. Nagaraja, H. Jung, D.R. Yang, K.-D. Jung, "Effect of potassium addition on bimetallic PtSn supported θ-Al_2O_3 catalyst for n-butane dehydrogenation to olefins", *Catal. Today* **232** (2014) 40.

[20] S.A. Bocanegra, A. Guerrero-Ruiz, O.A. Scelza, S.R. de Miguel, "$MgAl_2O_4$ spinel prepared by mechanochemical synthesis used as a support of multimetallic catalysts for paraffin dehydrogenation", *Catal. Ind.* **5** (2013) 61.

[21] O. Rubio, J. Herguido, M. Menendez, "Oxidative dehydrogenation of n-butane on V/MgO catalysts-kinetic study in anaerobic conditions", *Chem. Eng. Sci.* **58** (2003) 4619.

[22] M.J. Alfonso, M. Menendez, J. Santamaria, "Oxidative dehydrogenation of butane on V/MgO catalytic membranes", *Chem. Eng. J.* **90** (2002) 131.

[23] M.A. Chaar, D. Patel, M.C. Kung, H.H. Kung, "Selective oxidative dehydrogenation of butane over V-Mg-O catalysts", *J. Catal.* **105** (1987) 483.

[24] S. Ge, C. Liu, S. Zhang, Z. Li, "Effect of carbon dioxide on the reaction performance of oxidative dehydrogenation of n-butane over V-Mg-O catalyst", *Chem. Eng. J.* **94** (2003) 121.

[25] N. Kijima, M. Toba, Y. Yoshimura, "A chemical potential diagram and an in-situ X-ray diffraction analysis of a V-Mg-O catalyst used in the oxidative dehydrogenation of n-butane", *Catal. Lett.* **127** (2009) 63.

[26] I.-C. Marcu, I. Sandulescu, J.-M.M. Millet, "Effects of the method of preparing titanium pyrophosphate catalyst on the structure and catalytic activity in oxidative dehydrogenation of n-butane", *J. Mol. Catal. A: Chem.* **203** (2003) 241.

[27] F. Urlan, I.-C. Marcu, I. Sandulescu, "Oxidative dehydrogenation of n-butane over titanium pyrophosphate catalysts in the presence of carbon

dioxide", *Catal. Commun.* **9** (2008) 2403.

[28] I.-C. Marcu, I. Sandulescu, Y. Schuurman, J.-M.M. Millet, "Mechanism of n-butane oxidative dehydrogenation over tetravalent pyrophosphates catalysts", *Appl. Catal. A: Gen.* **334** (2008) 207.

[29] L.M. Madeira, R.M. Martin-Aranda, F.J. Maldonado-Hodar, J.L.G. Fierro, M.F. Portela, "Oxidative dehydrogenation of n-butane over alkali and alkaline earth-promoted α-$NiMoO_4$ catalysts", *J. Catal.* **169** (1997) 469.

[30] F.J. Maldonado-Hodar, L.M. Madeira, M.F. Portela, R.M. Martin-Aranda, F. Freire, "Oxidative dehydrogenation of butane: changes in chemical, structural and catalytic behavior of Cs-doped nickel molybdate", *J. Mol. Catal. A: Chem.* **111** (1996) 313.

[31] F.J. Maldonado-Hodar, L.M.P. Madeira, M.F. Portela, "The effects of coke deposition on $NiMoO_4$ used in the oxidative dehydrogenation of butane", *J. Catal.* **164** (1996) 399.

[32] H. Armendariz, G. Aguilar-Rios, P. Salas, M.A. Valenzuela, I. Schifter, "Oxidative dehydrogenation of n-butane on iron-zinc oxide catalysts", *Appl. Catal. A: Gen.* **92** (1992) 29.

[33] J.M.L. Nieto, A. Dejoz, M.I. Vazquez, W. O'Leary, J. Cunningham, "Oxidative dehydrogenation of n-butane on MgO-supported vanadium oxide catalysts", *Catal. Today* **40** (1998) 215.

[34] R. Vidal-Michel, K.L. Hohn, "Effect of crystal size on the oxidative dehydrogenation of butane on V/MgO catalysts", *J. Catal.* **221** (2004) 127.

[35] A. Dejoz, J.M. Lopez Nieto, F. Marquez, M.I. Vazquez, "The role of molybdenum in Mo-doped V-Mg-O catalysts during the oxidative dehydrogenation of n-butane", *Appl. Catal. A: Gen.* **180** (1999) 83.

[36] X. Gao, P. Ruiz, Q. Xin, X. Guo, B. Delmon,, "Effect of coexistence of magnesium vanadate phases in the selective oxidation of propane to

propene", *J. Catal.* **148** (1994) 56.

[37] A. Corma, J.M. Lopez Nieto, N. Paredes, "Influence of the preparation methods of V-Mg-O catalysts on their catalytic properties for the oxidative dehydrogenation of propane", *J. Catal.* **144** (1993) 425.

[38] X. Gao, P. Ruiz, Q. Xin, X. Guo, B. Delmon, "Preparation and characterization of three pure magnesium vanadate phases as catalysts for selective oxidation of propane to propene", *Catal. Lett.* **23** (1994) 321.

[39] D. Patel, P.J. Andersen, H.H. Kung, "Oxidative dehydrogenation of butane over orthovanadates", *J. Catal.* **125** (1990) 132.

[40] O.S. Owen, H.H. Kung, "Effect of cation reducibility on oxidative dehydrogenation of butane on orthovanadates", *J. Mol. Catal.* **79** (1993) 265.

[41] M.A. Chaar, D. Patel, H.H. Kung, "Selective oxidative dehydrogenation of propane over V-Mg-O catalysts", *J. Catal.* **109** (1988) 463.

[42] C. Tellez, M. Abon, J.A. Dalmon, C. Mirodatos, J. Santamaria, "Oxidative dehydrogenation of butane over VMgO catalysts", *J. Catal.* **195** (2000) 113.

[43] M.E. Harlin, V.M. Niemi, A.O.I. Krause, "Alumina-supported vanadium oxide in the dehydrogenation of butanes", *J. Catal.* **195** (2000) 67.

[44] L.M. Madeira, M.F. Portela, "Catalytic oxidative dehydrogenation of n-butane", *Catal. Rev. Sci. Eng.* **44** (2002) 247.

[45] S. Albonetti, F. Cavani, F. Trifiro, "Key aspects of catalyst design for the selective oxidation of paraffins", *Catal. Rev. Sci. Eng.* **38** (1996) 413.

[46] H. Lee, J.K. Lee, U.G. Hong, Y. Yoo, Y.-J. Cho, J. Lee, H.-S. Jang, J.C. Jung, I.K. Song, "Effect of oxygen capacity and oxygen mobility of supported $Mg_3(VO_4)_2$ catalysts on the performance in the oxidative dehydrogenation of n-butane", *J. Ind. Eng. Chem.* **18** (2012) 808.

[47] T. Blasco, J.M. Lopez Nieto, A. Dejoz, M.I. Vazquez, "Influence of the acid-base character of supported vanadium catalysts on their catalytic

properties for the oxidative dehydrogenation of n-butane", *J. Catal.* **157** (1995) 271.

[48] J.M. Lopez Nieto, P. Concepcion, A. Dejoz, F. Melo, H. Konzinger, M.I. Vazquez, "Oxidative dehydrogenation of n-butane and 1-butene on undoped and K-doped VO_x/Al_2O_3 catalysts", *Catal. Today* **61** (2000) 361.

[49] M.M. Bhasin, J.H. McCain, B.V. Vora, T. Imai, P.R. Pujado, "Dehydrogenation and oxydehydrogenation of paraffins to olefins", *Appl. Catal. A: Gen.* **221** (2001) 397.

[50] Y. Xu, J. Lu, M. Zhong, J. Wang, "Dehydrogenation of n-butane over vanadia catalysts supported on silica gel", *J. Nat. Gas Chem.* **18** (2009) 88.

[51] S.D. Jackson, S. Rugmini, "Dehydrogenation of n-butane over vanadia catalysts supported on θ-alumina", *J. Catal.* **251** (2007) 59.

[52] S.R. de Miguel, S.A. Bocanegra, I.M.J. Vilella, A. Guerrero-Ruiz, O.A. Scelza, "Characterization and catalytic performance of PtSn catalysts supported on Al_2O_3 and Na-doped Al_2O_3 in n-butane dehydrogenation", *Catal. Lett.* **119** (2007) 5.

[53] S.A. Bocanegra, P.D. Zgolicz, O.A. Scelza, S.R. de Miguel, "New trimetallic catalysts supported on coprecipitated $MgAl_2O_4$ for n-paraffins selective dehydrogenation processes", *Catal. Commun.* **10** (2009) 1463.

[54] S.A. Bocanegra, A. Guerrero-Ruiz, S.R. de Miguel, O.A. Scelza, "Performance of PtSn catalysts supported on MAl_2O_4 (M: Mg or Zn) in n-butane dehydrogenation: characterization of the metallic phase", *Appl. Catal. A: Gen.* **277** (2004) 11.

[55] A.D. Ballarini, P. Zgolicz, I.M.J. Vilella, S.R. de Miguel, A.A. Castro, O.A. Scelza, "n-Butane dehydrogenation on Pt, PtSn and PtGe supported on γ-Al_2O_3 deposited on spheres of α-Al_2O_3 by washcoating", *Appl. Catal. A: Gen.* **381** (2010) 83.

[56] J.K. Lee, H. Seo, U.G. Hong, G. Park, Y. Yoo, J. Lee, H. Chang, I.K. Song, "Platinum-tin nano-catalysts supported on alumina for direct dehydrogenation of n-butane", *J. Nanosci. Nanotechnol.* **15** (2015) 8305.

[57] S. He, C. Sun, Z. Bai, X. Dai, B. Wang, "Dehydrogenation of long chain paraffins over supported Pt-Sn-K/Al_2O_3 catalysts: a study of the alumina support effect", *Appl. Catal. A: Gen.* **356** (2009) 88.

[58] G.J. Siri, G.R. Bertolini, M.L. Casella, O.A. Ferretti, "PtSn/γ-Al_2O_3 isobutane dehydrogenation catalysts: the effect of alkaline metals addition", *Mater. Lett.* **59** (2005) 2319.

[59] M. Tasbihi, F. Feyzi, M.A. Amlashi, A.Z. Abdullah, A.R. Mohamed, "Effect of the addition of potassium and lithium in Pt-Sn/Al_2O_3 catalysts for the dehydrogenation of isobutane", *Fuel. Process. Technol.* **88** (2007) 883.

[60] C.L. Padro, S.R. de Miguel, A.A. Castro, O.A. Scelza, "Stability and regeneration of supported PtSn catalysts for propane dehydrogenation", *Stud. Surf. Sci. Catal.* **111** (1997) 191.

[61] M. Alifanti, B. Baps, N. Blangenois, J. Naud, P. Grange, B. Delmon, "Characterization of CeO_2-ZrO_2 mixed oxides. Comparison of the citrate and sol-gel preparation methods", *Chem. Mater.* **15** (2003) 395.

[62] C.-H. Lu, C.-T. Chen, B. Bhattacharjee, "Sol-gel preparation and luminescence properties of $BaMgAl_{10}O_{17}$: Eu^{2+} phosphors", *J. Rare Earths* **24** (2006) 706.

[63] A. Kahoul, P. Nkeng, A. Hammouche, F. Naamoune, G. Poillerat, "A sol-gel route for the synthesis of $Bi_2Ru_2O_7$ pyrochlore oxide for oxygen reaction in alkaline medium", *J. Solid State Chem.* **161** (2001) 379.

[64] J.K. Lee, H. Lee, U.G. Hong, J. Lee, Y.-J. Cho, Y. Yoo, H.-S. Jang, I.K. Song, "Oxidative dehydrogenation of n-butane to n-butene and 1,3-butadiene over $Mg_3(VO_4)_2$/MgO-ZrO_2 catalysts: effect of Mg:Zr ratio of

support", *J. Ind. Eng. Chem.* **18** (2012) 1096.

[65] H. Lee, J.K. Lee, U.G. Hong, I.K. Song, Y. Yoo, Y.-J. Cho, J. Lee, H. Chang, J.C. Jung, "Oxidative dehydrogenation of n-butane over vanadium magnesium oxide catalysts supported on nano-structured MgO and ZrO_2: effect of oxygen capacity of the catalyst", *J. Nanosci. Nanotechnol.* **12** (2012) 6045.

[66] J.G. Seo, M.H. Youn, D.R. Park, I. Nam, I.K. Song, "Hydrogen production by steam reforming of liquefied natural gas (LNG) over Ni-Al_2O_3 catalysts prepared by a sequential precipitation method: effect of precipitation agent", *Int. J. Hydrogen Energy* **34** (2009) 8053.

[67] G. Buelna, Y.S. Lin, "Sol-gel-derived mesoporous γ-alumina granules", *Microporous Mesoporous Mater.* **30** (1999) 359.

[68] T.F. Baumann, A.E. Gash, S.C. Chinn, A.M. Sawvel, R.S. Maxwell, J.H. Satcher, "Synthesis of high-surface-area alumina aerogels without the use of alkoxide precursors", *Chem. Mater.* **17** (2005) 395.

[69] Y. Bang, J.G. Seo, M.H. Youn, I.K. Song, "Hydrogen production by steam reforming of liquefied natural gas (LNG) over mesoporous Ni-Al_2O_3 aerogel catalyst prepared by a single-step epoxide-driven sol-gel method", *Int. J. Hydrogen Energy* **37** (2012) 1436.

[70] H. Yahiro, K. Nakaya, T. Yamamoto, K. Saiki, H. Yamaura, "Effect of calcination temperature on the catalytic activity of copper supported on γ-alumina for the water-gas-shift reaction", *Catal. Commun.* **7** (2006) 228.

[71] A. Burrows, C.J. Kiely, J. Perregaard, P.E. Hojlund-Nielsen, G. Vorbeck, J.J. Calvino, C. Lopez-Cartes, "Structural characterisation of a VMgO catalyst used in the oxidative dehydrogenation of propane", *Catal. Lett.* **57** (1999) 121.

[72] M.L. Occelli, R.S. Maxwell, H. Eckert, "The interaction of vanadia with

sepiolite. Structural studies by ^{51}V solid-state NMR and raman spectroscopy", *J. Catal.* **137** (1992) 36.

[73] M.K. Yurdakoc, R. Haffner, D. Honicke, "Characterization of V_2O_5/MgO catalysts", *Mater. Chem. Phys.* **44** (1996) 273.

[74] J.C. Jung, H. Kim, A.S. Choi, Y.M. Chung, T.J. Kim, S.J. Lee, S.-H. Oh, I.K. Song, "Effect of pH in the preparation of γ-Bi_2MoO_6 for oxidative dehydrogenation of n-butene to 1,3-butadiene: correlation between catalytic performance and oxygen mobility of γ-Bi_2MoO_6", *Catal. Commun.* **8** (2007) 625.

[75] J.C. Jung, H. Lee, D.R. Park, J.G. Seo, I.K. Song, "Effect of calcination temperature on the catalytic performance of γ-Bi_2MoO_6 in the oxidative dehydrogenation of n-butene to 1,3-butadiene", *Catal. Lett.* **131** (2009) 401.

[76] V.D. Sokolovskii, "Principles of oxidative catalysis on solid oxides", *Catal. Rev. Sci. Eng.* **32** (1990) 1.

[77] J.K. Lee, H. Lee, U.G. Hong, Y. Yoo, Y.-J. Cho, J. Lee, H. Chang, I.K. Song, "Oxidative dehydrogenation of n-butane over $Mg_3(VO_4)_2$/MgO-ZrO_2 catalysts: effect of oxygen capacity and acidity of the catalysts", *J. Ind. Eng. Chem.* **18** (2012) 1758.

[78] I.H. Cho, S.B. Park, S.J. Cho, R. Ryoo, "Investigation of Pt/γ-Al_2O_3 catalysts prepared by sol-gel method: XAFS and ethane hydrogenolysis", *J. Catal.* **173** (1998) 295.

[79] M.-Y. Kim, J.-H. Park, C.-H. Shin, S.-W. Han, G. Seo, "Dispersion improvement of platinum catalysts supported on silica, silica-alumina and alumina by titania incorporation and pH adjustment", *Catal. Lett.* **133** (2009) 288.

[80] Y. Zhang, Y. Zhou, L. Wan, M. Xue, Y. Duan, X. Liu, "Effect of magnesium addition on catalytic performance of PtSnK/γ-Al_2O_3 catalyst

for isobutane dehydrogenation", *Fuel Process. Technol.* **92** (2011) 1632.

[81] C.L. Pieck, C.R. Vera, J.M. Parera, G.N. Gimenez, L.R. Serra, L.S. Carvalho, M.C. Rangel, "Metal dispersion and catalytic activity of trimetallic Pt-Re-Sn/Al_2O_3 naphtha reforming catalysts", *Catal. Today* **107** (2005) 637.

[82] O.A. Barias, A. Holmen, E.A. Blekkan, "Propane dehydrogenation over supported Pt and Pt-Sn catalysts: catalyst preparation, characterization, and activity measurements", *J. Catal.* **158** (1996) 1.

[83] C. Yu, H. Xu, Q. Ge, W. Li, "Properties of the metallic phase of zinc-doped platinum catalysts for propane dehydrogenation", *J. Mol. Catal. A: Chem.* **266** (2007) 80.

[84] Y. Zhang, Y. Zhou, A. Qiu, Y. Wang, Y. Xu, P. Wu, "Propane dehydrogenation on PtSn/ZSM-5 catalyst: effect of tin as a promoter", *Catal. Commun.* **7** (2006) 860.

[85] J. Llorca, N. Homs, J. Leon, J. Sales, J.L.G. Fierro, P.R. de la Piscina, "Supported Pt-Sn catalysts highly selective for isobutene dehydrogenation: preparation, characterization and catalytic behavior", *Appl. Catal. A: Gen.* **189** (1999) 77.

[86] R. Morales, L. Melo, A. Llanos, F. Zaera, "Characterization of bifunctional PtSn/H[Al]ZSM5 catalysts: a comparison between two impregnation strategies", *J. Mol. Catal. A: Chem.* **228** (2005) 227.

[87] G.D. Angel, A. Bonilla, Y. Pena, J. Navarrete, J.L.G. Fierro, D.R. Acosta, "Effect of lanthanum on the catalytic properties of PtSn/γ-Al_2O_3 bimetallic catalysts prepared by successive impregnation and controlled surface reaction", *J. Catal.* **219** (2003) 63.

[88] D. Wang, F. Ammari, R. Touroude, D.S. Su, R. Schlogl, "Promotion effect in Pt-ZnO catalysts for selective hydrogenation of crotonaldehyde to crotyl alcohol: a structural investigation", *Catal. Today* **147** (2009) 224.

[89] K.S.W. Sing, D.H. Everett, R.A.W. Haul, L. Moscou, R.A. Pierotti, J. Rouquerol, T. Siemieniewska, "Reporting physisorption data for gas/solid systems with special reference to the determination of surface area and porosity", *Pure. Appl. Chem.* **57** (1985) 603.

[90] Q. Liu, A. Wang, X. Wang, T. Zhang, "Mesoporous γ-alumina synthesized by hydro-carboxylic acid as structure-directing agent", *Microporous. Mesoporous. Mater.* **92** (2006) 10.

[91] K.V.R. Chary, P.V.R. Rao, V.V. Rao, "Catalytic functionalities of nickel supported on different polymorphs of alumina", *Catal. Commun.* **9** (2008) 886.

[92] P. Burtin, J.P. Brunelle, M. Pijolat, M. Soustelle, "Influence of surface area and additives on the thermal stability of transitioin alumina catalyst supports. I: kinetic data", *Appl. Catal.* **34** (1987) 225.

[93] P. Burtin, J.P. Brunelle, M. Pijolat, M. Soustelle, "Influence of surface area and additives on the thermal stability of transition alumina catalyst supports. II: kinetic model and interpretation", *Appl. Catal.* **34** (1987) 239.

[94] R.-S. Zhou, R.L. Snyder, "Structures and transformation mechanisms of the η, γ and θ transition aluminas", *Acta. Crystallogr. B* **47** (1991) 617.

[95] U. Janosovits, G. Ziegler, U. Scharf, A. Wokaun, "Structural characterization of intermediate species during synthesis of Al_2O_3-aerogels", *J. Non-Cryst. Solids* **210** (1997) 1.

[96] B.K. Vu, M.B. Song, I.Y. Ahn, Y.-W. Suh, D.J. Suh, W.-L. Kim, H.-L. Koh, Y.G. Choi, E.W. Shin, "Propane dehydrogenation over Pt-Sn/Rare-earth-doped Al_2O_3: influence of La, Ce, or Y on the formation and stability of Pt-Sn alloys", *Catal. Today* **164** (2011) 214.

[97] Y. Zhang, Y. Zhou, X. Sheng, L. Wan, Y. Li, Y. Xiao, B. Yu, Z. Zeng, "Effect of the competitive adsorbates on the catalytic performances of

PtSnK/γ-Al_2O_3 catalyst for isobutane dehydrogenation", *Fuel Process. Technol.* **104** (2012) 23.

[98] L.S. Carvalho, C.L. Pieck, M.C. Rangel, N.S. Figoli, J.M. Grau, P. Reyes, J.M. Parera, "Trimetallic naphtha reforming catalysts. I. properties of the metal function and influence of the order of addition of the metal precursors on Pt-Re-Sn/γ-Al_2O_3-Cl", *Appl. Catal. A: Gen.* **269** (2004) 91.

[99] Y. Zhang, Y. Zhou, Y. Li, Y. Wang, Y. Xu, P. Wu, "Effect of calcination temperature on catalytic properties of PtSnNa/ZSM-5 catalyst for propane dehydrogenation", *Catal. Commun.* **8** (2007) 1009.

[100] H. Seo, J.K. Lee, U.G. Hong, G. Park, Y. Yoo, J. Lee, H. Chang, I.K. Song, "Direct dehydrogenation of n-butane over Pt/Sn/M/γ-Al_2O_3 catalysts: effect of third metal (M) addition", *Catal. Commun.* **47** (2014) 22.

[101] S. Zhang, Y. Zhou, Y. Zhang, L. Huang, "Effect of K addition on catalytic performance of PtSn/ZSM-5 catalyst for propane dehydrogenation", *Catal. Lett.* **135** (2010) 76.

초 록

노르말-부텐과 1,3-부타디엔과 같은 C4 올레핀은 화학 물질로서 광범위하게 사용되기 때문에 석유화학산업에서 중요한 원료이다. C4 올레핀은 합성 수지 (저밀도 폴리에틸렌 (LDPE)과 고밀도 폴리에틸렌 (HDPE))와 합성 고무 (아크릴로니트릴-부타디엔-스타이렌 (ABS), 폴리부타디엔 고무 (BR), 스타이렌-부타디엔 고무 (SBR), 스타이렌-부타디엔 라텍스 (SBL))와 같은 다양한 화학물질의 생산을 위한 주요 공급원료이다. C4 올레핀의 수요량은 개발도상국의 합성 고무 산업의 발전으로 꾸준히 증가하고 있다. 셰일가스 산업의 성장에 따라, 투입원료가 더 가벼운 물질로 변화 (나프타 → 에탄) 하기 때문에 C4 올레핀의 생산량은 감소되고 있다. 현재, 석유화학산업에서 노르말-부텐과 1,3-부타디엔은 주로 나프타 크래킹 공정에 의해 생산된다. 그러나 나프타 크래킹 공정은 상대적으로 높은 온도에서 운전 (>800 °C)되며, 이 공정은 부텐과 부타디엔을 생산할 뿐만 아니라 에틸렌, 프로필렌, 아이소부텐등을 생산하기 때문에 마케팅과 에너지 관리 측면에서 많은 문제점을 지니고 있다. 이러한 이유들로, 노르말-부탄의 탈수소화는 노르말-부텐과 1,3-부타디엔을 생산하기 위한 효과적인 방법으로 간주되고 있다. 본 연구에서는 노르말-부탄의 탈수소화를 위해 다양한 마그네슘 바나데이트와 백금-주석 촉매들을 이용하였다.

마그네슘 바나데이트 촉매는 고유의 높은 활성 때문에 노르말-부탄의 산화적 탈수소화 반응을 위한 가장 적합한 촉매로 알려져 있다. 그러나 $Mg_3(VO_4)_2$/MgO 촉매의 활성은 낮은 산소운동성 때문에 불안정하다고 알려져 있다. $Mg_3(VO_4)_2$/MgO

촉매의 낮은 산소운동성은 촉매 반응 중에 산소 보충을 방해하여, 노르말-부탄의 산화적 탈수소화 반응에서 심각한 촉매 비활성화를 일으킨다. 이러한 문제점을 극복하기 위해, $Mg_3(VO_4)_2$/MgO 촉매의 안정성을 향상시키는 금속 산화물 안정제 (TiO_2, Cr_2O_3, SiO_2, ZrO_2)의 도입 등의 많은 시도가 이루어지고 있다. $Mg_3(VO_4)_2$/MgO 촉매에 ZrO_2의 도입은 산소운동성이 향상되어 뛰어난 촉매 안정성의 결과를 가져왔다. 이는 잘 개발된 $Mg_3(VO_4)_2$/MgO-ZrO_2 촉매는 촉매의 산소운동성이 향상될 뿐만 아니라, 촉매의 고유 활성도 향상되어 촉매 비활성화 없이 높은 활성을 유발한다는 의미이다. 따라서 $Mg_3(VO_4)_2$/MgO-ZrO_2 촉매는 노르말-부탄의 산화적 탈수소화 반응에서의 촉매 활성 및 안정성 향상 측면에서 주목을 받고 있다. 본 연구에서는 노르말-부탄의 산화적 탈수소화 반응에서의 노르말-부텐과 1,3-부타디엔 생산 효율을 최적화하기 위해, 촉매의 바나듐 함량과 Mg:Zr 비율등과 같은 다양한 화학적 조성에 의해 $Mg_3(VO_4)_2$/MgO-ZrO_2 촉매를 제조하였다.

다양한 바나듐 함량 (X = 6.6, 9.9, 12.8, 15.2, and 19.1 wt%)에 따라 일련의 X-$Mg_3(VO_4)_2$/MgO-ZrO_2 촉매들을 시트르산 졸겔법과 습윤 함침법에 의해 제조하였다. X-$Mg_3(VO_4)_2$/MgO-ZrO_2 촉매를 통한 노르말-부탄의 산화적 탈수소화 반응에서 격자산소량 (반응에 참여할 수 있는 촉매 내 격자 산소의 양)과 격자 산소운동성 (반응에 참여하는 격자 산소의 고유의 운동성)이 반응활성에 미치는 영향이 조사되었다. X-$Mg_3(VO_4)_2$/MgO-ZrO_2 촉매의 반응 활성은 바나듐의 함량에 크게 의존하였다. TPRO 실험 결과, X-$Mg_3(VO_4)_2$/MgO-ZrO_2 촉매의 성능은 격자산소량 및 산소운동성과 밀접한 관련이 있음을 알아내었다. 실험결과, 노르말-부탄의 산화적 탈수소화 반응에서 격자 산소량은 산소의 활성과 밀접한 관련이 있고, 격자

산소운동성은 촉매 안정성에 중요한 역할을 하는 것으로 나타났다.

촉매의 Mg:Zr 비율이 촉매의 반응활성에 미치는 영향을 알아보기 위한 목적으로, 다양한 Mg:Zr 비율 (X = 16:1, 8:1, 4:1, 2:1, and 1:1)에 따라 $Mg_3(VO_4)_2/MgO-ZrO_2$ (X) 촉매들을 시트르산 졸겔법과 습윤 함침법에 의해 제조하였다. $Mg_3(VO_4)_2/MgO-ZrO_2$ (X) 촉매의 반응 활성은 Mg:Zr 비율에 따라 크게 달라졌다. 모든 촉매는 노르말-부탄의 산화적 탈수소화 반응 시간 동안 안정한 반응활성 성능을 보였다. 탈수소화 생성물 수율 (TDP, 노르말-부텐과 1,3-부타디엔)은 Mg:Zr의 비율에 따라 화산형 그래프를 보였다. 노르말-부탄의 산화적 탈수소화 반응에서 $Mg_3(VO_4)_2/MgO-ZrO_2$ (X) 촉매의 산소 특성이 촉매 반응활성에 미치는 영향을 살펴보았다. 실험결과, $Mg_3(VO_4)_2/MgO-ZrO_2$ (X) 촉매의 활성은 촉매의 격자산소량이 증가함에 따라 증가하는 것을 확인할 수 있었다.

Al_2O_3 에 담지된 Pt-Sn 촉매는 높은 촉매 활성과 노르말-부텐과 1,3-부타디엔의 높은 선택도을 갖기 때문에 노르말-부탄의 직접 탈수소화 반응에 널리 사용되고 있다. 노르말-부탄의 직접 탈수소화 반응에 사용되는 백금은 활성금속이고 주석은 백금을 위한 효과적인 활성 개선제의 역할을 하고 있다. 일반적으로 노르말-부탄의 직접 탈수소화 반응에서 알루미나에 담지된 백금 촉매의 백금과 산 특성은 중요한 역할을 하고 있는 것으로 알려져 있다. 백금은 활성금속 이고 백금의 높은 분산도는 주요반응을 촉진시켜 탈수소화 생성물의 높은 선택도를 얻을 수 있다. 일반적으로 사용되는 알루미나 담체는 산 특성을 가지게 되는데, 이는 이성질화, 크래킹, 중합, 코크 형성을 가속화시킨다. 더욱이, 해당 반응에서 높은 온도의 반응조건은 촉매 비활성화를 야기시키는 코크 형성을 피할 수 없다. 그러므로, 높은 활성과 촉매

안정성을 갖는 효과적인 $Pt/Sn/Al_2O_3$ 촉매의 개발은 매우 중요하다. 본 연구에서는 $Pt/Sn/M/Al_2O_3$ (M = Zn, In, Y, Bi, and Ga) 촉매, 다양한 Zn함량의 $Pt/Sn/Zn/Al_2O_3$ 촉매, $Pt/Sn/Al_2O_3$ (다양한 담체 제조방법), $Pt/Sn/Al_2O_3$ (다양한 담체 소성온도) 등의 다양한 백금-주석 촉매들을 연속 함침법에 의해 제조되었다.

다양한 3번째 금속 (M = Zn, In, Y, Bi, and Ga)을 갖는 일련의 $Pt/Sn/M/Al_2O_3$ 촉매는 연속 함침법에 의해 제조되었다. $Pt/Sn/M/Al_2O_3$ 촉매의 3번째 금속 (M)의 도입에 따른 물리화학적 특성과 촉매 활성의 영향에 대해 조사되었다. 촉매의 화학적 및 전자적 특성은 3번째 금속의 도입에 따라 영향을 받았음을 알 수 있었다. 탈수소화 생성물에 대한 수율은 촉매의 금속-담체의 상호작용과 백금 표면적이 증가함에 따라 증가하였음을 알 수 있었다. 금속-담체 상호작용과 백금 표면적은 촉매활성을 결정하는데 중요한 역할을 하였다. 노르말-부탄의 직접 탈수소화 반응에서 $Pt/Sn/Zn/Al_2O_3$ 촉매는 가장 우수한 활성을 보였다.

다양한 Zn 함량을 갖는 일련의 $Pt/Sn/XZn/Al_2O_3$ 촉매는 연속 함침법으로 제조되었다. 노르말-부탄의 직접 탈수소화 반응에서 $Pt/Sn/XZn/Al_2O_3$ 촉매의 아연의 양 (X)이 물리화학적 특성과 촉매활성에 미치는 영향에 대해 조사되었다. TPR 및 화학흡착 실험을 통해 촉매의 금속-담체 상호작용과 백금 표면적이 촉매활성과 밀접한 관련이 있다는 것을 확인하였다. 촉매 활성은 촉매의 금속-담체 상호작용과 백금 표면적이 증가함에 따라 증가하였다. 노르말-부탄의 직접 탈수소화 반응에서, 가장 강한 금속-담체 상호작용과 가장 큰 백금 표면적을 갖는 $Pt/Sn/0.5Zn/Al_2O_3$ 촉매가 노르말-부탄의 전환율과 탈수소화 생성물의 수율의 관점에서 가장 우수한 활성을 보였다.

Al_2O_3 (X) 담체는 침전법 (Al_2O_3(P)), 알콕사이드 기반

졸겔법 (Al_2O_3(AS)), 에폭사이드 유도 졸겔법 (Al_2O_3(ES))에 의해 제조되었다. 비교를 위해, 상업적으로 구입할 수 있는 Al_2O_3를 담체로서 사용하였다 (Al_2O_3 (C)). Pt/Sn/Al_2O_3 (X) 촉매는 연속 함침법에 의해 제조되었다. 노르말-부탄의 직접 탈수소화 반응에서 Pt/Sn/Al_2O_3 (X) 촉매의 알루미나 담체 제조법이 촉매의 물리화학적 특성과 활성에 미치는 영향이 조사되었다. Pt/Sn/Al_2O_3 (X) 촉매의 BET 표면적과 기공 부피는 Pt/Sn/Al_2O_3 (ES) > Pt/Sn/Al_2O_3 (AS) > Pt/Sn/Al_2O_3 (P) > Pt/Sn/Al_2O_3 (C) 촉매의 순서로 감소하였다. Pt/Sn/Al_2O_3 (X) 촉매의 백금 분산도와 백금 표면적은 Pt/Sn/Al_2O_3 (ES) > Pt/Sn/Al_2O_3 (AS) > Pt/Sn/Al_2O_3 (P) > Pt/Sn/Al_2O_3 (C) 촉매의 순서로 감소하는 것을 확인 할 수 있었다. 노르말-부탄의 직접 탈수소화 반응에서, 가장 큰 백금 표면적을 가진 Pt/Sn/Al_2O_3 (ES) 촉매가 가장 우수한 활성을 보였다.

졸겔법으로 제조된 Al_2O_3-X 담체는 다양한 온도에서 소성을 하였고, Pt/Sn/Al_2O_3-X 촉매는 연속 함침법에 의해 제조되었다. 노르말-부탄의 직접 탈수소화 반응에서 Pt/Sn/Al_2O_3-X 촉매의 알루미나 소성온도에 대한 촉매의 활성에 대한 영향이 조사되었다. Pt/Sn/Al_2O_3-X 촉매의 물리화학적 특성은 알루미나 소성온도에 의해 강하게 영향을 받았다. Pt/Sn/Al_2O_3-X 촉매의 백금 표면적과 산량은 알루미나의 소성온도가 증가함에 따라 감소함을 확인할 수 있었다. 노르말-부탄의 직접 탈수소화 반응에서, Pt/Sn/Al_2O_3-X 촉매의 백금표면적과 산량은 각각 노르말-부탄의 전환율과 탈수소화 생성물의 선택도와 밀접하게 관련이 있었다. 노르말-부탄의 전환율은 촉매의 백금 표면적이 감소함에 따라 감소하였고, 탈수소화 생성물의 선택도는 촉매의 산량이 증가함에 따라 감소하였다. 실험한 촉매들 중에서, Pt/Sn/Al_2O_3-700 (700도로

소성한 알루미나에 담지된 백금-주석 촉매)이 탈수소화 생성물 수율에 관하여 가장 우수한 촉매 활성을 보였다.

요약하면, 본 연구에서는 다양한 마그네슘 바나데이트 촉매와 백금-주석 촉매를 제조하여 노르말-부탄의 탈수소화 반응을 통해 노르말-부텐과 1,3-부타디엔을 얻기 위한 반응에 적용하였다. 준비된 촉매의 노르말-부탄의 탈수소화 반응에서의 촉매 활성을 설명하기 위해 질소 흡탈착 분석, XRD, 라만분광기, TPR, TPRO, HR-TEM, 화학흡착 및 NH_3-TPD 등의 다양한 특성 분석기법이 수행되었다. 실험 결과로부터 마그네슘 바나데이트 촉매의 격자 산소량과 격자 산소운동성은 노르말-부탄의 산화적 탈수소화 반응에서 촉매 활성을 결정하는 중요한 요소이며, 백금-주석 촉매의 백금 표면적과 산량은 노르말-부탄의 직접 탈수소화 반응에서 촉매활성을 결정하는 주요 역할을 하는 것으로 밝혀졌다.

주요어: 산화적 탈수소화, 직접 탈수소화, 노르말-부탄, 노르말-부텐, 1,3-부타디엔, 마그네슘 바나데이트 촉매, 백금-주석 촉매

학 번: 2011-21067

List of publications

Papers

International papers published (First author)

1. **J.K. Lee**, J.K. Kim, K.H. Kang, I.K. Song, "Direct Dehydrogenation of n-Butane over Platinum-tin Catalysts Supported on Alumina", *Journal of Nanoscience and Nanotechnology* (Submitted).

2. **J.K. Lee**, H. Seo, J.K. Kim, H. Seo, H.-R. Cho, J. Lee, H. Chang, I.K. Song, "Direct Dehydrogenation of n-Butane over Pt/Sn/Zn-K/Al_2O_3 Catalyst: Effect of Hydrogen in the Feed", *Journal of Nanoscience and Nanotechnology* (In Press).

3. **J.K. Lee**, H. Seo, U.G. Hong, G. Park, Y. Yoo, J. Lee, H. Chang, I.K. Song, "Platinum-tin Nano-catalysts Supported on Alumina for Direct Dehydrogenation of n-Butane", *Journal of Nanoscience and Nanotechnology,* 15(10), pp.8305-8310 (2015).

4. **J.K. Lee**, H. Seo, U.G. Hong, Y. Yoo, Y.-J. Cho, J. Lee, G. Park, H. Chang, I.K, Song, "$Mg_3(VO_4)_2$-MgO-ZrO_2 Nano-catalysts for Oxidative Dehydrogenation of n-Butane", *Journal of Nanoscience and Nanotechnology*, 14(11), pp.8879-8883 (2014).

5. **J.K. Lee**, U.G. Hong, Y. Yoo, Y.-J. Cho, J. Lee, H. Chang, I.K. Song, "Oxidative Dehydrogenation of n-Butane over Magnesium Vanadate Nano-Catalysts Supported on Magnesia-Zirconia: Effect of Vanadium Content", *Journal of Nanoscience and Nanotechnology*, 13(12), pp.8110-8115 (2013).

6. **J.K. Lee**, H. Lee, U.G. Hong, Y. Yoo, Y.-J. Cho, J. Lee, H. Chang, I.K. Song, "Oxidative Dehydrogenation of n-Butane over $Mg_3(VO_4)_2$/MgO-ZrO_2 Catalysts: Effect of Oxygen Capacity and Acidity of the Catalysts", *Journal of Industrial and Engineering Chemistry*, 18(5), pp.1758-1763 (2012).

7. **J.K. Lee**, H. Lee, U.G. Hong, J. Lee, Y.-J. Cho, Y. Yoo, H.-S. Jang, I.K. Song, "Oxidative Dehydrogenation of n-Butane to n-Butene and 1,3-Butadiene over $Mg_3(VO_4)_2$/MgO-ZrO_2 Catalysts: Effect of Mg:Zr Ratio of Support", *Journal of Industrial and Engineering Chemistry*, 18(3), pp.1096-1101 (2012).

International papers published (Co-author)

1. J.K. Kim, **J.K. Lee**, K.H. Kang, J.W. Lee, I.K. Song, "Catalytic Decomposition of Phenethyl Phenyl Ether to Aromatics over Pd-Fe Bimetallic Catalysts Supported on Ordered Mesoporous Carbon", *Journal of Molecular Catalysis A: Chemical*, 410, pp.184-192 (2015).

2. J.K. Kim, **J.K. Lee**, K.H. Kang, J.C. Song, I.K. Song, "Selective Cleavage of C-O Bond in Benzyl Phenyl Ether to Aromatics over Pd-Fe Bimetallic Catalyst Supported on Ordered Mesoporous Carbon", *Applied Catalysis A: General,* 498, pp.142-149 (2015).

3. J.H. Choi, T.H. Kang, Y. Bang, **J.K. Lee**, J.C. Song, I.K. Song, "Effect of Metal-substitution on the Redox Behaviors of Mono-transition metal-substituted Wells-Dawson Tungstoarsenates", *Catalysis Communications*, 65, pp.66-71 (2015).

4. H. Seo, **J.K. Lee**, U.G. Hong, G. Park, Y. Yoo, J. Lee, H. Chang, I.K. Song, "Direct Dehydrogenation of n-Butane over Pt/Sn/Zn/γ-Al_2O_3 Nano-catalyst: Effect of Zn Content", *Journal of Nanoscience and Nanotechnology,* 15(10),

pp.8318-8823 (2015).

5. K.H. Kang, U.G. Hong, Y. Bang, J.H. Choi, J.K. Kim, **J.K. Lee**, S.J. Han, I.K. Song, "Hydrogenation of Succinic Acid to 1,4-Butanediol over Re-Ru Bimetallic Catalysts Supported on Mesoporous Carbon", *Applied Catalysis A: General*, 490, pp.153-162 (2015).

6. U.G. Hong, H.W. Park, J. Lee, **J.K. Lee**, J. Yi, I.K. Song, "Conversion of Succinic Acid to 1,4-Butanediol via Dimethyl Succinate over Rhenium Nano-catalyst Supported on Copper-containing Mesoporous Carbon", *Journal of Nanoscience and Nanotechnology*, 14(11), pp.8867-8872 (2014).

7. H. Seo, **J.K. Lee**, U.G. Hong, G. Park, Y. Yoo, J. Lee, H. Chang, I.K. Song, "Direct Dehydrogenation of n-Butane over Pt/Sn/M/γ-Al_2O_3 Catalysts: Effect of Third Metal (M) Addition", *Catalysis Communications*, 47, pp.22-27 (2014).

8. U.G. Hong, J.K. Kim, J. Lee, **J.K. Lee**, J.H. Song, J. Yi, I.K. Song, "Hydrogenation of Succinic Acid to Tetrahydrofuran over Ruthenium-carbon Composite Catalysts: Effect of HCl Concentration in the Preparation of the Catalysts", *Journal of Industrial and Engineering Chemistry*, 20(5), pp.3834-3840 (2014).

9. Y. Bang, S.J. Han, J. Yoo, J.H. Choi, **J.K. Lee**, J.H. Song, J. Lee, I.K. Song, "Hydrogen Production by Steam Reforming of Simulated Liquefied Natural Gas (LNG) over Nickel Catalyst Supported on Mesoporous Phosphorus-modified Alumina Xerogel", *Applied Catalysis B: Environmental*, 148-149, pp.269-280 (2014).

10. U.G. Hong, J.K. Kim, J. Lee, **J.K. Lee**, J.H. Song, J. Yi, I.K. Song, "Hydrogenation of Succinic Acid to Tetrahydrofuran (THF) over Ruthenium-carbon Composite (Ru-C) Catalyst", *Applied Catalysis A: General*, 469,

pp.466-471 (2014).

11. H. Lee, **J.K. Lee**, U.G. Hong, I.K. Song, Y. Yoo, Y.-J. Cho, J. Lee, H.-S. Chang, J.C. Jung, "Oxidative Dehydrogenation of n-Butane over Vanadium Magnesium Oxide Catalysts Supported on Nano-structured MgO and ZrO_2: Effect of Oxygen Capacity of the Catalyst", *Journal of Nanoscience and Nanotechnology*, 12(7), pp.6045-6050 (2012).

12. H. Lee, **J.K. Lee**, U.G. Hong, Y. Yoo, Y.-J. Cho, J. Lee, H.-S. Jang, J.C. Jung, I.K. Song, "Effect of Oxygen Capacity and Oxygen Mobility of Supported $Mg_3(VO_4)_2$ Catalysts on the Performance in the Oxidative Dehydrogenation of n-Butane", *Journal of Industrial and Engineering Chemistry*, 18(2), pp.808-813 (2012).

Patents

International registered patents

1. 조영진, 유연식, 이진석, 장호식, 송인규, 이호원, **이종권**, "正丁烷氧化脱氢催化剂的氧化镁-氧化锆复合载体及其制备方法 ", 중국 특허출원 201210377874.X, 중국 공고번호 CN 103028446 B (2015).

2. Y.J. Cho, Y.S. Yoo, J.S. Lee, H.S. Chang, I.K. Song, H.W. Lee, **J.K. Lee**, "Single-step precipitation method of producing magnesia-zirconia complex carrier for catalyst for oxidative dehydrogenation of n-butane, magnesium orthovanadate catalyst supported on magnesia-zirconia complex carrier, and method of producing n-butene and 1,3-butadiene using said catalyst", US Patent Application No. 13/645,189, US Patent No. 8,927,455 B2 (2015).

International applied patents

1. 박글, 유연식, 이진석, 장호식, 최창현, 송인규, **이종권**, 서현, "用于正丁烷直接脱氢的铂/锡/氧化铝催化剂的制备方法以及使用所述催化剂制备C4 烯烃的方法", 중국 특허출원 201410145496.1 (2014).

2. G. Park, Y.S. Yoo, Y.J. Cho, J.S. Lee, H.S. Chang, C.H. Choi, I.K. Song, **J.K. Lee**, H. Seo, "Preparation method of platinum/tin/alumina catalyst for direct dehydrogenation of n-butane and method for producing C4 olefins using said catalyst", US Patent Application No. 14/249,955 (2014).

3. 박글, 유연식, 이진석, 장호식, 최창현, 송인규, **이종권**, 서현, "노르말-부탄의 직접 탈수소화 반응용 백금-주석-알루미나 촉매의 제조방법 및 상기 촉매를 이용한 C4 올레핀의 제조방법", 일본 특허출원 2013-259201 (2013).

Domestic registered patents

1. 송인규, 김정권, 홍웅기, 강기혁, **이종권**, "술폰산기 (-SO3H) 가 도입된 산점을 포함한 정렬된 구조의 중형기공성탄소에 담지된 귀금속 촉매, 그 제조방법 및 상기 촉매를 이용한 리그닌 모델 화합물 분해 방법", 대한민국 특허출원 10-2014-0057290 (2014), 대한민국특허 제 1,536,623호 (2015).

2. 박글, 유연식, 이진석, 장호식, 송인규, **이종권**, 서현, "알콕사이드 기반의 졸겔법에 의한 노르말-부탄의 직접 탈수소화 반응 촉매용 알루미나 담체의 제조방법, 그에 의해 제조된 알루미나 담체에 담지된 주석을 포함하는 백금 촉매 및 상기 촉매를 이용한 C4 올레핀 제조방법", 대한민국 특허출원 10-2013-0150440 (2013), 대한민국특허 제 1,522,250호 (2015).

3. 박글, 유연식, 이진석, 장호식, 최창현, 송인규, 서현, **이종권**, "노르말-부탄의 직접 탈수소화 반응용 백금-주석-금속-알루미나 촉매의 제조방법 및 상기 촉매를 이용한 C4 올레핀의 제조방법", 대한민국 특허출원 10-2013-0090456 (2013). 대한민국특허 제 1,477,413호 (2014).

4. 박글, 유연식, 조영진, 이진석, 정호식, 최창현, 송인규, **이종권**, 서현, “노르말-부탄의 직접 탈수소화 반응용 백금-주석-알루미나 촉매의 제조방법 및 상기촉매를 이용한 C4 올레핀의 제조방법”, 대한민국 특허출원 10-2013-0039749, 대한민국특허 제 1,452,102호 (2014).

5. 유연식, 조영진, 이진석, 장호식, **이종권**, 송인규, “이산화탄소와 산소를 산화제로 이용하는 노르말-부탄의 산화적 탈수소화 반응용 마그네슘 오르소바나데이트 촉매의 제조방법 및 상기 촉매를 이용한 노르말-부텐과 1,3-부타디엔의 제조방법”, 대한민국 특허출원 10-2012-0142941 (2012), 대한민국특허 제 1,437,744호 (2014).

6. 유연식, 조영진, 이진석, 장호식, **이종권**, 이호원, 송인규, “노르말-부탄의 산화적 탈수소화 반응 촉매용 마그네시아-지르코니아 복합담체의 제조방법, 그에 의해 제조된 마그네시아-지르코니아 복합담체에 담지된 마그네슘 오르소바나데이트 촉매의 제조방법 및 상기 촉매를 이용한 노르말-부텐과 1,3-부타디엔의 제조 방법”, 대한민국 특허출원 10-2012-0006693 (2012), 대한민국특허 제 1,419,995호 (2014).

7. 조영진, 유연식, 이진석, 장호식, 송인규, 이호원, **이종권**, “노르말-부탄의 산화적 탈수소화 반응 촉매용 마그네시아-지르코니아 복합담체의 단일 단계 침전법에 의한 제조방법, 그에 의해 제조된 마그네시아-지르코니아 복합담체에 담지된 마그네슘 오르소바나데이트 촉매 및 상기 촉매를 이용한 노르말-부텐과 1,3-부타디엔의 제조 방법” 대한민국 특허출원 10-2011-0101954 (2011), 대한민국특허 제 1,338,637호 (2013).

8. **이종권**, 송인규, 유연식, 조영진, 이진석, 장호식, “단일단계 졸-겔 법에 의해 제조된 노르말-부탄의 산화적 탈수소화 반응용 마그네슘 오르소바나데이트-마그네시아-지르코니아 촉매의 제조방법 및 상기 촉매를 이용한 노르말-부텐과 1,3-부타디엔의 제조방법”, 대한민국 특허출원 10-2012-0086839 (2012), 대한민국특허 제 1,341,242호 (2013).

Domestic applied patents

1. 조혜란, 서한욱, 이진석, 장호식, 송인규, **이종권**, 서현, 김정권, “다양한 결정상을 갖는 노르말-부탄의 탈수소화 반응 촉매용 알루미나 담체의 제조방법, 그에 의해 제조된 알루미나 담체에 담지된 주석을 포함하는 백금 촉매 및 상기 촉매를 이용한 노르말-부텐과 1,3-부타디엔 제조방법”, 대한민국 특허출원 10-2014-0095885 (2014).

2. 송인규, 이종협, 홍웅기, 김정권, **이종권**, “중형 기공성 탄소에 담지된 귀금속 담지촉매, 그 제조방법 및 상기 촉매를 이용하여 숙신산으로부터 사수소화퓨란을 제조하는 방법”, 대한민국 특허출원 10-2014-0064910 (2014).

3. 박글, 유연식, 이진석, 장호식, 최창현, 송인규, **이종권**, 서현 “노르말-부탄의 직접 탈수소화 반응 촉매용 알루미나 담체의 침전법에 의한 제조방법, 그에 의해 제조된 알루미나 담체에 담지된 백금-주석 촉매의 제조방법 및 상기 촉매를 이용한 C4 올레핀의 제조방법”, 대한민국 특허출원 10-2013-0065336 (2013).

Conferences

International conferences (First author)

1. **J.K. Lee**, J.K. Kim, K.H. Kang, I.K. Song, "Direct Dehydrogenation of n-Butane over Platinum-tin Catalysts Supported on Alumina", *NANO KOREA 2015*, P1503_099, COEX, Seoul, Korea (2015/7/1-3).

2. **J.K. Lee**, H. Seo, U.G. Hong, G. Park, Y. Yoo, J. Lee, H. Chang, I.K. Song, "Platinum-tin Nano-catalysts Supported on Alumina for Direct Dehydrogenation of n-Butane", *NANO KOREA 2014*, P1403_004, COEX, Seoul, Korea (2014/7/2-4).

3. **J.K. Lee**, H. Seo, U.G. Hong, Y. Yoo, Y.-J. Cho, J. Lee, H. Chang, I.K. Song, "Production of C4 Olefins by Oxidative Dehydrogenation of n-Butane over $Mg_3(VO_4)_2$ Catalysts", *The 14th Korea-Japan Symposium on Catalysis*, GP20, Nagoya, Japan (2013/7/1-3).

4. **J.K. Lee**, H. Seo, U.G. Hong, Y. Yoo, Y.-J. Cho, J. Lee, G. Park, H. Chang, I.K, Song, "$Mg_3(VO_4)_2$-MgO-ZrO_2 Nano-catalysts for Oxidative Dehydrogenation of n-Butane", *NANO Korea 2013 Symposium*, P1303_008, Coex, Seoul, Korea (2013/7/10-12).

5. **J.K. Lee**, U.G. Hong, Y. Yoo, Y.-J. Cho, J. Lee, H. Chang, I.K. Song, "Oxidative Dehydrogenation of n-Butane over Magnesium Vanadate Nano-catalysts Supported on Magnesia-zirconia: Effect of Vanadium Content", *The 10th NANO KOREA 2012 Symposium*, P1208-001, COEX, Korea (2012/8/16-18).

International conferences (Co-author)

1. K.H. Kang, T.H. Kim, **J.K. Lee**, S.J. Han, W.C. Choi, Y.-K. Park, I.K. Song, "Dehydrogenation of Propane to Propylene over Cr-based Catalysts", *NANO KOREA 2015*, P1503_101, COEX, Seoul, Korea (2015/7/1-3).

2. J.K. Kim, K.H. Kang, **J.K. Lee**, J.W. Lee, I.K. Song, "Catalytic Decomposition of Phenethyl Phenyl Ether to Aromatics over Pd-Fe Bimetallic Catalysts Supported on Ordered Mesoporous Carbon", *NANO KOREA 2015*, P1506_104, COEX, Seoul, Korea (2015/7/1-3).

3. K.H. Kang, J.K. Kim, **J.K. Lee**, S.J. Han, I.K. Song, "Re-Ru Bimetallic Catalysts for Hydrogenation of Succinic Acid to 1,4-Butanediol", *The 15th Korea-Japan Symposium on Catalysis,* GP56, Busan, Korea (2015/05/26-28).

4. Y. Bang, S.J. Han, J. Yoo, J.H. Choi, **J.K. Lee**, I.K. Song, "Hydrogen Production by Steam Reforming of Liquefied Natural Gas (LNG) over Nickel Catalyst Supported on Mesoporous Phosphorus-modified Alumina Xerogel", *20th WHEC(World Hydrogen Energy Conference) 2014*, 58, Kwangju, Korea (2014/6/15-20).

5. H. Seo, **J.K. Lee**, U.G. Hong, G. Park, Y. Yoo, J. Lee, H. Chang, I.K. Song, "Direct Dehydrogenation of n-Butane over Pt/Sn/Zn/γ-Al_2O_3 Nano-catalyst: Effect of Zn Content", *NANO KOREA 2014*, P1403_010, COEX, Seoul, Korea (2014/7/2-4).

6. U.G. Hong, H.W. Park, J. Lee, **J.K. Lee**, J. Yi, I.K. Song, "Conversion of Succinic Acid to 1,4-Butanediol via Dimethyl Succinate over Rhenium Nano-catalyst Supported on Copper-containing Mesoporous Carbon", *NANO Korea 2013 Symposium*, P1303_004, Coex, Seoul, Korea (2013/7/10-12).

7. H. Lee, **J.K. Lee**, I.K. Song, Y. Yoo, Y.-J. Cho, J. Lee, H.-S. Jang, J.C. Jung, "Oxidative Dehydrogenation of n-Butane over V-Mg-O Catalysts Supported on Nano-structured MgO-ZrO_2Mixed Oxides", *The 9th International Nanotech Symposium & Exhibition in Korea* (NANO KOREA 2011), P1103_009, Kintex, Seoul, Korea (2011/8/24-26).

Domestic conferences (First author)

1. **이종권**, 김정권, 강기혁, 이진석, 장호식, 송인규, "노르말-부탄의 직접 탈수소화 반응에서 소성온도가 다른 알루미나에 담지된 백금-주석 촉매가 노르말-부텐과 1,3-부타디엔 생성에 미치는 영향", 2015년 한국화학공학회 춘계학술회의, P촉매목-2, 제주 ICC (2015/4/22-24).

2. **이종권**, 김정권, 서한욱, 조혜란, 이진석, 장호식, 송인규, "알루미나 담체에 담지된 백금-주석 촉매의 제조 및 이를 활용한 노르말-부탄의 직접 탈수소화 반응을 통한 부텐과 부타디엔 생성", 2014년 한국화학공학회 추계학술회의, P촉매금-3, 대전 DCC (2014/10/22-24).

3. **이종권**, 서현, 이진석, 서한욱, 유연식, 장호식, 송인규, "알루미나에 담지된 백금-주석 촉매가 노르말-부탄의 직접 탈수소화 반응을 통한 부텐과 부타디엔 생성에 미치는 영향", 2014년 한국공업화학회 춘계학술회의, 1P-263, 제주 ICC (2014/4/30-5/2).

4. **이종권**, 서현, 이진석, 서한욱, 유연식, 장호식, 송인규, "노르말-부탄의 직접 탈수소화 반응을 통한 부텐과 부타디엔 제조에서알루미나 담체에 담지된 백금-주석 촉매의 영향", 2014년

한국화학공학회 춘계학술회의, P촉매금-5, 창원 컨벤션센터 (2014/4/23-25).

5. **이종권**, 서현, 이진석, 박글, 유연식, 장호식, 송인규, "노르말-부탄의 직접 탈수소화 반응에서 백금/주석/알루미나 촉매의 알루미나 담체가 촉매 활성에 미치는 영향", 2013년 한국공업화학회 추계학술회의, 2P-182, 대전 컨벤션센터 (2013/10/30-11/1).

6. **이종권**, 서 현, 이진석, 박 글, 유연식, 장호식, 송인규, "주석을 포함한 알루미나 담체에 담지된 백금 담지 촉매의 제조 및 노르말-부탄의 직접 탈수소화 반응으로의 적용", 2013년 한국화학공학회 추계학술회의, P촉매목-11, 대구 EXCO (2013/10/23-25).

7. **이종권**, 서현, 이진석, 조영진, 유연식, 장호식, 송인규, "노르말-부탄의 직접 탈수소화 반응을 위한 주석이 포함된 알루미나에 담지된 백금 촉매의 제조 및 특성에 관한 연구", 2013년 한국공업화학회 춘계학술회의, 1P-411, 제주 국제컨벤션센터 (2013/5/1-3).

8. **이종권**, 서현, 이진석, 조영진, 유연식, 장호식, 송인규, "백금/주석/알루미나 촉매의 제조 및 이를 이용한 C4 파라핀의 직접 탈수소화 반응을 통한 C4 올레핀의 생산", 2013년 한국화학공학회 춘계학술회의, P촉매금-5, 광주 김대중컨벤션센터 (2013/4/24-26).

9. **이종권**, 이진석, 조영진, 유연식, 장호식, 송인규, "졸겔법으로 제조된 마그네슘 오르소바나데이트-마그네시아-지르코니아 촉매가 노르말-부탄의 산화적 탈수소화 반응에 미치는 영향", 2012년

한국공업화학회 추계학술회의, 2P-182, 대전컨벤션센터 (2012/10/31-11/2).

10. **이종권**, 이진석, 조영진, 유연식, 장호식, 송인규, "마그네시아와 지르코니아가 포함된 마그네슘 오르소바나데이트 촉매의 제조 및 노르말-부탄의 산화적 탈수소화 반응으로의 적용", 2012년 한국화학공학회 추계학술회의, P촉매수-10, 부산 BEXCO (2012/10/24-26).

11. **이종권**, 이진석, 조영진, 유연식, 장호식, 송인규, "n-Butane의 산화적 탈수소화 반응에서 VMgO/MgO-ZrO_2 촉매의 산화물 담체가 촉매 활성에 미치는 영향", 2012년 한국공업화학회 춘계학술회의, 2P-187, 김대중컨벤션센터 (2012/5/9-11).

12. **이종권**, 이진석, 조영진, 유연식, 장호식, 송인규, "마그네시아-지르코니아에 담지된 마그네슘 오르소바데이트 촉매를 이용한 n-butane의 산화적 탈수소화 반응에 대한 연구", 2012년 한국화학공학회 춘계학술회의, P촉매금-35, 제주ICC (2012/4/25-27).

13. **이종권**, 이호원, 이진석, 조영진, 유연식, 장호식, 송인규, "n-butane의 산화적 탈수소화 반응에서 VMgO/MgO-MeO_x 촉매의 복합 금속산화물 담체가 촉매 활성에 미치는 영향", 2011년 한국공업화학회 추계학술회의, 1P-265, 경원대학교 (2011/11/2-4).

14. **이종권**, 이호원, 이진석, 조영진, 유연식, 장호식, 송인규, "다양한 복합 금속산화물에 담지된 VMgO 촉매를 이용한 n-butane의

산화적 탈수소화 반응에 대한 연구", 2011년 한국화학공학회 추계학술회의, P촉매목-14, 송도컨벤시아 (2011/10/26-28).

Domestic conferences (Co-author)

1. 김정권, **이종권**, 강기혁, 이종원, 송인규, "중형기공성 탄소에 담지된 Pd-Fe 촉매를 통한 리그닌 내부의 선택적인 탄소-산소 분해반응 및 리그닌 모델 화합물의 분해경로 규명", 2015년 한국화학공학회 추계학술회의, O촉매D목-2, 일산 KINTEX (2015/10/21-23).

2. 김태협, 강기혁, **이종권**, 한승주, 최원춘, 박용기, 송인규, "크로미아 기반 금속 산화물 촉매 상에서 프로판의 탈수소화 반응을 통한 프로필렌의 제조", 2015년 한국화학공학회 추계학술회의, P촉매금-14, 일산 KINTEX (2015/10/21-23).

3. 강기혁, 김정권, **이종권**, 한승주, 김태협, 송인규, "레늄-루세늄 이중금속 촉매 상에서 숙신산의 수소화를 통한 1,3-부탄디올으 제조", 2015년 한국화학공학회 춘계학술회의, P촉매목-6, 제주 ICC (2015/4/22-24).

4. 김정권, 강기혁, **이종권**, 송인규, "전이금속 복합 촉매상에서 리그닌 내부의 선택적인 탄소-산소 분해반응을 통한 방향족 생성 및 리그닌 모델 화합물의 분해경로 규명", 2015년 한국화학공학회 춘계학술회의, P촉매목-7, 제주 ICC (2015/4/22-24).

5. 김정권, 박해웅, **이종권**, 이어진, 송인규, "전이금속 및 귀금속이 담지된 중형기공성 탄소 담체를 이용한 리그닌 모델화합물의 분해반응 및 분해경로 규명", 2014년 한국화학공학회 추계학술회의, P촉매금-9, 대전 DCC (2014/10/22-24).

6. 서현, **이종권**, 이진석, 서한욱, 유연식, 장호식, 송인규, "아연을 조촉매로 도입한 백금/주석/아연/알루미나 촉매의 제조 및 노르말-부탄의 직접 탈수소화 반응으로의 적용", 2014년 한국공업화학회 춘계학술회의, 1P-260, 제주 ICC (2014/4/30-5/2).

7. 홍웅기, 강기혁, 김정권, 이중원, **이종권**, 이종협, 송인규, "염산을 조절한 단일공정 계면활성-주형법으로 제조된 귀금속-탄소 복합체 촉매의 숙신산 수소화 반응활성", 2014년 한국공업화학회 춘계학술회의, 1P-266, 제주 ICC (2014/4/30-5/2).

8. 서현, **이종권**, 이진석, 서한욱, 유연식, 장호식, 송인규, "$Pt/Sn/xZn/Al_2O_3$ 촉매 상의 노르말-부탄의 직접 탈수소화 반응에서 Zn 조성(X)이 미치는 영향", 2014년 한국화학공학회 춘계학술회의, P촉매금-4, 창원 컨벤션센터 (2014/4/23-25).

9. 홍웅기, 강기혁, 김정권, 이중원, **이종권**, 이종협, 송인규, "숙신산으로부터 사수소화퓨란 생성 반응에서 촉매 표면 형태에 따른 루테늄-탄소 복합체 촉매의 반응 활성", 2014년 한국화학공학회 춘계학술회의, P촉매금-53, 창원 컨벤션센터 (2014/4/23-25).

10. 홍웅기, 김정권, 이중원, **이종권**, 이종협, 송인규, "단일공정 계면활성 주형법으로 제조된 루테늄-탄소 복합체 촉매의 숙신산 수소화

반응활성", 2013년 한국공업화학회 추계학술회의, 2P-254, 대전 컨벤션센터 (2013/10/30-11/1).

11. 서현, **이종권**, 이진석, 박글, 유연식, 장호식, 송인규, "노르말-부탄의 직접 탈수소화 반응을 위한 조촉매가 도입된 백금/주석/알루미나 촉매의 제조 및 특성에 관한 연구", 2013년 한국공업화학회 추계학술회의, 2P-178, 대전 컨벤션센터 (2013/10/30-11/1).

12. 홍웅기, 김정권, 이중원, **이종권**, 이종협, 송인규, "숙신산으로부터 사수소화퓨란 생성 반응에서 귀금속-지지체 결합 온도에 따른 루테늄-탄소 복합체 촉매의 반응 활성", 2013년 한국화학공학회 추계학술회의, P촉매목-1, 대구 EXCO (2013/10/23-25).

13. 서현, **이종권**, 이진석, 박 글, 유연식, 장호식, 송인규, "$Pt/Sn/M/Al_2O_3$ 촉매의 전이금속(M)이 노르말-부탄의 직접 탈수소화 반응에서 부텐과 1,3-부타디엔 생성에 미치는 영향", 2013년 한국화학공학회 추계학술회의, P촉매목-7, 대구 EXCO (2013/10/23-25).

14. 홍웅기, 김정권, 이중원, **이종권**, 이종협, 송인규, "구리를 포함한 중형기공 탄소담체에 담지된 레늄 담지촉매를 이용한 숙신산의 수소화 반응에서 구리의 포함량에 따른 반응 활성", 2013년 한국공업화학회 춘계학술회의, 1P-414, 제주 국제컨벤션센터 (2013/5/1-3).

15. 서현, **이종권**, 이진석, 조영진, 유연식, 장호식, 송인규, "$Pt/Sn/M/Al_2O_3$ 촉매의 금속(M)이 노르말-부탄의 직접 탈수소화 반응에서 부텐과 1,3-부타디엔 생성에 미치는 영향", 2013년

한국공업화학회 춘계학술회의, 1P-425, 제주 국제컨벤션센터 (2013/5/1-3).

16. 홍웅기, 김정권, 이중원, **이종권**, 이종협, 송인규, “레늄-구리 촉매를 이용하여 숙신산으로부터 디메틸숙시네이트를 통해 1,4-부탄디올을 생산하는 촉매공정에서 구리 비율에 따른 반응 활성”, 2013년 한국화학공학회 춘계학술회의, P촉매금-2, 광주 김대중컨벤션센터 (2013/4/24-26).

17. 서현, **이종권**, 이진석, 조영진, 유연식, 장호식, 송인규, “노르말-부탄의 직접 탈수소화 반응을 위한 조촉매가 도입된 백금/주석/알루미나 촉매의 제조 및 특성에 관한 연구”, 2013년 한국화학공학회 춘계학술회의, P촉매금-11, 광주 김대중컨벤션센터 (2013/4/24-26).

18. 이호원, **이종권**, 홍웅기, 정지철, 장호식, 이진석, 유연식, 조영진, 송인규, “n-Butane의 산화적 탈수소화 반응을 위한 VMgO/MgO-ZrO_2, VMgO/MgO/ZrO_2, VMgO/ZrO_2/MgO 촉매들의 제조 및 특성에 관한 연구”, 2011년 한국공업화학회 추계학술회의, 1P-258, 경원대학교 (2011/11/2-4).

19. 이호원, **이종권**, 홍웅기, 정지철, 장호식, 이진석, 유연식, 조영진, 송인규, “n-Butane의 산화적 탈수소화 반응을 위한 VMgO/MgO-ZrO_2 촉매에서 다양한 MgO-ZrO_2 복합산화물 담체가 촉매의 활성에 미치는 영향”, 2011년 한국화학공학회 추계학술회의, P촉매목-9, 송도컨벤시아 (2011/10/26-28).

20. 홍웅기, 이중원, 황선환, **이종권**, 송인규, “숙신산의 수소화 반응에서 졸-겔 법으로 제조된 팔라듐-알루미나 복합체 촉매의 반응 활성”, 2011년 한국화학공학회 춘계학술회의, P촉매목-4, 창원켄벤션센터 (2011/4/27-29).